Soot Formation in Direct Injection Spark Ignition Engines Under Cold-Idle Operating Conditions

by

Justin Edward Ketterer

B.A.Sc., Honours Mechanical Engineering with Automotive Option
University of Windsor (2008)
M.A.Sc., Mechanical Engineering
University of Toronto (2010)

Submitted to the Department of Mechanical Engineering
in partial fulfillment of the requirements for the degree of

Doctor of Philosophy in Mechanical Engineering

at the

MASSACHUSETTS INSTITUTE OF TECHNOLOGY

September 2013

Author .....
Department of Mechanical Engineering
29 August, 2013

Certified by..... .....
Wai K. Cheng
Professor of Mechanical Engineering
Thesis Supervisor

Accepted by .....
David E. Hardt, Professor of Mechanical Engineering
Chairman, Department Committee on Graduate Theses

Soot Formation in Direct Injection Spark Ignition Engines Under Cold-Idle Operating Conditions

by

Justin Edward Ketterer

Submitted to the Department of Mechanical Engineering
on 29 August, 2013, in partial fulfillment of the
requirements for the degree of
Doctor of Philosophy in Mechanical Engineering

Abstract

Direct injection spark ignition engines are growing rapidly in popularity, largely due to the fuel efficiency improvements in the turbo-downsized engine configuration that are enabled by direct injection technology. Unfortunately, direct injection spark ignition engines also emit higher concentrations of particulate matter than conventional port fuel injected engines. In light of evidence linking particulate matter to adverse human health impacts, particulate emissions standards have been strengthened in both the United States and in Europe. A great deal of research seeking particulate emissions reductions is ongoing. This study contributes to this body of research by offering a refined explanation of the soot formation process in direct injection engines under cold-idle operating conditions. A number of engine and rapid compression machine experiments were conducted in order to understand the impacts of engine operating conditions and fuel composition on particulate matter emissions. Using these data, a conceptual model describing the formation of soot in direct injection engines is outlined. This model suggests that soot forms after the main combustion event in fuel vapour plumes surrounding liquid fuel films on cylinder surfaces through pyrolytic reactions enabled by heat transfer from burned gases from the primary combustion event.

Thesis Supervisor: Wai K. Cheng
Title: Professor of Mechanical Engineering

Acknowledgments

There are many people I would like to thank for their help and support in my time at MIT. The kindness and brilliance of those with whom I've worked and formed friendships is astounding. Without them, I would never have finished this thesis.

I would, firstly, like to thank my supervisor, Prof. Wai Cheng for the opportunity to work at MIT, as well as his help, guidance and patience throughout this project. I deeply appreciate his willingness to answer questions and give advice while still providing the opportunity to have an active role in determining the direction of my research. I would also like to thank Prof. John Heywood and Prof. Bill Green for sitting on my thesis committee. Our discussions were invaluable in the quest to interpret my experimental results.

Funding for this project came from the Engine and Fuels Research Consortium. I would like to thank the members of the Consortium, General Motors, Ford, Chrysler and Borg Warner, for the resources they've provided, since, without them, this project could not have been undertaken. I would also like to thank Rick Davis, Yangbing Zheng and Minghua Yang, of General Motors, for their help with engine hardware, setup and CFD modelling and Tom Leone, of Ford, for his valuable input.

I've been very fortunate to be a part of the Sloan Automotive Lab and would like to thank all of the staff and my fellow students for their support. Raymond, Thane, Eric, Wen, Tomas, Mike, Jake, Patrick, Amir, Kenneth, Joe, Felipe, Camille and Mathieu helped to make my time in the Sloan Lab productive and truly enjoyable. I would especially like to thank Kevin Cedrone for his help with my experiments and his willingness to co-operate while sharing a test-cell. I would also like to thank the friends I've made outside of the Sloan Lab, especially those in the Tech Catholic Community at MIT. Their support and friendship is sincerely appreciated.

Finally, and most importantly, I would like to thank my parents, Ed and Sherry, my brother Jordan and my wonderful fiance Katie for their love and support throughout my studies at MIT.

This page intentionally left blank

Contents

This page intentionally left blank

List of Figures

List of Tables

This page intentionally left blank

Abbreviations

CA	Crank Angle Degrees
ATDC	After Top Dead Centre
BDC	Bottom Dead Centre
BTDC	Before Top Dead Centre
COV	Coefficient of Variation
CPC	Condensation Particle Counter
DAQ	Data Acquisition
DISI	Direct Injection Spark Igntion
DMA	Differential Mobility Analyzer
EGR	Exhaust Gas Recirculation
GPF	Gasoline Particulate Filter
IMEP	Indicated Mean Effective Pressure
MAP	Manifold Absolute Pressure
NDIR	Non-Dispersive Infrared
NIMEP	Net Indicated Mean Effective Pressure
PAH	Polycyclic Aromatic Hydrocarbons
PM	Particulate Matter
PMP	Particle Measurement Programme
PMT	Photomultiplier Tube
PN	Particle Number
RCM	Rapid Compression Machine
SMPS	Scanning Mobility Particle Sizer
SOI	Start of Injection
SOI_2	Start of Second Injection
SY	Soot Yield
TDC	Top Dead Centre
UEGO	Universal Exhaust Gas Oxygen Sensor
VVT	Variable Valve Timing

This page intentionally left blank

Chapter 1

Introduction

Few inventions have impacted society as profoundly as the internal combustion engine. Its development enabled accessible, reliable, affordable and relatively rapid transportation which has changed our outlook on distance and has forever reshaped our landscape. Unfortunately, this transportation revolution has been accompanied by severe environmental challenges, most notably air pollution. While there have been vast improvements since the advent of emissions controls in the early 1970s, the transportation sector remains a significant contributor to air pollution [1]. Emissions of greenhouse gases, such as carbon dioxide, are of particular interest recently, owing to their impact on global climate change, but particulate matter (PM) emissions are also a major (and growing) concern because of their health effects.

Efforts to reduce greenhouse gas emissions have led to investment and innovations oriented toward limiting fuel consumption. To this end, we have witnessed widespread adoption of Direct Injection, Spark Ignition (DISI) engine technology [2]. DISI engines, which see the air/fuel charge prepared in-cylinder, have enabled improved engine efficiency, especially in turbo-downsized configurations. Unfortunately, these engines are also associated with increased PM emissions when compared to conventional SI engines [3]. This is especially apparent during cold-start and cold-idle operating conditions [4].

In light of the health impacts associated with PM exposure, PM emissions limits are being strengthened [5] and automakers are making strong efforts to reduce PM

emissions from their vehicles. Progress is being made in the reduction of PM emissions, but cold-start and cold-idle PM emissions remain a significant challenge; there remains a lack of understanding of the fundamental processes through which PM is formed in-cylinder.

1.1 Background

Throughout the past decade, DISI has rapidly progressed from an emerging technology to a fully mainstream technology. DISI engines are found in all segments of the automotive market from economy cars to high-performance sports cars. Like traditional spark ignition (SI) engines, in DISI engines, a pre-mixed mixture of fuel and air is ignited by a spark. The difference lies in the method of mixture preparation. Carburetion was the dominant method until being replaced in the mid 1980s with throttle body and later multi-port fuel injection. In the case of carburetion, mixing should be essentially complete within the intake manifold, since the fuel is well-atomized and there is a long mixing distance. In the case of port fuel injection, the process is somewhat more complicated. In this case, the liquid fuel is sprayed toward the back of the intake valve, which is relatively hot, vaporizing much of the liquid. In part-load conditions, upon the intake valve opening, there will then be a flow of hot residual gases into the intake runner, which will further help to vaporize remaining liquid fuel. Finally, when flow begins into the cylinder, the turbulent flow through the intake valve serves to further enhance mixing [6]. The result is a well-mixed, homogeneous charge being admitted to the engine cylinder.

In a DISI engine, by contrast, only air is inducted to the cylinder. The fuel is injected inside the cylinder and all air/fuel mixing occurs in-cylinder. The heat of vaporization for fuel evaporation is drawn from the air charge, or from engine surfaces, and mixing is largely dependent on charge motion. This presents some benefits in terms of engine efficiency. Volumetric efficiency is improved by inducting only air as well as by the charge cooling effect of vaporizing fuel, which increases charge density [2]. This charge cooling effect also increases the maximum cylinder pressure allowable

before knock is likely. This has enabled the recent increase in popularity of downsized and turbocharged engines [2, 7].

The liquid fuel in cylinder and resulting compromises related to mixing, however, contribute to difficulties in limiting PM emissions. DISI engines emit substantially more PM than PFI engines and in some cases more even than Diesel engines equipped with particulate filters [8]. This PM is attributed to the presence of liquid fuel in-cylinder during the combustion event. This fuel may be present in the form of free droplets, but of most importance to PM formation is liquid films on cylinder surfaces. It is generally reported that these films result in diffusion flames in which soot inception takes place [9]. This is especially true during cold-start and cold-idle operating conditions when cold engine surfaces and inlet air do not support evaporation and low engine speeds may not provide adequate charge motion for good mixing [10]. Compounding this problem is the issue that the engine operating conditions under these cases may be more susceptible to soot formation due to efforts to reduce other emissions. In particular, the spark and injection timings are sometimes retarded to promote faster catalyst light-off with the goal of reducing hydrocarbon emissions [11, 12].

In response to these emissions challenges, engine researchers in both industry and academia have been undertaking studies designed to better understand PM emissions in the context of SI engines and to develop strategies for reducing emissions in order to meet government emissions standards.

1.1.1 Literature Review

The study detailed in this thesis is not the first to address PM emissions in DISI engines, nor will it be the last. In order to appreciate this study's contribution to this field of study, one must be familiar with the state of research regarding PM and DISI engines. This section offers a summary of those previous works that are relevant to this study of PM from DISI engines. When viewed as a collection, it is possible to identify the weaknesses present in the current understanding of PM emissions from DISI engines, serving as motivation for the research objectives of this study.

Health and Environmental Impacts of Particulate Matter

Soot, a carbonaceous form of PM, has long been associated with negative health impacts. In fact, it was the first substance identified as an occupational carcinogen based on cancers caused in chimney sweeps in the 18^{th} century [13]. Since that time, suspicion of PM as a cause or contributor to a wide variety of illnesses and environmental impacts has continued to grow.

Today, few people are employed as chimney sweeps, but there remain many sources of PM, a major one being transportation [1]. A number of studies have identified relationships between PM and human mortality. For example, a review of European studies by Pelucchi et al. [14] found that while there was some heterogeneity in results based on exposures and locations, total mortality rates were directly asscoiated with long-term exposure to PM. The excess mortality seen in these studies was due mainly to cardiovascular and respiratory illnesses. Questions were raised about the mechanisms through which PM impacts health. In particular, there remains uncertainty over whether the health impacts are caused by PM mass or chemical composition.

Atmospheric PM typically displays a tri-modal size distribution [15], but most studies have narrowed in on fine particles as the likely culprits in health impacts. Also in Europe, Boldo et al. [16] have studied the public health of $PM_{2.5}$ (the collection of particulates smaller than 2.5μm in diameter), finding that reductions in exposure to $PM_{2.5}$ may increase life expectancy in European cities. Kaiser et al. [17] notes that the link between $PM_{2.5}$ exposures and long-term mortality risks have been largely confirmed, with increases in the long-term death risk estimated to be 4% for every $10\mu g/m^3$ increase in $PM_{2.5}$ concentrations. Short-term exposure to $PM_{2.5}$ is also identified as a potential health risk. Some people may experience a tripling of their risk of heart attack in the hour following exposure to traffic-related PM [17, 18]. Peters et al. [18], in discussing the cardiac risk of traffic-related PM exposure note that ultrafine particles are especially prevalent in traffic-related PM emissions. Based on this idea, it has been suggested that ultrafine particles, that is, particles smaller than 0.1μm, may be the main culprits in PM-related illnesses. This hypothesis is supported

by PM respiratory deposition modeling which suggests that smaller particles are far more efficiently deposited in the human respiratory tract than larger particles [19]. Kaiser et al. [17] note that it is not clear whether it is the small size or the chemical composition of ultrafine particles that may enable the added risk. It is suggested that the risk may be due to some combination of size and chemistry.

While this idea remains controversial [20], it has found support in other studies as well. McCreanor et al. [21] found that lung function is negatively affected by PM exposure. This was found to be especially true for those suffering from asthma or other existing respiratory illnesses and was most consistently associated with ultrafine particles and elemental carbon.

The growing understanding of these health impacts have largely been the motivation behind increasingly stringent emissions limits. DISI engines emit particles much smaller than 2.5μm, tending toward sub-micron particles with mean diameters between 60 and 100nm [22]. It is in light of this that engine manufacturers are seeking strategies for limiting PM emissions from DISI engines.

Emissions Legislation

In light of the potential health impacts, government regulations limiting PM are increasingly stringent, for the first time intending to limit SI engine emissions of PM. In the United States, thus far, the limits remain measured on a mass basis. In Europe, however, a particle number limit has been enacted in addition to a mass limit [23]. The final number limit will be $6x10^{11}$ particles/km, measured with a lower size limit of 23nm and a 50% upper cut size of 2.5μm. For vehicles emitting small particles, this number limit of $6x10^{11}$ particles/km ($6x10^{12}$ particles/km during the phase-in) is more difficult to satisfy than the mass limit as DISI engines typically emit a reasonably low mass of PM, but relatively high numbers of small particles. In fact, it was reported in 2008, that many then-current DISI engines would emit more PM on a number basis than modern Diesel engines equipped with particulate filters [8]. Few would be surprised if a similar limit were mandated in the United States at some point in the future.

Engine emissions have been under scrutiny since an understanding of the adverse effects of vehicle emissions began to emerge in the 1940s and 1950s, but it was not until the early 1960s that governments began establishing programs targeted to reduce emissions. The first such effort came in California when it was mandated that vehicles be equipped with crankcase ventilation systems that recirculate the blowby gases into the intake air to be burned. By the late 1960s, photochemical smog was acknowledged as a problem outside of California and a desire for nationwide emissions standards emerged. In 1970, the U.S. Environmental Protection Agency (EPA) was authorized to set these emissions standards by amendments to the Clean Air Act [24]. The Clean Air Act was further amended in 1977 and again in 1990, when the Tier I and Tier II emissions programmes were established. The Tier I emissions standards were phased-in between 1994 and 1997 [25], and the Tier II standards were phased in between 2004 and 2009 [26].

While studies of the impacts of PM were required by the Clean Air Act as early as 1977 [27], until now, particulate emissions standards have not been aimed at SI engines. This will change, however, as the recently finalized Tier III rules come into effect. While lacking the number limit seen in Europe, there is a stringent mass limit of 3mg/mi attached to the new standards [28]. The efforts in the U.S. and in Europe to reduce PM emissions have provided a strong driving force behind research oriented toward understanding PM emissions.

PM Emissions Measurement

The particle concentrations permissible under upcoming emissions standards in the U.S. and in Europe are low enough that they pose a measurement challenge for traditional PM measurement techniques. When discussing mass measurements, as are used in the U.S., for DISI and clean-Diesel engines, the mass of PM deposited on the filters is so small that it may be on the same order of magnitude as the deposited mass attributed to the background PM and condensed gaseous hydrocarbons in the sampling system [29]. In addition, number measurements, as are performed in this study, are also difficult since PM is not an easily defined substance because it does

not have a uniform composition [30]. Instead, PM is a mixture of solid particles, largely carbonaceous soot (but also some metal particles), and droplets of volatile liquids. The volatile fraction is a major contributor to the difficulty of measuring PM for regulatory purposes, since the volatile fraction is very sensitive to the emissions sampling techniques. With diluted samples, for example, the dilution ratio can have a profound effect on the PM composition [10]. With the advent of number-based emissions standards in Europe, it has been necessary to standardize PM measurement techniques to allow repeatable measurements of particle number concentrations in a number of different locations.

Toward this end, the Particle Measurement Programme (PMP) was started. The PMP includes an international effort to develop a standard measurement technique for PM emissions. These standards were initially set with Diesel engines in mind, but have been adapted to consider DISI engines as well. Changes to the initial protocol have been suggested by various members en route toward the final protocol. For example, the UK recommended the addition of a cyclone pre-classifier and changes to the filtration setup for mass measurements [31].

For this study, the PMP protocol for number measurements was of particular interest as it helped to guide the design of the sampling system. One of the major goals of the protocol for number emissions is to eliminate the volatile PM component, since the solid particles can be measured more repeatably. This was accomplished through the use of a condensation particle counter measuring only particles between 23nm and 2.5μm. The lower size cut-off helps to eliminate volatile particles. In addition, the sample is pre-conditioned in an evaporation tube heated to 300°C. These techniques were validated by using a single, "golden" test vehicle. Emissions from this vehicle were measured in a number of regulatory labs in various countries in Europe as well as in the United States. A summary of this inter-laboratory correlation report is included in [32].

Soot Formation

A high fraction of the PM from DISI engines is soot [33]. Thus, in order to gain a full understanding of PM formation in engines, it is helpful to be familiar with the fundamentals of soot formation in flames. A review by Haynes and Wagner [34] offers a thorough overview of the processes involved in soot formation. Two separate stages are discussed in the initial soot formation process. The first is particle inception and the second is particle surface growth. Surface growth is then followed by growth via coalescence. All of these processes are taking place in competition with oxidation processes.

In the particle inception stage, gaseous products of fuel oxidation or pyrolysis reactions condense to form particles with diameters of approximately $20\mathring{A}$. Unsaturated hydrocarbons such as acetylene or polycyclic aromatic hydrocarbons (PAH) are thought to be the most likely precursors of these particle nuclei. This process takes place near the primary reaction zone in a flame and defines the initial number of soot particles.

In the particle surface growth stage, the mass (or volume fraction) of soot is increased, while the number of particles remains constant. During surface growth, gas phase hydrocarbons readily deposit or release from the soot surface, which is highly reactive. These primary particles then may undergo coalescence to form chain-like agglomerates. In this case, the number will decrease while the total soot mass remains constant. Soot formation and growth is occuring at the same time as oxidation processes. In typical flames, most of the soot formed will be oxidized prior to be being emitted, OH being the primary oxidant.

Mansurov [35] offers a similarly thorough review, describing essentially the same processes. Here, particle nucleation is explained by a process through which large PAH are formed through reactions of smaller PAH with acetylene, other PAH or PAH radicals, with the main nucleation path being via reactions between PAH and PAH radicals. Surface growth reactions are described as being similar to the aforementioned PAH reactions, with acetylene and PAH as the growth species. This growth

competes with surface oxidation. Finally, coalescence is described in two stages. In the early stages of coalescence, collisions between growing particles yields new, larger spherical particles. In the later stages, the particles agglomerate into chain-like structures.

Brezinsky et al. [36] discusses this process in the context of different flame types. In premixed flames, sooting is observed to decrease with increased flame temperature. This is explained by noting that attack by OH increases more rapidly with temperature than does the formation of soot precursors. The formation of OH and soot precursors both depend on the number of carbon-carbon bonds in the fuel, but, otherwise, the fuel composition has little effect. In diffusion flames, by contrast, the rate of soot formation increases with increasing temperature and is affected by the fuel structure which impacts how the fuel pyrolytically decays. This study also looks at the formation of soot in an oxidative pyrolysis, offering some insight into the formation of soot in diffusion flames. This study agrees with those above in the understanding that PAH are the precursors leading to nucleation, though it is not confirmed experimentally.

Nucleation and surface growth driven by acetylene has been described by the Hydrogen Abstraction, C_2H_2 Addition (HACA) mechanism. In cases where acetylene concentrations are much larger than those of aromatics, it is expected that the PAH leading to nucleation grow by the addition of acetylene molecules to the aromatic rings, forming additional rings in the process. When the aromatic concentration is closer in magnitude to that of acetylene, it may be more likely that the PAH growth will occur through the condensation of existing aromatic rings. These mechanisms do not address the formation of the initial aromatic rings which grow to form PAH, but it is suggested that this likely proceeds from a polymerization of acetylene molecules [37].

In studies of pyrolysis, there has been, however, some debate over the mechanism of nucleation. Krestinin [38] in outlining a model of soot formation, questions the "aromatic model" discussed above. Instead, the model was based on the "acetylene pathway." In this model, acetylene, which, unlike other hydrocarbons, increases in

thermodynamic stability at elevated temperatures, along with polyacetylenes and PAH are formed in pyrolysis reactions. Acetylenes, considered a major intermediate in both pyrolysis and flames, grow simply and quickly, while PAH grow relatively slowly in a multi-stage process. The breeding of radical sites in polyacetylenes permits fast polymerization, which may lead to nucleation, growing into a polymeric globule (primary soot particle). In this model, coalescence forming new spherical particles continues until polymeric growth ceases, at which point agglomeration may take place. The application of this mechanism to traditional flames is not clear, since the lack of oxygen in pyrolysis simplifies the chemical pathways greatly.

These questions about the roles of aromatics or acetylenes are not new. They were raised in 1965 by Scully and Davies [39] who were able to identify PAH in their experiments of carbon black production. It was unclear at that time whether the PAH were side-products, or intermediates in the combustion and soot formation processes.

Looking more practically at flames, a number of studies have examined the locations of soot formation in flames and have attempted modelling of soot formation. Moss et al. [40] identified soot formation in a fuel rich pyrolysis region of an ethylene-oxygen laminar diffusion flame. Santoro et al. [41] similarly examined soot formation in an ethylene-air flame, looking at soot growth by observing soot characteristics at different points along the flame. By observing the particle concentrations along the length of the flame, some insight was gained into the temperature-time history of soot particles in flames. The soot was found to form in the annular flame region, on the fuel side of the flame. Through modelling and experiments, Smooke et al. [42] similarly outline soot formation and evolution through the flame with the main soot formation regions appearing to be in the annular region of the flame in a fuel-rich region on the fuel-side of the reaction.

While fuel structure impacts on soot formation rates are not entirely clear when discussing nucleation and suface growth, in practical applications, sooting tendencies do vary with fuel type. As outlined in Glassman and Yetter [43], early attempts to establish sooting trends for premixed flames or laminar diffusion flames met with some difficulty due to confounding variables such as flame temperature changes ac-

companying fuel changes. Controlling flame temperature, however, it was possible to obtain a more reliable index of fuel sooting tendencies based on fuel structure. It was found that sooting tendency correlates closely to the number of carbon-carbon bonds contained in a fuel, with the sooting tendency increasing with more carbon-carbon bonds. Similar results were obtained by Ladommatos et al. [44], who found sooting tendencies to increase with carbon number for paraffins, olefins and acetylenes. The trends reported for cyclic hydrocarbons were more complicated, depending on the type and location of side chains, though it was clear that aromatics had a higher sooting tendency than naphthalenic rings.

Soot Formation in DISI Engines

For more than a decade, PM emissions from DISI engines have proven to be of great interest to engine developers and researchers. A large number of studies have been completed with the intent of understanding PM formation in the context of DISI engine combustion. Most of these studies have focused on the mechanical processes through which soot forms, while some effort to understand the chemical pathways to soot has also been made.

Early in the development of modern DISI engines, the fuel/air mixing process was identified as a major contributor to engine emissions. Efforts to understand these mixing processes drove much of the early research [45]. PM emissions were linked to the mixing process early on as well. Early experiments noted changes in PM emissions with spark timing, which were related to the cylinder temperature and pressure changes associated with varied combustion phasing, but injection timing was identified as having a very strong impact on PM emissions. With late injection timings found to increase PM emissions, mixing time and charge stratification were identified as likely culprits in PM formation [46].

Optical Experiments In order to examine the mixing process, a number of studies have made use of optical engines to observe the fuel injection and mixture preparation processes. The work of Stevens and Steeper [47] made use of an optical engine,

equipped with laser-induced fluorescence imaging of the fuel injection process. They found that the cylinder pressures and temperatures affected the spray morphology. Their work was extended, in a second paper, to examine the formation of PM [9]. They found that the fuel impingement on cylinder surfaces persits throughout the combustion and exhaust processes, giving rise to soot-producing reactions described as pool fires. The soot formed in these pool fires was observed to persist throughout the exhaust stroke, being emitted with the bulk gases.

Alger et al. [48], also completed optical experiments. These used Schlieren imaging to observe the evaporation process for piston fuel films. It was observed that the fuel films evaporate late in the power stroke, resulting in fuel vapour plumes. The fuel volatility was found to play an important role as it determined the time needed for evaporation. More volatile fuels weren't necessarily better. In warm engines, with hot piston surfaces, volatile fuel components may experience film boiling. This Leidenfrost effect creates a layer of vapour which insulates the less-volatile fuel components from the piston surface, extending their lifetime. It was found that, in some cases, fuel films may persist for several cycles.

In [49], it was similarly found that mixture stratification is an important issue, as soot forms in fuel-rich regions. It was found that there were no droplets remaining in the bulk charge by the time combustion occurs, but significant liquid fuel mass remained as fuel films. In [50], yet another optical study, a distinction was made between soot forming early in the cycle and that which forms late in the cycle. Early soot was observed to form in rich, but pre-mixed regions of the cylinder, while late soot was found to form in the type of pool fire suggested in [9]. Through the imaging of piston fuel films, it was found that only approximately 0.1% of the injected fuel typically forms a fuel film, yet the smoke emissions remain closely related to the maximum wall film mass.

Even recently, optical experiments have continued to be employed in studies of PM formation. Velji et al. [51] used the light extinction technique and laser-induced incandescence to visualize soot and fuel sprays. Again, pool fires were considered to be the main cause of soot formation, but, in stratified operation, soot formation was

also observed in rich pre-mixed regions in the cylinder. Similar observations were made in [4]. Here, inadequate mixing and stratification were again implicated in soot formation, but, some effort was also made to understand the impacts of the fuel spray on the formation of liquid films. It was found that there is a tradeoff between fuel atomization and impingement. Better atomization, with the intent of improving in-flight evaporation, achieved through increased fuel pressures also resulted in increased spray penetration, increasing impingement. Costanzo et al., visualized the ignition of diffusion flames around liquid films after the main combustion event in an experimental, square-piston optical engine [52]. Here, it was seen that the luminous soot particles persisted into the exhaust stroke.

While in cold engines it seems that most PM is produced in reactions surrounding surface films, it was found in [53] that for warm engines, soot producing reactions are also likely around the injector tip (especially if it is coked) as well as other regions of the cylinder containing carbon deposits. This study urged a focus on the injector tip as a source of PM in warm engines.

The impact of fuel composition on PM emissions has also been studied. In an optical experiment similar to those discussed above, the same observations of soot being emitted in proportion to spray impingement were made, but a look at the formation of films was examined with varied injection timing as well as varied fuel composition. In this case, ethanol/gasoline blends were examined, with wider spray cone angles observed for ethanol blends [54]. The dependence on fuel composition had earlier been observed in [55]. In this optical study, it was found that the fuel composition impact was also related to the coolant temperatures as the spray was strongly affected by coolant temperature for fuels with boiling points near the coolant temperature.

Emissions Measurements Optical experiments offer good insight into soot formation mechanisms, but emissions measurements are also very useful for understanding the impact of engine operation on PM emissions. Many studies have been able to detail the impacts of mixture composition through exhaust PM measurements. For

example, a direct correlation between PM emissions and the engine body temperature was observed in [10]. In [56], it was similarly observed that particle number emissions decreased with increasing coolant temperature (up to 50°C). In addition, it was found that rich mixtures increased particle number emissions as did low fuel pressures. The injector spray angle was also found to be important. A high sensitivity to equivalence ratio was observed through emissions measurements in [57]. This study also identified long injection durations as problematic, reinforcing the idea that poor mixing leads to soot formation. Excursions into rich operation, or high fuelling rates in a transient manner are not always easily avoided. For this reason, it has been suggested that efforts are needed to achieve PM reductions when operating outside of the optimal engine settings, although it is often difficult to reduce particle number and mass emissions simultaneously [58].

Through a more thorough analysis of exhaust emissions, including speciation, it was possible to correlate nanoscale particles to gaseous species [59]. Here it was found that slight chemical differences can make large differences in PM emissions. It was found that acetylene and benzene play key roles in the nucleation phase of particle development, as is expected based on fundamental studies of soot formation. It was, however, found that benzene and other aromatics played a larger role in the growth of particles than acetylene. Thorough analyses of the soot composition have also been completed. As an example, a study of cold-start emissions found that PM was dominated by volatile materials, but that in the solid fraction, both amorphous and graphitic particles were observed [60]. The fuel temperatures were also observed to affect the composition of particles, with higher temperatures resulting in decreased mass and decreased particle diameters [61].

Fuel Effects Much of the effort in understanding PM formation and emissions has gone into understanding the impacts of fuel composition with a fairly strong focus on alcohol blends. This is largely for practical reasons. One of the reasons is that pump fuel in the United States already contains ethanol. A second relates to the synergies between decreased PM and improved knock resistance afforded by ethanol/gasoline

blends [62, 63].

One study of oxygenated fuels attributed decreases in PM emissions, in part, to changes in volatility with the addition of alcohol. The addition of ethanol, for example, despite its high latent heat of vaporization, may improve the mid-range volatility of a gasoline blend, improving mixing and reducing PM [64]. While some studies report decreased number emissions with no change in size distribution [65], it should be noted that the decreases observed in PM emissions with ethanol addition were not uniform for all particles. In some cases, increases were seen in nucleation mode particles, but decreases were seen in accumulation mode particles. The mixing benefits with ethanol blending were not universally observed. In [66], less homogeneous mixtures were observed with ethanol blending. Other studies did find improvements associated with ethanol, but the improvements did not necessarily correlate linearly with increased ethanol content. One study found better evaporative properties with ethanol blends, but the PM reductions began to decrease when the ethanol fraction was increased above 10% [67]. It was thought that the higher ethanol content may actually impede the evaporation of heavier gasoline components due to the charge cooling effect. In addition to the ethanol experiments, this study also looked at fuels more generally to try to find relations between the composition and the PM emissions. In this case, high boiling point aromatics were found to be the best predictor of PM emisisons.

There have been several attempts to develop predictive models relating fuel properties to vehicle PM emissions. In a study conducted at Honda [68], it was found that high boiling point, and high double-bond-equivalent aromatics were associated with increased particle number emissions while high boiling point, low double-bond-equivalent components had only a minor effect on PM. Here, a PM index was developed, which was then verified for different fuels and engines, with a specific effort to ensure it applied for fuels available in a variety of countries. In a study by Leach et al. [69], a refinement to this index for particle number emissions was validated with fuel mixtures carefully blended to offer independent control of volatility and aromatic content.

PM Control Strategies

Much work has gone into attempts to understand the processes through which PM is formed in DISI engines. As discussed above, the main contributor to PM seems to be soot formed in reactions involving fuel from liquid films, with contributions from pre-mixed combustion in locally rich regions. While there may be some detail lacking in these explanations of soot formation, they nevertheless provide a practical framework that enables the development of systems designed to limit PM emissions. Strategies to reduce PM emissions fall into two broad types: in-cylinder strategies and aftertreatment strategies. Owing to the cost and complexity of aftertreatment systems, in-cylinder PM reduction strategies are more desirable. These generally involve efforts to improve the mixture homogeneity through injection strategies,or the control of combustion parameters.

Early attempts at reduced emissions through injection design included Toyota's development of a fan-shaped injector for use in stratified charge operation [70]. This was targeted at reductions in emissions at moderate loads and engine speeds. Under cold-start conditions, the goal was to use this system while reducing wetting [71]. In the experiments, this was accomplished by injecting heated fuel and using careful injection strategies to minimize wetting with stratification and the aforementioned fan-shaped sprays. More recently, the prospects of lean, stratified charge combustion seem less promising, but similar spray optimization efforts are ongoing. For example, in developing the combustion system for their 3.6L DISI V6 engine, GM engineers optimised the injector flowrate, orifice geometry and spray pattern to balance the power, torque, fuel consumption, driveability and emissions needs of the engine [72]. This engine does still incorporate a piston bowl for cold-start, but efforts were made to characterize the interactions between the fuel spray and this bowl.

The work of Whitaker et al. [4] offers a thorough review of some of the options currently available for reducing PM emissions with in-cylinder strategies. The focus was on the optimization of the fuel injection system and the combustion system. A tradeoff between fuel atomization and impingement was identified, with the key

to reduced emissions being the reduction of impingement. Four distinct operating regimes were identified, and soot reduction strategies were offered for each. Most relevant to this study are the cold-start and catalyst-heating operating conditions. Under both conditions, optimized injection strategies are important. In addition to the injector design, high injection pressures have been used to aid in atomization and multiple injections are used to limit penetration. For the catalyst light-off phase, the cam timing and ignition timing were also identified as areas with potential for optimization. These parameters are related to the combustion phasing and temperatures, influencing the soot formation and oxidation reactions. The multiple injection strategy has been studied in several locations and is seen as a promising technology for the reduction of other emissions, such as hydrocarbons, in addition to PM [73]. Other strategies have also been considered for improving injection characteristics. One example is the use of supercritical injection pressures [74]. In this system, at high pressures, good mass flow can be maintained despite being supercritical, and the fuel condenses to very small droplets, which should evaporate easily, after injection.

Piock et al. [3] offer similar injection strategies for the reduction of PM emissions. They suggest increased fuel pressures and temperatures, multiple injections, minimized wall wetting, careful control of the equivalence ratio, good atomization and optimized spray patterns. An emphasis, in this paper, seems to be on maintaining elevated temperatures to reduce the effects of fuel impingement. In addition, heated inlet air, and optimized valve timing and residual gas mixing are suggested. Control of the cam timing seems geared toward controlling internal exhaust gas recirculation (EGR) rates. External EGR has also been considered as a means of reducing PM emissions. Cooled EGR has been found to be effective at reducing particle number and mass emissions [58]. Though it is generally a challenge to reduce mass and number emissions simultaneously, it was found that the use of EGR can help to reduce emissions when operating outside the optimal settings. Of course, most of these strategies will require different optimizations depending on the fuel being used.

While injection and combustion optimization are promising strategies for PM reductions, it is possible that they may not be sufficient. In this case, revised or ex-

panded aftertreatment systems may be necessary. For meeting particle number limits, it has been suggested that three-way catalysts (TWC) could be effectively optimized to reduce the concentration of small particles in the exhaust, though the concentration of large particles will likely experience modest increases [75, 76]. Should this still not be sufficient, it may be necessary to follow the lead of Diesel manufacturers and use particulate filters. Recent studies of "gasoline particulate filters" (GPF) have demonstrated efficiencies of approximately 80% [22]. Since cold start is a major area of concern, a study was conducted to examine GPF performance at cold ambient temperatures. For cold engines, when filter regeneration could be avoided, the ambient temperature had little effect on the filtration efficiency, even though the engine-out particulate emissions changed. During regeneration at cold temperatures, however, the filtration efficiencies were significantly reduced, with similar concentrations of ultrafine particles observed upstream and downstream of the filter [77].

1.2 Research Objective

This study was intended to examine the physical processes leading to the formation of particulate matter, in cylinder, during cold-idle operation in DISI engines. The primary goal was to offer a thorough explanation of the mechanism through which liquid fuel films on cylinder surfaces give rise to reactions supporting soot formation.

A complete conceptual model of particulate formation, including a full understanding of the reactions involving liquid fuel would be of great value to the automotive industry as it strives to meet increasingly stringent emissions standards. When equipped with a full understanding of the underlying processes leading to particulate formation, it is expected that combustion specialists will be better able to design engine combustion systems which successfully avoid particulate formation.

1.3 Research Approach

The ultimate goal of this research project was to gain a more complete understanding of the soot formation processes in DISI engines. In working toward this goal, the research effort was guided by two hypotheses. The first was referred to as the "residual fuel effects" hypothesis and the other was the "fuel effects" hypothesis.

Based on observations reported in previous works [9, 47, 52], the residual fuel effects hypothesis suggests that, in cold engines, PM results primarily from residual fuel, present after the wetting of in-cylinder surfaces, which will be burned with residual oxygen from burned gases. It was thought that this combustion would behave as a very fuel-rich flame with the associated sooting propensity.

In the fuel effects hypothesis it was predicted that differences in PM emissions observed [78] for different fuels could be related to physical or chemical properties of those fuels. Different evaporation properties would affect the residual fuel composition, the mixture stoichiometry would affect the sooting propensity given constant mixing properties (i.e. with a given amount of fuel and air, a fuel with a higher stoichiometric air/fuel ratio would yield a more fuel-rich mixture) and soot formation chemistry may result in different emissions based on the soot formation pathways followed.

An experimental approach was chosen for this work, but this had to be accomplished without the ability to visualize the combustion process. Instead a series of engine and rapid compression machine (RCM) experiments were designed to allow inferences of the in-cylinder soot formation processes based on the emissions response to changes in engine operating conditions or fuel compositions.

1.3.1 Engine Experiments

In order to measure engine exhaust concentrations of PM, a particulate sampling system was installed on a 2.0L, turobcharged, DISI engine. These experiments provided an opportunity to test the residual fuel effects hypothesis. Experiments were designed to allow some inference of the impacts of engine operating parameters on PM forma-

tion, with a focus on examinations of the effects of piston fuel films. The emissions response to spark timing, injection timing, coolant temperature, fuel volatility, fuel composition and residual oxygen content were examined.

These experiments were chosen since they provide some insight into the dynamics involved in the fuel-film soot generation. The size and location of fuel films are affected by these parameters, as are the conditions of the residual gases with which it is expected fuel arising from surface films must react.

1.3.2 Rapid Compression Machine Experiments

The rapid compression machine (RCM) offers an opportunity to observe PM formation under carefully-controlled mixture conditions. In an engine, it is difficult to know the mixture composition for an individual cycle, and, further to that, it was not possible to measure particulate matter emissions on a cycle-resolved basis. The RCM was equipped with optical access, so, using the light extinction technique, it was possible to measure the soot volume fraction for an individual combustion event. Granted, the combustion process is not representative of what takes place in an engine, but, it provides a useful tool for characterizing the sooting propensity of fuels. These experiments provided useful data for examining the fuel effects hypothesis.

The fuel/air mixture was controlled very precisely and the mixture of intert gases in the synthetic air could be chosen in order to provide known temperatures upon compression. Heaters in the RCM combustion chamber allowed specification of the initial temperatures, allowing measurements of soot formation threshold for a variety of ignition temperatures, pressures and fuel compositions.

Chapter 2

Experiments

This chapter provides a detailed description of the experiments conducted in this study. In the first section, the physical implementation of the experiments is detailed, while the second section outlines the procedures which were followed during the experiments.

2.1 Experimental Setup

In this section, details of the physical set-up and instrumentation of the experiments will be discussed. This includes both engine experiments as well as RCM experiments.

2.1.1 Engine Experiments

The bulk of the experiments used to test the hypotheses laid out in this thesis were based on measurements of engine emissions. A 2.0L, 4 cylinder, turbocharged, DISI engine was used. This engine, which has been used in a variety of vehicles including the Chevrolet Cobalt SS, the Pontiac Solsice GXP and the Saturn Sky Redline, is illustrated in figure 2-1. with a focus on the exhaust system.

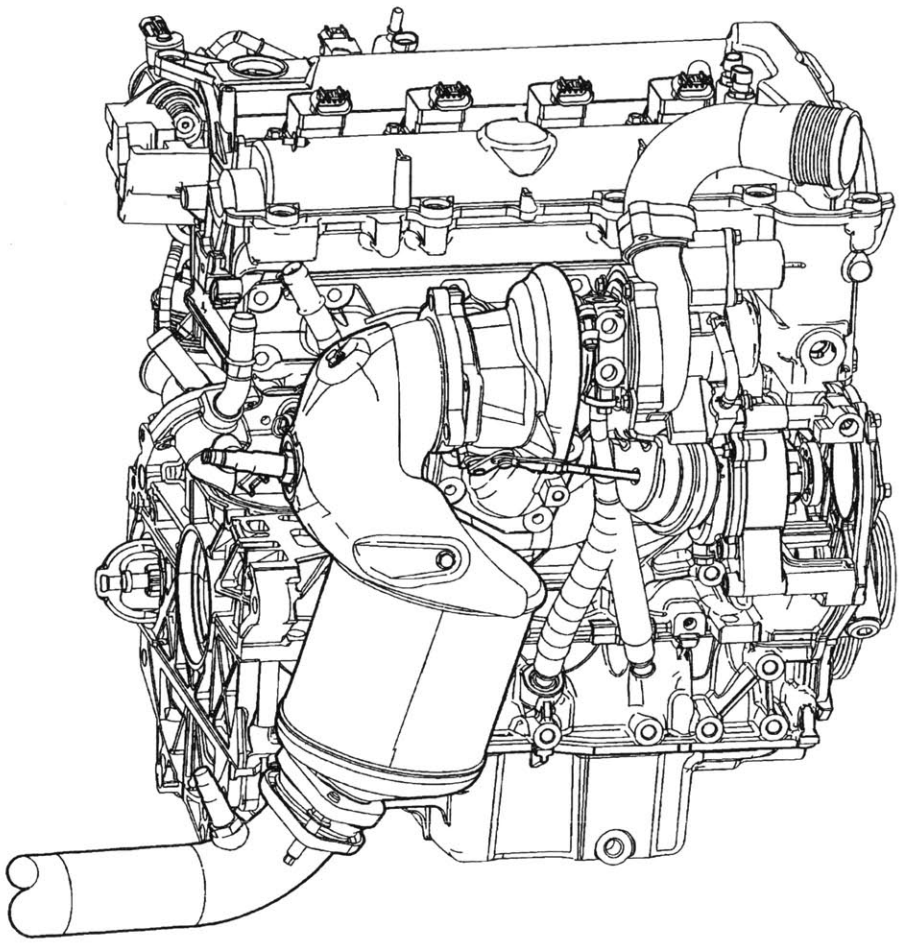

Figure 2-1: 2.0L, Turbocharged, Direct Injection Spark Ignition Engine ©GM Company.

Engine Specifications

The engine was manufactured by General Motors and is code-named LNF. It is a spray-guided engine, with side-mounted injectors, 4 valves per cylinder and centrally-mounted spark plugs. The engine is equipped with variable valve timing (VVT) for both the intake and exhaust valves. This engine was used for this study of PM as well as a parallel study of unburned hydrocarbon emissions. The basic specifications of this engine are shown in table 2.1.

As mentioned, this is engine was equipped with VVT. The VVT system uses vane-type hydraulic camshaft phasers and is capable of advancing the inlet valve timing by

Table 2.1: LNF engine layout and geometry information

Engine type	In-line 4 cylinder
Displacement [cc]	1998
Bore [mm]	86
Stroke [mm]	86
Wrist pin offset [mm]	0.8
Connecting rod [mm]	145.5
Compression ratio	9.2:1
Fuel system	Side-mounted gasoline direct injection
Valve configuration	16 valve DOHC, dual cam phaser 35.1 mm intake valve diameter 30.1 mm exhaust valve diameter
Max. torque	353 N·m at 2500 rpm
Max. power	194 kW at 5300 rpm

up to 50°CA and retarding the exhaust valve timing by up to 50°CA. The valvetrain specifications along with the VVT system capabilities are summarized in table 2.2.

Table 2.2: Basic valve timing and lift (cam phasers inactive)

		Opens	Max opening	Closes
Intake valve	Base timing	+11°ATDC$_{compr.}$	+126°ATDC$_{gas.ex.}$	+61°ABDC$_{compr.}$
	Max advance	-39°ATDC$_{compr.}$	+76°ATDC$_{gas.ex.}$	+11°ABDC$_{compr.}$
	Lift [mm]	0.25	10.3	0.25
Exhaust valve	Base timing	+52°BBDC$_{exp.}$	-125°ATDC$_{gas.ex.}$	-10°ATDC$_{compr.}$
	Max retard	+2°BBDC$_{exp.}$	-75°ATDC$_{gas.ex.}$	+40°ATDC$_{compr.}$
	Lift [mm]	0.25	10.3	0.25

Engine Controls, Installation and Modifications

The engine was installed on a test-bed, mated to a Froude-Consine AG-80 eddy current dynamometer and an electric motor via a driveshaft and compliant rubber coupling. The setup of the engine and instrumentation is illustrated schematically in figure 2-2. The coupling served to damp out fluctuations in engine torque. There was also an enlarged flywheel assembly used to minimize speed fluctuations. The test-bed motor was not powerful enough to start the engine, so the stock starter motor was

retained and was used to crank the engine before engaging the test-bed motor.

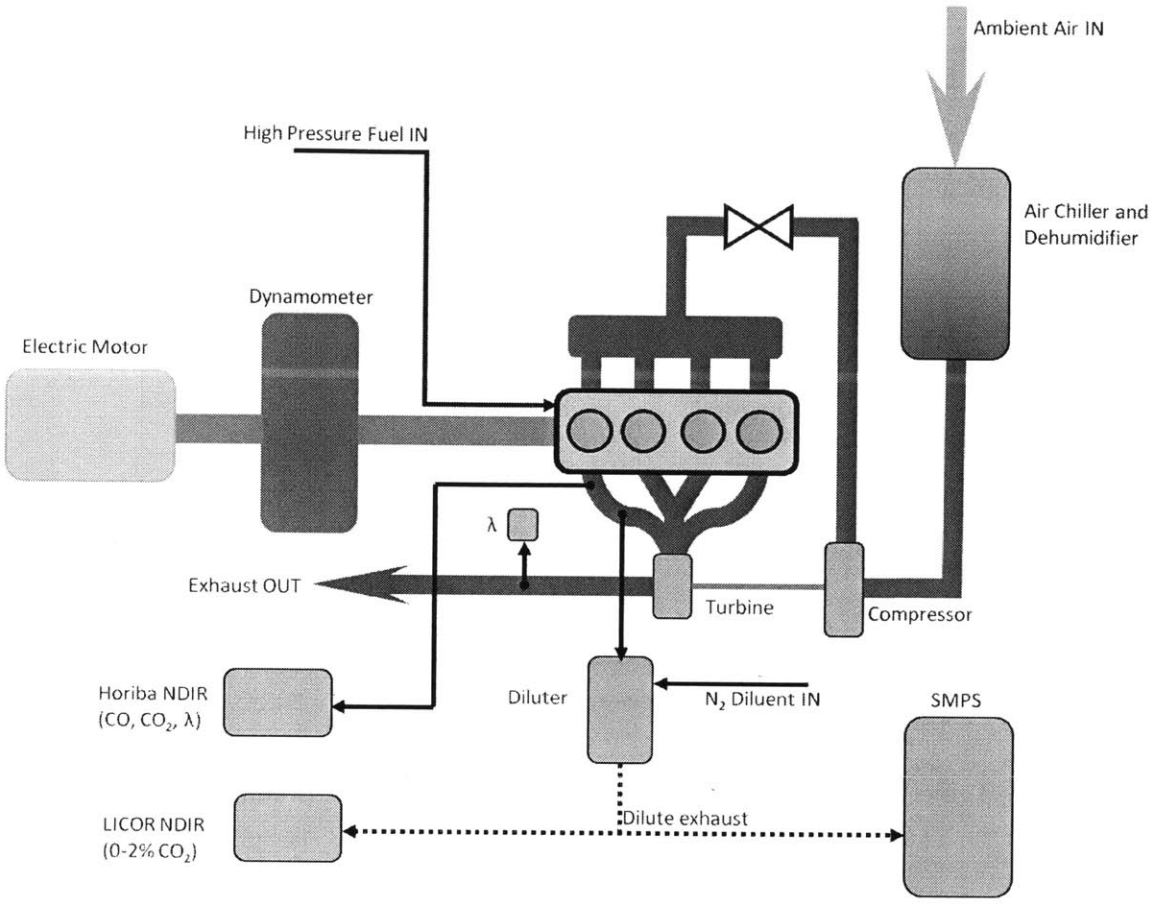

Figure 2-2: The engine is equipped with inlet air conditioning and instrumented with emissions analyzers.

Intake and Exhaust The intake and exhaust manifolds were modified by adding ports to allow pressure and temperature measurements. Also, the catalytic converter and housing were removed. This study was interested in PM formation and, as such, measured engine-out emissions, upstream of the usual catalyst location. Since the catalyst was not used, it was replaced with an empty housing in order to avoid damaging a catalyst due to prolonged operation at high exhaust temperatures.

Engine Control The engine was controlled electronically using a C-based code, developed at MIT. The control code operates on a pair of PCs. Using the "Master" computer, a variety of engine operating parameters were specified. These data were

sent to the "Slave" computer on which the control code was executed. The computer was equipped with digital-to-analogue and analogue-to-digital capabilities and, as such, is capable of reading engine sensor outputs and sending control signals. On the "Master" computer, spark timing, injection timing, injection duration, number of injections, spark dwell and valve timing were specified. The code then executes the control commands in an infinite loop following a set schedule which is timed using the crankshaft encoder signal. There are cut-off switches for the injector and spark signals, as well as a main kill switch which may be used to terminate the control loop. All four cylinders received the same control signals in this configuration, though it is possible to modify the code to support cylinder-to-cylinder differences.

Fuel Supply The engine's mechanical fuel pump was bypassed and replaced with a fuelling system consisting of a hydro-pneumatic accumulator, pressurized by a compressed nitrogen cylinder, feeding the fuel rail directly. The accumulator was filled by venting the pneumatic side and filling the fuel side using an automotive low-pressure electric fuel pump. This accumulator system allows constant fuel pressures regardless of engine speed or operating condition. The pressure could be specified between 30bar and 150bar. A chiller was used, along with a single pass counter-flow heat exchanger to control the fuel temperature.

The injectors were controlled using the aforementioned C code in tandem with a Siemens injector driver. This injector driver converts the injector control pulse from the slave computer into to the high peak current, low-hold current injection pulse used to actuate the fuel injectors. The high initial current enables fast injector opening. After the injector has begun to open, a lower current is used to hold it open.

Valve Timing The VVT system discussed earlier was also controlled using MIT's custom code. The lift profile and duration were constant. but, by varying the phaser position, the timing could be changed. The system is controlled by energizing a solenoid valve which controls the oil flow to the camshaft phasers. When not energized, the phasers remain locked in their parked position. When energized, the

solenoids allow a flow of oil, proportional to the energizing voltage, to flow into the phaser. This moves the vanes, resulting in relative motion between the rotor (attached to the camshaft) and the stator, which is driven by the timing chain.

Lambda The equivalence ratio was not controlled by a feedback loop, but was monitored using an ETAS LA-4 wideband UEGO oxygen sensor and chosen manually through specification of intake manifold pressure (via throttle position) and fuel injection rate (pulse width and pressure). The lambda sensor was mounted in the exhaust, downstream of the turbocharger in a custom housing that was built to replace the catalytic converter. The throttle position was controlled using a custom microcontroller host H-bridge PWM (pulse-width modulation) controller. This allowed the user to specify the throttle plate angle. It was also built with the capability to control the intake manifold absolute pressure (MAP) or the net Indicated Mean Effective Pressure (IMEP), though these capabilities were not employed in this study.

Cooling and Air Conditioning The engine was cooled using an electric chiller which circulated a 50/50 mixture of water and ethylene glycol through the engine's existing cooling circuit. The chiller was capable of controlling the coolant temperature over a wide range, including the ability to chill the coolant to below 0°C.

Alternatively, a coolant heating/cooling circuit was installed to allow high-temperature experiments with minimal warm-up time. This system consisted of a coolant storage vessel equipped with a heater as well as a liguid-to-liquid heat exchanger which was used for cooling. City water was used on the cold side of this heat exchanger. The solenoid valve controlling water flow as well as the heater were controlled using an Omega CN7800 digital PID controller.

The test bed was equipped with an oil cooling system, but it was not used during the experiments conducted for this project. Instead, the production oil cooler installed on the engine was used, with the coolant supplied from the main engine cooling circuit.

The engine was also equipped with an inlet air conditioning system consisting of a air-to-liquid intercooler, an electric chiller, a condensate trap and an air heater.

The electric chiller, equipped with a temperature controller, circulated chilled coolant through the intercooler circuit to cool the inlet air. The inlet air could be heated with the resistive heater (controlled by an Omega CN7800 digital PID controller).

The humidity could also be specified psychrometrically by first chilling the air, until it is at the desired saturation temperature, then heating the air to the desired temperature and relative humidity.

Engine Instrumentation

The engine was thoroughly instrumented for the purposes of engine control and combustion analysis. The instrumentation included a series of thermocouples, pressure transducers, exhaust gas analyzers and a crankshaft position encoder. Data from most of these instruments were collected using a National Instruments data acquisition (DAQ) system along with National Instruments LabView software. Those instruments connected to the DAQ are summarized in table 2.3.

Table 2.3: DAQ sensor details

Crankshaft position	BEI encoder, 360° per rev.
Cylinder pressure	Kistler 6125A sensor, Kistler 5010b charge amplifier
Intake pressure (MAP)	Honeywell SA-001-BAC1DE sensor
Exhaust pressure	OMEGA PX209-030A5V sensor
Fuel pressure	OMEGA PX309-3KG5V pressure transducer
Intake cam timing	OEM intake cam sensor
Exhaust cam timing	OEM intake cam sensor
Temperature	K-type thermocouples
Air-fuel ratio	ETAS LA-4 Lambda Meter
Exhaust composotion	Horiba MEXA-554JU and Horiba MEXA-584L

Crankshaft Position The crankshaft position is measured using the optical encoder which is connected to front of the crankshaft. The encoder's bottom dead centre (BDC) signal was aligned with that of cylinder #4 on the engine using an AVL-428 capacitive piston position sensor.

Pressure Measurements The pressure of cylinder #4 was measured using a Kistler 6125A pressure transducer. The signal was routed through a type 5010b

charge amplifier before being recorded by the DAQ system. To minimize the effects of thermal shock caused by the flame, the transducer is fitted with a flame arrestor. This transducer and charge amplifier combination experiences an offset drift, requiring the signal to be pegged to a value provided from another pressure measurement. In this case, the intake pressure was used for pegging. The pegging routine is completed in the LabView software and is detailed in [79].

The intake manifold absolute pressure (MAP) sensor was located in the intake runner for cylinder #4, approximately 5cm upstream of the port. Usually, the MAP would be measured in the intake plenum, but, for the pegging purposes mentioned above, this location provided a good compromise of MAP measurement and utility in pegging the cylinder pressure to the intake runner pressure at BDC. The exhaust manifold pressure was measured in the runner of cylinder #4, approximately 8cm downstream of the exhaust port. The fuel pressure sensor was located in the fuel supply line, upstream of the fuel rail.

Cam Timing The intake and exhaust cam timing were measured using the production Hall-effect sensors mounted at the rear of the camshafts.

Temperatures A number of K-type thermocouples were mounted on the engine. These included three thermocouples in the intake. One was upstream of the compressor, but downstream of the inlet air heater, another was downstream of the compressor and the third was in the intake runner for cylinder #4. There were also three thermocouples mounted in the engine cooling circuit. One was at the coolant inlet to the engine, one was at the coolant outlet and the third was mounted in the heated coolant reservoir. The exhaust was fitted with a total of four thermocouples. One was in the exhaust runner of cylinder #4, approximately 8cm from the exhaust port. This thermocouple was equipped with an aspirated radiation shield in an attempt to measure accurate exhaust thermal enthalpy data [80]. The other three were mounted downstream of the turbine and were not equipped with radiation shields, so for high temperatures (above 700°C) some error (up to 50°C)is expected in the temperature

measurement. One of these was located close to the turbine outlet, one was mounted upstream of the production catalyst location and the third was mounted downstream of the catalyst location. The fuel inlet temperature was measured with a thermocouple mounted upstream of the fuel rail and the lubricating oil temperature was measured using thermocouples mounted at the inlet and outlet of the oil cooling circuit.

Air and Fuel Flowrates The inlet airflow rate was measured using an EPI Flow thermal air flow meter (model number 8716-MPNH-SSS-133-AC115-AIR). This flow meter is mounted horizontally upstream of the inlet air conditioning system.

The fuel system is not equipped with a flowmeter, but, instead, the mass per injection was measured against injection pulsewidth signal to provide a calibration allowing the fuel flow rate to be calculated. These calibration data are found in Appendix A.

The air/fuel ratio can, theoretically, be calculated using the airflow and fuel flow measurements, but, due to uncertainties over the amount of fuel contributing to oil dilution (oil dilution has been observed), the air/fuel ratio was instead measured using a lambda sensor.

Lambda and Exhaust Gas Analysis The air/fuel ratio was measured using an ETAS LA-4 UEGO sensor. The catalyst housing, where it would normally be mounted was replaced by a hollow housing, but an attempt was made to locate the UEGO sensor close to the stock location. The sensor was located downstream of the turbocharger, and thus measured the average equivalence ratio across all cylinders.

It was noted during experiments that there were significant cylinder to cylinder variations in equivalence ratio (cylinder #4 ran substantially more rich than the average). In situations where the equivalence ratio for cylinder #4 was important, the Horiba gas analyzer could be used. Using the CO and CO_2 measurements and given the fuel properties, it performed an internal carbon balance to calculate lambda. The sampling line was located in the same position as the exhaust manifold pressure

transducer. Initially, a MEXA-554JU analyzer was used. This was a Non-Dispersive Infrared (NDIR) analyzer which measured CO, CO_2, unburned hydrocarbons (HC) and O_2 concentrations. This analyzer was damaged and was replaced by a Horiba MEXA-584L analyzer. This analyzer was also an NDIR analyzer, but it was not equipped with an O_2 measurement cell.

The Horiba analyzers measure emissions on a dry basis. In order to dehumidify the exhaust gases, a condensate trap was included upstream of the NDIR. The condensate trap consists of coiled copper tubing submerged in an ice reservoir. The condensate and exhaust gases then flow into a pyrex flask. The gases are sampled by the NDIR from a position near the top of this flask, while the condensate collects in the bottom of the flask. The sample is also drawn through a Drierite desiccant.

Particulate Instrumentation

In addition to those instruments discussed in the previous section, series of instruments were installed to measure PM emissions. These included a custom dilution system, a Scanning Mobility Particle Sizer (SMPS) and two NDIR sensors measuring CO_2 emissions for dilution purposes. The exhaust sample for particulate analysis was collected in the exhaust runner of cylinder #4, approximately 10cm from the exhaust port.

SMPS For this study, a TSI model 3934 SMPS was used. The SMPS system consists of a model 3071A Electrostatic Classifier and a model 3010 Condensation Particle Counter (CPC). The Electrostatic Classifier operates by first imparting a known charge distribution on the aerosol sample using a bi-polar charger, which contains Kr^{85}. Then, the particles are separated based on mobility. In the classifier, there is a Differential Mobility Analyzer (DMA) column. The DMA consists of a rod and an outer tube, between which there is a voltage difference. The aerosol sample is admitted along the inner diameter of the tube, separated from the rod by a sheath flow of filtered air. The flow velocities of the aerosol sample and the sheath flow are equalized using a series of flowmeters and needle valves. When a voltage difference is

applied between the rod and the inner tube, particle paths will be deflected toward the rod depending on the charge which they acquired in the neturalizer. There is a slot in the bottom of the inner tube which feeds an outlet tube. Those particles which are deflected such that they enter a flowstream leaving the DMA through the slot in the inner rod will proceed to enter the CPC as a monodisperse aerosol flow. This is shown in figure 2-3. In the CPC, the particle-laden flow passes over a bath of n-butanol, which condenses onto the particles, increasing their size such that they can be counted optically (see figure 2-4). The voltage difference is scanned such that the particle sizes sampled will change to span the entire range of interest. The particles are counted in discrete bins of particles sizes. The SMPS functions (DMA voltage scanning and CPC number data collection) are managed using TSI's Scanning Mobility Particle Sizer software, version 3.2, which communicates with the SMPS via a serial connection.

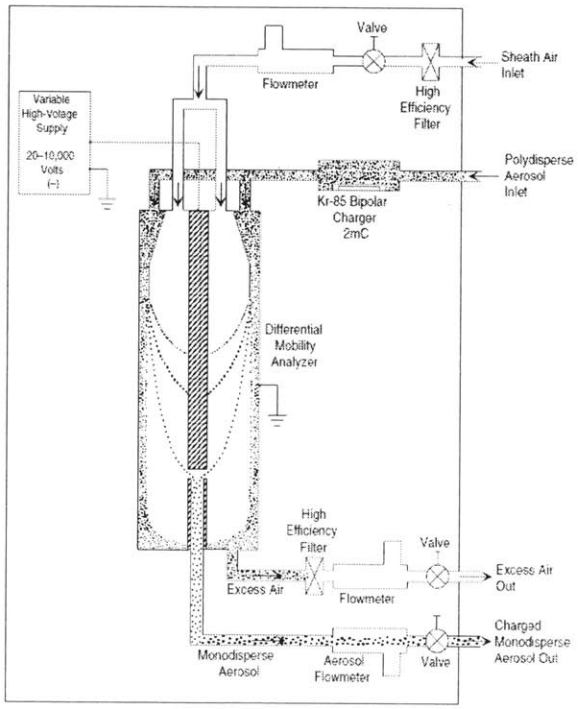

Figure 2-3: The Operation of the TSI Model 3071A Electrostatic Classifier [81]

This SMPS model was designed primarily for use in sampling atmospheric aerosols, but it has been widely used in engine emissions research [83–87]. It is not suitable

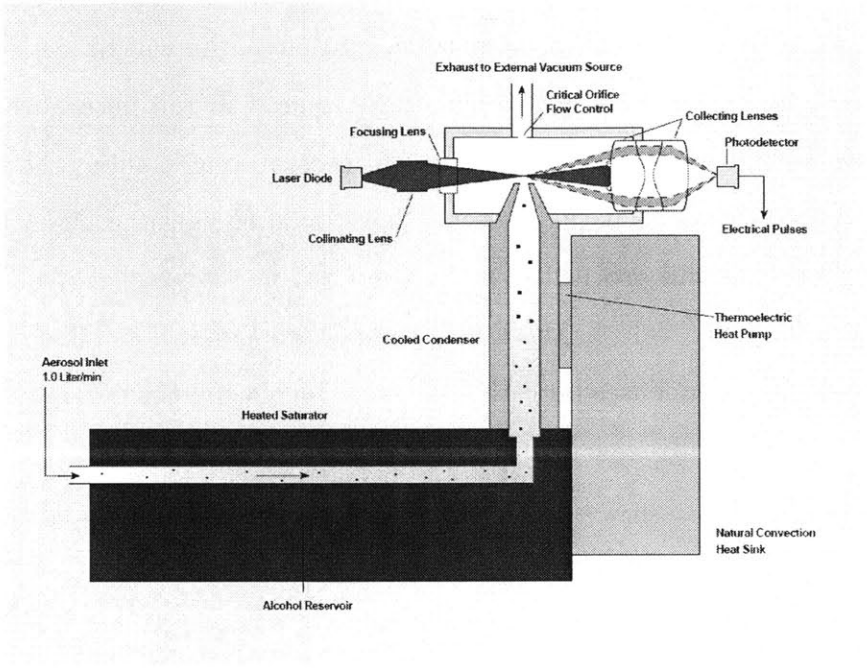

Figure 2-4: The Operation of the TSI Model 3010 Condensation Particle Counter [82]

for engine-out emissions, but with proper dilution, it can effectively measure engine exhaust PM emissions. Perhaps the largest compromise that is made is that the measurements are limited to steady-state experiments due to the long sampling intervals (in this case, 90 seconds) needed to complete a full scan.

The SMPS is configured with a 0.0457cm diameter orifice in the impactor assembly and the flowrate is set at 0.7slpm. This results in a size measurement range of 9.31 to 365nm. The SMPS is operated in the under-pressure mode, meaning that the sample is drawn through the system by a vacuum pump rather than being driven through by a pressure differential.

Dilution The diluter is an integral part of the PM sampling system. Broadly speaking, exhaust dilution serves three roles. The first is to reduce the exhaust concentration to a level that can be measured by the instrumentation. The second is to keep the sample sufficiently dilute to prevent agglomeration. The third is to attempt to replicate the processes undergone by tailpipe emissions as they are mixed with the atmosphere. This is important because engine-out emissions are not what

affects the environment or human health. It is, instead those emissions which have dispersed in the atmosphere which affect air quality and health.

In this study, since the exhaust was sampled upstream of the turbocharger, two additional concerns had to be addressed when designing a dilution system. The first is that the SMPS is designed to accomodate samples at atmospheric pressure. Because the sample is drawn upstream of the turbocharger, the sample pressure is slightly above atmospheric. This was especially true under exceptionally inefficient operating condtions (e.g. a very late spark requires relatively high fuelling and airflow rates to maintain the desired load). Thus, the dilution system had to be designed to minimize the effects of the elevated exhaust pressure on the analyzer. The second concern was the pressure pulses that are encountered when sampling in an exhaust runner. Typically, exhaust is sampled much farther downstream in the exhaust system, where the pulses from several cylinders effectively average to a steady pressure. In this case, however, since engine out exhaust was desired, it was necessary to sample upstream of the turbocharger, where pressure pulses are present. It was necessary for the dilution system to dampen the effects of these pressure pulses, since the oscillatory nature of flow in this case may not allow the flow within the DMA to remain laminar. The flow through the DMA must remain laminar in order for particles to be properly classified according to diameter.

In order to accomplish the dilution task while accounting for these concerns, a new dilution system was designed for this project. It consists of a heated aluminium block containing two 0.020"x2" orifice tubes and a sampling chamber as shown in figure 2-5. The first orifice tube is mounted between the exhaust manifold and the sampling chamber. This orifice was sized to dampen the pressure pulsations while allowing adequate flow for the sampling devices. The sampling chamber is connected to a large-diameter chamber open to atmosphere. This ensures that the sample drawn into the dilution tube is always at atmospheric pressure. The constant outward flow of exhaust (at a larger volume rate than is sampled) ensures there is no back-flow of air into the sampling chamber.

The second orifice was located between the sampling chamber and the dilution

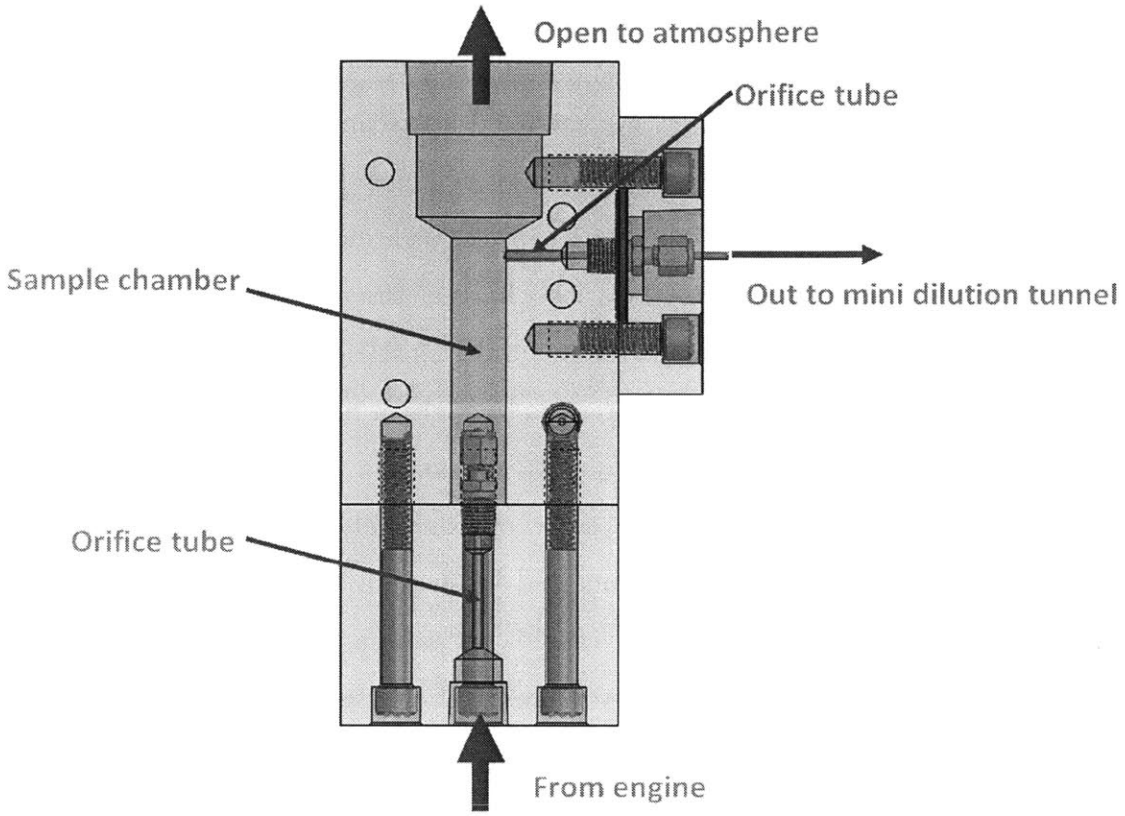

Figure 2-5: The dilution block provides a sampling location at constant atmospheric pressure.

tube. A vacuum supply is connected to the opposite end of the dilution tube which creates a slight vacuum, drawing a sample into the dilution tube. The diluent (nitrogen) is injected into the tube perpendicular to the exhaust flow. The length of the dilution tube was chosen to permit adequate mixing of the exhaust sample with the dilution gas. Nitrogen was chosen to eliminate any oxidation reactions, but air or another diluent could also be used. At the end of the dilution tube, the sample is drawn for the SMPS measurement. The vacuum level in the dilution tube is controlled by way of a needle valve which throttles a flow of air into the vacuum pump. Closing the valve permits less ambient air to be drawn by the pump, causing a decreased pressure in the dilution tube. The diluter assembly is shown in figure 2-6.

In order to replicate the action of a thermodenuder, the use of which is specified in the Particle Measurement Programme (PMP) protocol [88], the dilution block is fitted

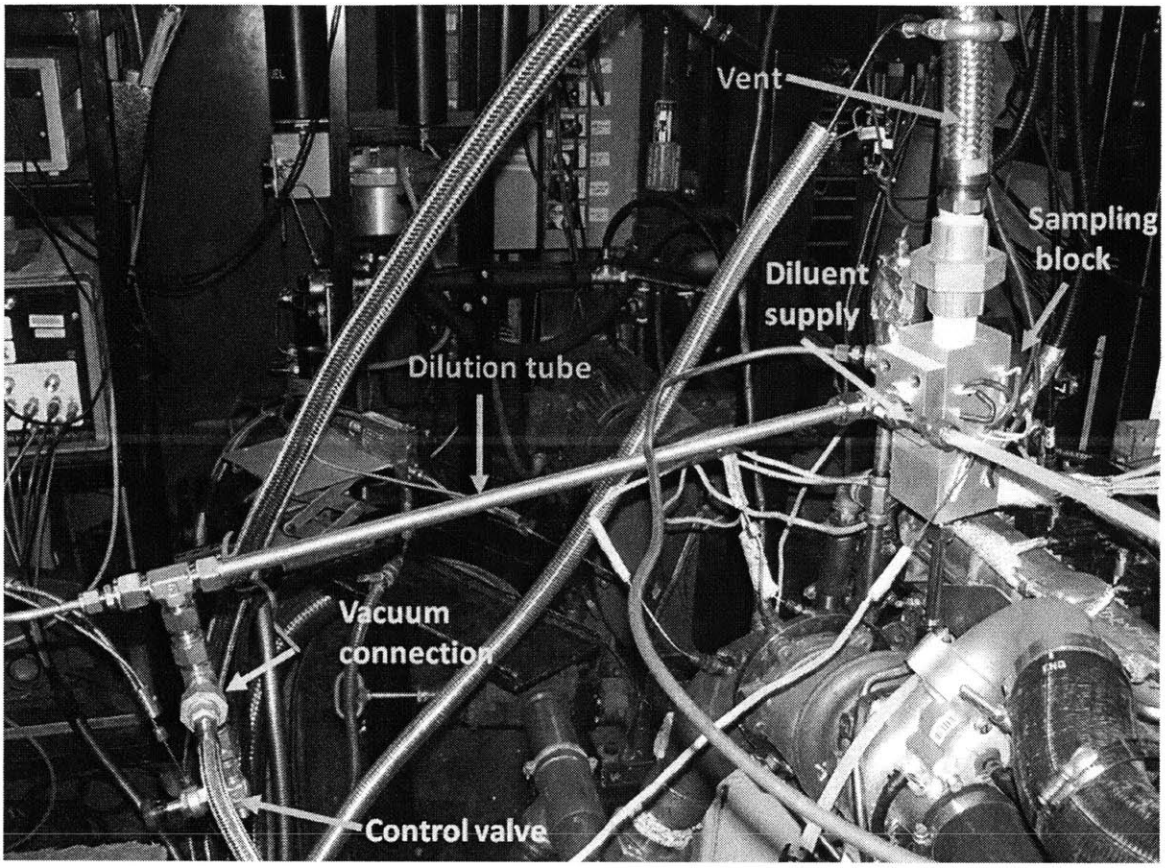

Figure 2-6: Custom dilution system.

with 6 cartridge heaters controlled by a PID controller. These are used to heat the block to a temperature of 200°C. This accomplishes two things. Firstly, the elevated surface temperatures in the sampling block help to minimize thermophoretic losses in the orifice tubes. Secondly, the high temperature prevented volatile hydrocarbons from condensing before dilution. After dilution, the hydrocarbon concentrations were likely too low to permit nucleation. Few nucleation mode particles were observed in the PM data.

In order to quantify the dilution ratio, a differential measurement of CO_2 concentrations is used. The upstream (undiluted) concentration is measured using the Horiba NDIR gas analyzer. The Horiba NDIR measures CO_2 concentrations between 0 and 20%vol. The downstream (diluted) CO_2 concentration is measured using a Li-Cor LI-820 NDIR CO_2 analyzer, which measures over the range of 0-20,000ppm with an error of less than 3% of the reading. The diluted sample is drawn approximately

5cm upstream of the SMPS inlet (impactor). To allow simple calculations, this measurement is also on a dry basis, being dehumidified using the same condensate trap setup as the Horiba NDIR.

2.1.2 Rapid Compression Machine

A rapid compression machine is a device commonly used to study fuel ignition characteristics under conditions approximating the pre-mixed combustion phase in a Diesel engine [89]. It works by compressing a uniform mixture of fuel and oxidant in a combustion chamber. The rapid rise in temperature and pressure associated with compression causes the mixture to autoignite. An RCM is a single-stroke device which provides a force balancing the combustion pressure in order to enable a constant volume combustion event.

RCM Design MIT's RCM #1 was used in this study. It consists of a combustion cylinder, a hydraulic cylinder, a pneumatic cylinder and a compressed air tank (see figure 2-7). The compressed air tank provides the driving pressure for the pneumatic cylinder which powers the piston assembly. The ball valve is in place to allow the compressed air tank to be pressurized without pressurizing the pneumatic cylinder. The hydraulic piston is equipped with a face seal, which, when sealed allows the hydraulic cylinder to be pressurized, resisting the force from the pneumatic cylinder. This serves as a lock on the piston assembly. The hydraulic cylinder is filled with silicone oil. Since the compressibility of this fluid is very low, when the gas pressure used to pressurize the hydraulic cylinder is released, the hydraulic pressure releases nearly instantly, allowing the pneumatic pressure to force the piston assembly forward. This compresses the air/fuel mixture in the combustion cylinder, resulting in the autoignition of that mixture. The design of this RCM is detailed in the doctoral thesis of Ioannis Kitsopanidis [89]. The only changes made to this design was the addition of a second seal on the combustion piston, and the replacement of the 1/4" capscrews on the pneumatic shaft with 3/8" capscrews.

To measure the cylinder pressure during the combustion event, the RCM com-

bustion chamber is equipped with a Kistler 6125A pressure transducer, connected to the National Instruments PCI-6025E data acquisition card through a Kistler type 5010 charge amplifier and a National Instruments BNC 2090 terminal block. The transducer is oriented perpenicular to the axis of the RCM.

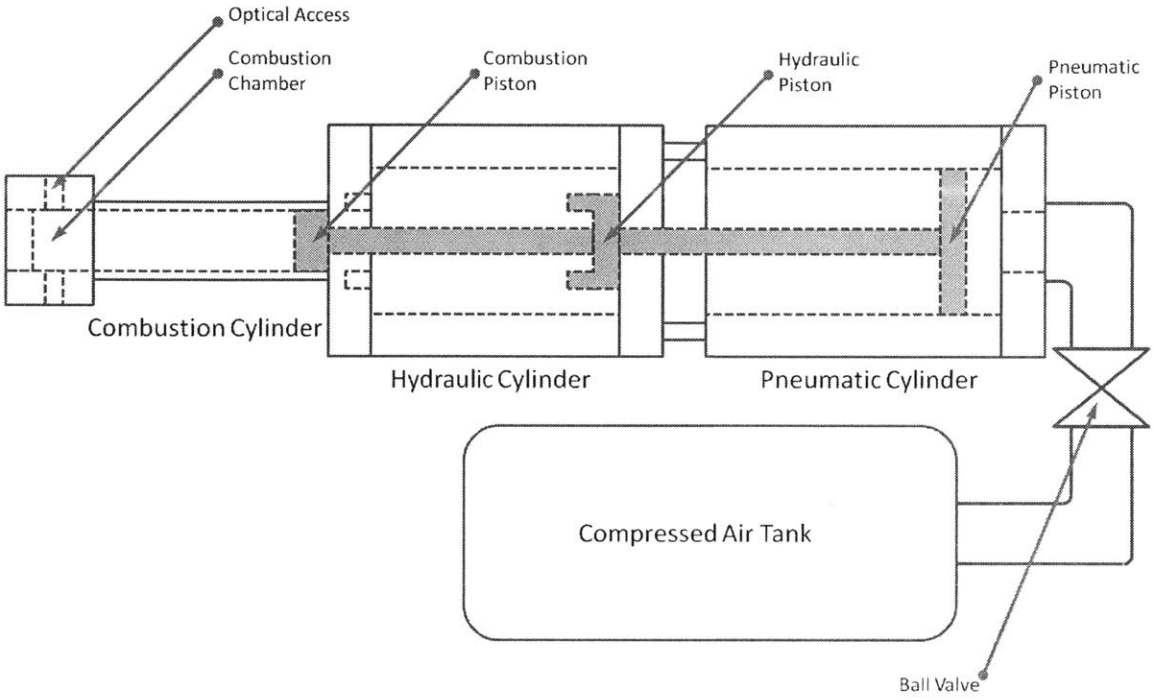

Figure 2-7: The MIT Rapid Compression Machine

Soot Measurement Optical access windows allow the Light Extinction Method to be used to measure the soot formation in the combustion chamber. In this implementation, the light source is a 30mW He-Ne LASER with a wavelength of 632.8nm. The LASER beam is directed through the combustion chamber into an integrating sphere, which transforms the concentrated LASER light into a diffuse light source, the intensity of which is then measured using a photomultiplier tube. The photomultiplier tube is equipped with a line filter, which seeks to minimize the transmission of light at wavelengths other than 632.8nm. It is also equipped with a collimator, which serves to keep any light passing through the line filter perpendicular to the filter face, since its effectiveness decreases sharply as the light beams stray from perpendicular. The LASER measurement system layout is shown in figure 2-8.

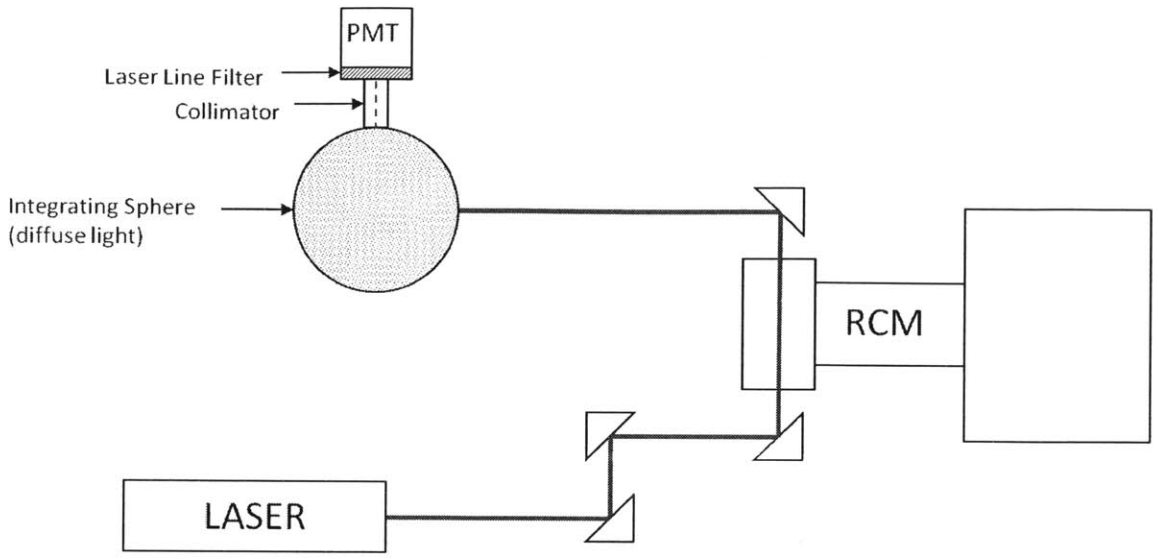

Figure 2-8: The MIT Rapid Compression Machine Light Extinction Method Apparatus

Mixture Preparation In addition to the RCM is a mixture preparation apparatus which is used to prepare a homogeneous mixture of fuel, oxidizer and inert gases. The apparatus consists of a pressure vessel fitted with a vacuum septum, three metering valves, two "high" pressure transducers (1000 Torr), one "low" pressure transducer (100 Torr), a mixing fan (driven through a magnetic vacuum pass-through), an array of heaters and a pressure-relief valve. The vessel is fitted to a vacuum pump. The low pressure transducer is used measure the vacuum level in the vessel. One of the high pressure transducers is used to measure the partial pressures of gases in the mixing process and the other is used to measure the pressure in the feed line to the RCM combustion chamber. Liquid fuel is injected through the septum. The fuel vapourizes because the vessel is under vacuum and heated. This mixture preparation system is a tremendous improvement over the system used in previous work at MIT [89] as it allows not only easier mixture preparation, but also a larger volume of mixture to be prepared at one time, allowing the RCM to be fired several times with a consistent mixture.

2.2 Experimental Procedures

This section outlines the procedures that are followed to collect data during engine and RCM experimentation. Data processing will also be discussed.

2.2.1 Engine Experiments

Engine experiments yielded the bulk of the data used in this project. This section describes the experimental and analytical procedures followed during the course of this study.

Engine and Instrumentation Preparations

Engine Before beginning experiments, the engine must be chilled to operating temperature and fuelled. To bring the engine to operating temperature, first the city water valve is opened until enough water pressure (approximately 25psi) is available. The laboratory water recirculating pump should be enabled during all experiments. Then the large chiller is powered by first turning on the circulating pump, then the compressor. When running chilled experiments, the chiller was allowed to run for approximately 1 hour to allow the engine to reach operating temperature. When experiments are performed on a warm engine, using the heated coolant system, the coolant was recirculated for less time before firing and the engine was then allowed to reach its operating temperature while firing. If the air chiller is being used, this chiller should also be powered in order to cool the intercooler body.

To fill the fuel delivery system, the "pressure cooker" fuel tank is first filled and then the lid is sealed. With the accumulator pneumatic bypass valve opened, the low pressure fuel pump is powered with the valve assembly directing fuel to the hydraulic side of the accumulator. When the accumulator is full, the pressure in the fuel delivery system will rise. This can be seen on the pressure regulator pressure gauge. At this time, the pump may be turned off, and the fuel 3-way directional valve may be turned to supply the engine. Finally, the compressed gas bypass valve is closed and the fuel accumulator is pressurized by opening the compressed nitrogen

valve. The fuel pressure is specified using the tank-mounted regulator.

The fuel system chiller should be powered during the warm-up period to allow the fuel system components to be brought to operating temperature before starting the engine.

Instrumentation A number of sensors and analyzers must be warmed up, configured or calibrated before beginning an experiment. The following devices require some action before beginning experiments:

- UEGO Sensor
- Horiba NDIR exhaust gas analyzer
- Li-Cor NDIR CO_2 analyzer
- Exhaust dilution system
- Scanning Mobility Particle Sizer
- Data acquisition system
- Cylinder pressure transducer

The UEGO sensor has to be configured for the fuel composition. The H/C ratio, C/O ratio, stoichiometric air/fuel ratio and H_2O content are input. These values are needed for the wideband action of the sensor. The UEGO should be powered before beginning experiments.

The Horiba and Li-Cor NDIR analyzers must be warmed-up and calibrated before experiments may begin. The Horiba analyzer performs a 5-minute warm-up routine following application of power. The Li-Cor analyzer requires approximately 30 minutes of warm-up time. For both anlayzers, during the warm-up period and for approximately one half-hour following, dry air is used to purge the detector before calibration. The air is dried using the condensate trap which should be filled with ice upon powering the NDIR analyzers.

Before calibration, the Horiba analyzer is first leak-checked using the internal function. To do so, first close the 3-way valve at the inlet of the condenser coil and then enable the leak-check in the calibration menu. If it passes, continue with the

calibration following the instructions provided on-screen. Air is used as the zero gas, and a mixture of 1600ppm propane, 1.9% CO and 13% CO_2 with a nitrogen balance is used as the span gas. The Li-cor analyzer is calibrated using nitrogen as the zero gas and a custom mixture of 15000ppm CO_2 in a nitrogen balance is used as the span gas. This calibration is performed by connecting the calibration gases to the ambient side of the 3-way valve on the Li-cor sampling line. The gases are then admitted to the analyzer and the needle valve is used to ensure the flowrate is below 1 slpm.

The dilution system and SMPS both require approximately one hour to warm to operating temperature. During the warm-up phase, the CPC should be inspected to ensure an adequate fluid (n-butanol) level. Also, the SMPS inlet impactor surface must be cleaned and a thin film of vacuum grease applied to the surface (this helps to trap large particles which strike the impactor, preventing them from being re-entrained in the flow). During the warm-up period, a flow of ambient air is allowed through the SMPS system, with no volage applied across the DMA.

To enable the data acquisition system, the test-cell power must be on, and the instrument power must be switched on at the front panel. Then the National Instruments SCXI DAQ chassis is turned on. The cylinder pressure transducer can be enabled by switching the charge amplifier to operate mode.

Starting the Engine

Once the engine and instrumentation are warmed-up and calibrated, the engine may be started. The procedure for starting the engine and preparing to collect data is outlined below:

1. Ensure that the front-panel and instrumentation circuits are powered.
2. Ensure that the cooling water is flowing and that the laboratory trench exhaust fan is running.
3. Apply power to the electric motor and motor controller by closing the breaker labelled "motor."
4. Apply power to the dynamometer controller.

5. Configure the Siemens injector driver for the appropriate operating pressure range.
6. On the Master computer, run the program Multi_06am.exe and specify the spark dwell, the ignition timing, the injector pulsewidth, the start of the first injection, the start of the second injection, the fraction of fuel injected in the first injection, the fraction of fuel injected during the second injection, the intake valve advance and the exhaust valve retard.
7. Turn on power to the throttle controller and ensure the throttle is wide-open.
8. Enable the starter motor.
9. Enable the test-bed electric motor.
10. Turn the key to crank the engine using the starter motor. When the starter motor is no longer audibly strained (at a speed of approximately 300rpm), release the key. The test-bed motor should continue bringing the engine up to speed.
11. Set the electric motor speed to be slightly slower than the intended operating speed (e.g. in the case of a 1200rpm operating case, the electric motor is set to run at approximately 1180rpm). This ensures that the motor is not over-loaded when the dynamometer is engaged.
12. Start the LabView DAQ interface.
13. With the engine motoring, ensure the cylinder pressure trace is correct. If it is out of phase, flip the phase switch which is located on the platform above the engine.
14. With the engine motoring, check the oil pressure and perform a walk-through in the test cell to ensure normal operation.
15. With the engine motoring, begin the dilution gas flow by opening the nitrogen cylinder valve and turning on the mass-flow controller.
16. Ensure the engine controller is powered and that the "kill switch" is in the "on" position.
17. Ensure the fuel injector switch is in the "off" position.

18. Engage the dynamometer clutch.
19. On the Slave computer, run the program Multi_06.exe.
20. Set the throttle position to achieve the appropriate MAP value for the desired start-up fuelling.
21. Move the injector switch to the "on" position.
22. Adjust the throttle position to ensure the equivalence ratio is stoichiometric.
23. Turn directional 3-way valves on the NDIR analyzers to sample from the engine.
24. Fine tune the operating parameters to reach the desired operating condition.
25. Allow the engine to run for approximately 15 minutes to reach a steady-state.

Setting the Dilution Ratio

After the engine has been allowed to reach steady-state, then emissions and combustion data may be collected, but first, in order collect PM data, the dilution ratio must be set. This should be done while the engine is running at the desired operating point. With all sampling equipment connected to the dilution system, begin with the vacuum bypass valve open $10^3/_4$ turns and a diluent flow of at least 5 slpm. Observe the Li-Cor NDIR CO_2 concentration and wait until it reaches a steady-state. At this point, adjust the diluent flowrate to achieve the desired dilution ratio.

Once the dilution ratio is specified, the SMPS flowrates must be set according to the procedures laid out in the operating manual [81]. The process of setting the SMPS flowrates and the dilution ratio may include some fine-tuning.

Collecting Data

Data are collected using 3 parallel data acquisition systems. Engine and combustion data are collected using the National Instruments DAQ in conjunction with LabView software, the PM data are collected using a serial connection to a desktop computer and TSI's SMPS software and the diluted CO_2 concentration data are collected with a serial connection to the same computer, but using Li-Cor's sampling software.

To collect PM data, the SMPS is set-up to run a 60 second upward scan and

a 30 second downward scan. Before beginning a scan, the Li-Cor NDIR sampling sofware should be run to collect data continuously. Then 3 consecutive SMPS scans are completed at each operating point.

Also, at the beginning of each scan the DAQ is triggered to collect engine and combustion data. The quantity and sampling frequencies of the engine data collected are described in table 2.4.

Table 2.4: Typical data collection quantity and frequency

Signal	**Collection Frequency**	**Amount collected**
Cylinder pressure, intake manifold pressure, exhaust manifold pressure	1/[CA]	100 consecutive cycles
Ignition, start of injection, camshaft position	1/[CA]	10 consecutive cycles
Engine speed, equivalence ratio, NDIR emissions, air flow meter, oil pressure, fuel pressure	1/[cycle]	5 consecutive cycles
Temperatures (13 ch.)	1/[cycle]	5 cycles
Injector pulse width	100 [kHz]	3.0 [s]
Transient temperatures	1 [Hz]	User set

Data Processing Post-processing of PM data is relatively straightforward. The size and number data are corrected for dilution and then the three runs are averaged. The dilution ratio is determined by comparing the upstream CO_2 concentration measured with the Horiba NDIR to the downstream CO_2 concentration measured with the Li-Cor NDIR analyzer. The upstream CO_2 value is taken from the DAQ data matching the corresponding SMPS scan. The downstream value was obtained by finding the CO_2 concentration recorded at the time corresponding to the beginning of the corresponding SMPS scan.

Processing of the engine and combustion data is far more complex. A MATLAB code developed for the processing of these data (with minor modifications) was used. Details of the post processing program are found in the PhD thesis of Kevin Cedrone [79].

Experimental Descriptions

This section will describe the details of the experiments that were conducted for this project. These experiments included spark sweeps, injection timing sweeps, dual injection timing sweeps, investigations of fuel composition and fuel volatility, engine speed investigations and an investigation of the impact of burned gas oxygen concentrations. All of these experiments are focused on examining the formation of PM in-cylinder during the cold-idle engine operating condition. The basic cold-idle operating condition is defined in table 2.5. This operating point was defined in collaboration with industrial sponsors and was designed to represent a realistic cold-idle period operation.

Table 2.5: Cold-idle operating point specification

Engine parameter	**Value**	**Units**
Engine Speed	1200	rpm
NIMEP	2	bar
Spark	Varied	CAD $ATDC_{compr.}$
Fuel/Air Equiv. Ratio (Φ)	1	
Dilution External EGR	0	%
Coolant/Oil Temperature	20	°C
Fuel Inj. Timing	Production intent	CAD $ATDC_{gasex.}$
Fuel Inj. Pressure	5.0	MPa
Ambient pressure	100	kPa
Intake Air Temperature	20	°C
Intake Air Vapour Pressure	1	kPa
Exhaust Back Pressure	0.5	kPa

It was discovered early in the course of experiments that there are sinificant cylinder to cylinder variations in equivalence ratio, with cylinder #4 running significantly more rich than the global equivalence ratio suggested by the UEGO sensor. For this reason, in all of the experiments described below, the equivalence ratio is specified using the lambda value calculated through a carbon balance done by the Horiba NDIR. Due to the sampling location, this value offers an estimate of the local equivalence ratio in cylinder #4.

Spark sweep The spark sweep was used to gain some understanding of the impact of mixing time, combustion phasing and in-cylinder temperatures on the formation and emission of PM. The experiment was completed beginning with the default cold idle condition shown in table 2.5 with a spark timing of 25°CA $BTDC_{comp}$. From this point, the spark was gradually retarded until reaching a limit of engine stability beyond which it was not possible to ensure 3 SMPS scans could be completed without the engine stalling.

At each new spark timing point, the fuelling rate and throttle position were adjusted to maintain a constant load of 2 bar net IMEP as well as a constant equivalence ratio. Also, the dilution ratio was adjusted to maintain a roughly constant value.

Injection timing investigation The injection timing sweep was used to gain some insight into the effects of fuel impingement on various cylinder surfaces. In this case, the spark timing was held constant at 25°CA $BTDC_{comp}$ while the start of injection timing for a single injection was varied between TDC_{intake} and the limit of engine stability in increments of 20°CA. At each operating point, the injector pulsewidth and throttle position were adjusted to maintain a constant load of 2 bar net IMEP as well as a constant equivalence ratio. The dilution ratio was also adjusted to maintain a constant value.

Dual injection timing investigation The sweep of second injection timing was used to further gain insight into the effects of fuel impingement on in-cylinder surfaces, wetting of the piston crown, in particular. The spark timing was kept constant at 11°CA $ATDC_{comp}$. This was the latest stable spark timing studied in the single injection spark sweep and it was chosen in order to allow some insight into the interactions between the fuel spray and the piston crown bowl, which is designed to direct the fuel spray toward the spark plug, creating a slightly rich mixture near the spark plug which enables improved stability at late spark timings. The first injection timing was set at 80°CA $ATDC_{intake}$, which is an injection timing that was observed to produce little soot in the single injection timing sweep. The second injection was then

varied between 200°CA $ATDC_{intake}$ and 340°CA $ATDC_{intake}$. Again, fuelling and throttle position were adjusted to maintain a constant load and equivalence ratio. The dilution ratio was adjusted as needed to keep it roughly constant.

Fuel composition investigation For the study of fuel composition, the spark sweep, injection timing sweep and second injection timing sweep were conducted as described in the previous paragraphs. In order to use different fuels, however, the fuelling system had to be drained and purged, the fuel characteristics had to be changed in the ETAS UEGO sensor controller as well as in the Horiba NDIR and, of course, the fuels had to be prepared.

The fuelling system is drained by applying a vacuum to the drain port on the fuel system valve panel. The vacuum is drawn until the flow ceases, at which time the fuel filter is replaced with a clean filter (a different filter is used for each fuel) and the fuel system is filled with the new fuel. Upon initial startup with the new fuel, the engine is allowed to run at a steady state until a change is seen in the lambda value reported by the UEGO sensor, indicating a change in the fuel composition being combusted. This is a signal that the old fuel has been purged from the system. At this time, experiments can proceed as usual.

The fuel mixtures are prepared by splash-blending. All fuels are blended on a volume basis, using the same Haltermann HF0 437 certification fuel as the base. For this study, mixtures of gasoline and ethanol were used to study the sensitivity to oxygenate/alcohol content, and gasoline and toluene were used to study the sensitivity to aromatic content.

Fuel volatility investigation In addition to the fuel studies discussed previously, an additional study was performed to examine the effects of fuel volatility more closely. In this case, an abridged version of the dual injection timing investigation was performed for a variety of mixtures of isooctane and isopentane. Isooctane served as the low-volatility fraction of the fuel while isopentane served as the high-volatility fraction. Pure isooctane as well as mixtures of 10%, 20%, 30% and 40% (by volume)

isopentane in isooctane were examined. The intent was to examine the impact of smaller fuel films present due to an increased volatile fraction. The load was kept constant at 2 bar net IMEP, and the tests were conducted at a stoichiometric equivalence ratio.

Engine speed investigation The engine speed variation experiment was performed to obtain a general understanding of the impact of in-cylinder mixing time on PM formation. The dual injection timing investigation was repeated at 1500rpm and 1800rpm, while maintaining the same load of 2 bar net IMEP. This is a low load for this engine speed, but it was chosen in an attempt to limit the fuelling increase that would be necessary were a more realistic load chosen. The fuelling rate is very important as it has a strong impact on the fuel impingement on cylinder surfaces. All of these experiments were conducted under stoichiometric conditions.

Burned gas oxygen content investigation Finally, the burned gas oxygen content investigation was performed to examine the impact of changing the end gas oxygen content on the growth and oxidation of PM in-cylinder. In order to examine this, the engine was operated at a steady gasoline fuelling rate, and the overall mixture was then enriched by adding propane to the intake manifold. The experiment was conducted in two different ways in an attempt to confirm the trends that were observed. In the first, the engine was first run at the standard cold-idle operating point and the mixture was then leaned-out by opening the throttle without changing the fuelling rate. The mixture was then enriched by propane addition in equivalence ratio increments of 0.05.

In the second method, the same initial point was chosen, but instead of first leaning-out the mixture, the propane was immediately used to enrich the mixture beginning from the stoichiometric case. This was repeated at spark timings of 25°CA $BTDC_{comp}$ and 11°CA $ATDC_{comp}$. In the early spark case, injection timings of 40°CA $ATDC_{intake}$ and 100°CA $ATDC_{intake}$ were considered, offering one highly sooting condition and one low sooting condition, respectively. At the late spark timing, a second

injection at 320°CA $ATDC_{intake}$ was studied to examine a highly-sooting condition with late fuel interaction with the piston. In these experiments, the engine load was permitted to float, instead keeping the throttle position and liquid fuelling rates constant.

Experimental Matrix

The series of experiments to be completed using the engine is summarized in table 2.6.

Table 2.6: Experimental matrix for engine-based experiments

	Spark Sweep	SOI Sweep	SOI_2 Sweep	Resid. O2	Speed	Temp. Study
Gasoline	• (x2)	• (x5)	• (x3)	•	•	•
Gasoline + 15% Toluene	•	•	•			•
Gasoline + 30% Toluene	•	•	•			•
Gasoline + 15% Ethanol	•	•	•			•
Gasoline + 30% Ethanol	•	•	•			•
Iso-octane	•	•	•			
Isooctane + 10% Isopentane			•			
Isooctane + 20 % Isopentane			•			
Isooctane + 30 % Isopentane			•			
Isooctane + 40 % Isopentane			•			

2.2.2 Rapid Compression Machine

The RCM is a bench-scale experiment designed primarily to study the ignition characteristics of fuels, but, in this case, to offer insight into the sooting tendencies of fuels. Here, the experimental procedures and data processing will be discussed.

Pre-experiment Preparations

Before beginning experiments, the RCM assembly and mixture preparation system should be inspected to ensure they are in proper working order. It should be verified that the nitrogen cylinders powering the device are full (one feeds the compressed gas tank for the pneumatic circuit, while the other is used to pressurize the oil cylinder). The optical windows should be inspected for cleanliness and should be removed for cleaning if any soot build-up is visible. Once clean, the LASER alignment is verified. If it is acceptable, then the combustion cylinder heaters and the mixture preparation heaters are turned on and the system is allowed to reach its operating temperature. Once at the operating temperature, experiments may proceed.

Mixture Preparation

The mixture is prepared using the apparatus discussed in the previous section. The mixture composition is chosen in order to specify the equivalence ratio as well as the temperature and pressure upon compression. The ratio of specific heats of the mixture determines the temperature and pressure following compression. In addition to changing the mixture composition, the temperature upon compression can also be varied by varying the initial mixture temperature. The air mixture was composed of 21% oxygen with a balance of nitrogen and argon. The nitogen/argon ratio was varied in order to specify the ratio of specific heats. In order to determine the necessary mixture composition, the fuel, equivalence ratio, initial temperature and fuel concentration upon compression were input to a FORTRAN code which performed stoichiometry and thermodynamic calculations yielding estimates of the temperature after compression, the peak temperature of combustion, the ratio of specific heats and the mole fractions of each mixture component for a range of nitrogen/argon ratios. The nitrogen/argon ratio was then interpolated based on the desired temperature after compression.

Knowing the mixture composition, the component partial pressures were calculated by scaling the mixture fractions by the desired mixture mass. The mixture

mass was chosen to permit a series of tests using the same mixture while maintaining an above-atmospheric pressure in the mixture preparation vessel. This is in order to avoid contamination with ambient air should the vessel leak.

In order to prepare the mixture, first the mixture preparation vessel is evacuated. All valves were kept closed during this process except the valve to the vacuum pump and the valve to the low-pressure Baratron pressure transducer, which is used to measure the vacuum pressure. When the vacuum level was adequate, the valve to the vacuum pump was closed, isolating the mixture preparation vessel. While under vaccuum, the desired volume of liquid fuel was injected through the septum. The pressure on the low pressure vacuum gauge was observed until the reading stabilized, indicating complete vaporization of the fuel. At this point, the low-pressure vacuum gauge was isolated by closing the valve.

Then, the simulated air mixture is prepared. Using the mixture preparation pressure gauge, first the oxygen micrometer valve is slowly opened to admit oxygen to the vessel until the total absolute pressure is equal to the sum of the partial pressures of fuel and oxygen. Then, the same process is followed for nitrogen and argon. When the mixture has been prepared, the mixing fan is turned on for 10 minutes to ensure that the mixture is homogeneous.

RCM Firing Sequence

While the mixing fan is running, the combustion chamber should be evacuated. To do so, first a vaccuum is applied to the pneumatic cylinder, drawing the piston assembly backward until the hydraulic piston strikes the sealing surface, creating a face seal. At this time, the hydraulic chamber may be pressurized by opening the valve connecting it to the compressed nitrogen supply. This locks the piston assembly in place. Once retracted, the combustion chamber 3-way valve was turned toward the mixture preparation unit and the vacuum valve is opened. It was found that approximately 10 minutes of evacuation was sufficient. The pressure of the combustion cylinder could be monitored using the "high"-pressure Baratron pressure transducer. When evacuated, the vacuum valve is closed and the pressure is monitored briefly to ensure

that there are no leaks in the combustion chamber. If the chamber is air-tight, the mixture is admitted by slowly opening the valve connecting the mixture preparation unit to the heated transfer line to the combustion cylinder. This valve is closed when the desired pressure is reached in the combustion cylinder. This pressure is important as it determines the mixture density. That is, the amount of fuel and air participating in the combustion event. Once the mixture is admitted at the proper pressure, the mixture is allowed to equilibrate with the RCM temperature for 10 minutes. This determines the initial temperature of the mixture. The 3-way valve is kept open to allow verification that the combustion chamber is not leaking.

After the equilibration period, with the hydraulic chamber pressurized, the compressed gas bypass valve is opened to equilibrate the pressure in the pneumatic cylinder with that in the compressed gas tank. Then, the 3" ball valve is then opened and the combustion chamber 3-way valve is closed. Finally, the DAQ recorder is started and then the RCM is fired by releasing the pressure in the hydraulic chamber. The DAQ is configured to record based on a pressure-rise trigger and 1 second of data are collected at 100kHz. Pressure data and light intensity data from the photomultiplier tube (PMT) are collected.

Data Processing

Using a MATLAB script, the raw data are first passed through a filter to eliminate the mechanical noise present in the pressure and LASER signals. With the clean signal, a simple analysis is performed by identifying the decrease in the measured light intensity. With the change in intensity, the volume fraction of soot can then be calculated using the following formula where C_v is the volume fraction of soot, λ is the light wavelength, L is the length of light travel through the combustion chamber, m is the refractive index of soot, I is the attenuated light intensity and I_0 is the initial light intensity [90].

$$C_v = \frac{\lambda}{6\pi L I m \left\{\frac{m^2-1}{m^2+2}\right\}} ln\left(\frac{I}{I_0}\right)$$

The volume fraction of soot in the cylinder is used to calculate a soot yield, which is a useful measure of the sooting tendencies of a combustion event. It is the mass of soot formed, normalized by the mass of fuel carbon present in the initial mixture. It is calculated as shown below, where SY is the soot yield, ρ_s is the density of soot, C_v is the volume fraction of soot, M_C is the molecular mass of carbon and $[C]_{comp}$ is the molar concentration of fuel carbon in the unburned mixture upon compression [89].

$$SY = \frac{\rho_s C_v}{M_C [C]_{comp}}$$

Using these values, a measure of the equivalence ratio threshold for soot formation was determined. On a soot yield versus equivalence ratio plot, the sooting threshold was initially identified as the point at which the slope of the curve increased most rapidly (i.e. the point on the curve with the highest second derivative). It was found that this value coincided closely with the point of 50% attenuation on a LASER attenuation versus equivalence ratio curve. In the interest of simplicity (and quick diagnosis), it was decided to define this point as the threshold equivalence ratio for soot formation.

This page intentionally left blank

Chapter 3

Results

A large number of experiments were conducted over the course of this study. This chapter discusses those experiments which are relevant to the objective of understanding the mechanism of PM formation during cold-idle operating conditions. The first section will discuss results from the study of engine emissions. The second section will discuss results from the study of fuel sooting tendencies completed using the rapid compression mchine.

3.1 Engine Experiment Results

Here, the results of a series of engine experiments will be presented. These results are those which are relevant to the questions laid out in the experimental hypotheses defining this program of study. An attempt will be made here to explain the observations drawn from the experimental results. Further discussion of these results in a broader context are included in chapter 4.

3.1.1 Spark Timing Sweep

The experimental investigation of the impact of spark timing on particulate matter was completed for two reasons. Firstly, spark retard is commonly used as a cold start strategy as the associated elevated exhaust temperatures accelerate catalyst light-off [11]. The experiment was also intended to offer some insight into the effects

of mixing time, combustion phasing and cylinder temperatures on PM emissions. In some capacity, this was meant to test the residual fuel effects hypothesis. A retarded spark timing results in more time for fuel and air mixing, but the change in cylinder temperature and pressure profiles may also change the evaporation properties of deposited fuel. With retarded spark, the exhaust gas and, consequently, the residual gas temperatures are elevated when compared to more advanced spark timings [91]. Further to this, due to changes in combustion phasing the peak temperatures and combustion durations are changed, with lower peak temperatures (depending on load) and extended combustion durations.

In previous studies, it was found that PM, on both a number and mass basis, does not vary monotonically with spark timing. Instead, at advanced ignition timings (25°CA $BTDC_{comp}$ to 45°CA $BTDC_{comp}$), retarding the spark will reduce PM emissions. This was attributed to an increased time for mixing as well as increased post-flame oxidation. At retarded spark timings (later than 20°CA bTDC), however, it was found that retarding the spark increased PM emissions. This was attributed to reduced combustion quality [66].

In these experiments, it was similarly found that retarding the spark timing (at late timings) results in an increase in particulate number emissions with spark retard. This is shown for gasoline fuelling in figure 3-1.

Similar to the conclusions drawn in [66], it was seen that along with increased PM emissions, the combustion stability was decreased, as indicated by an increased coefficient of variation (COV) of the gross IMEP. This is shown in figure 3-2. Also, it was observed, as expected, that the combustion phasing is later with retarded spark. This is seen in figure 3-3. The late combustion phasing leads to increases in late-cycle charge temperatures and pressures, which may both impact soot formation and oxidation processes (high temperatures can increase the rate of soot oxidation, while high pressures may increase soot formation)[3, 34], though their combined impact is unclear in this case.

One should note that, in this experiment, the engine speed, load and equivalence ratio were held constant. Consequently, due to the reduced efficiency associated with

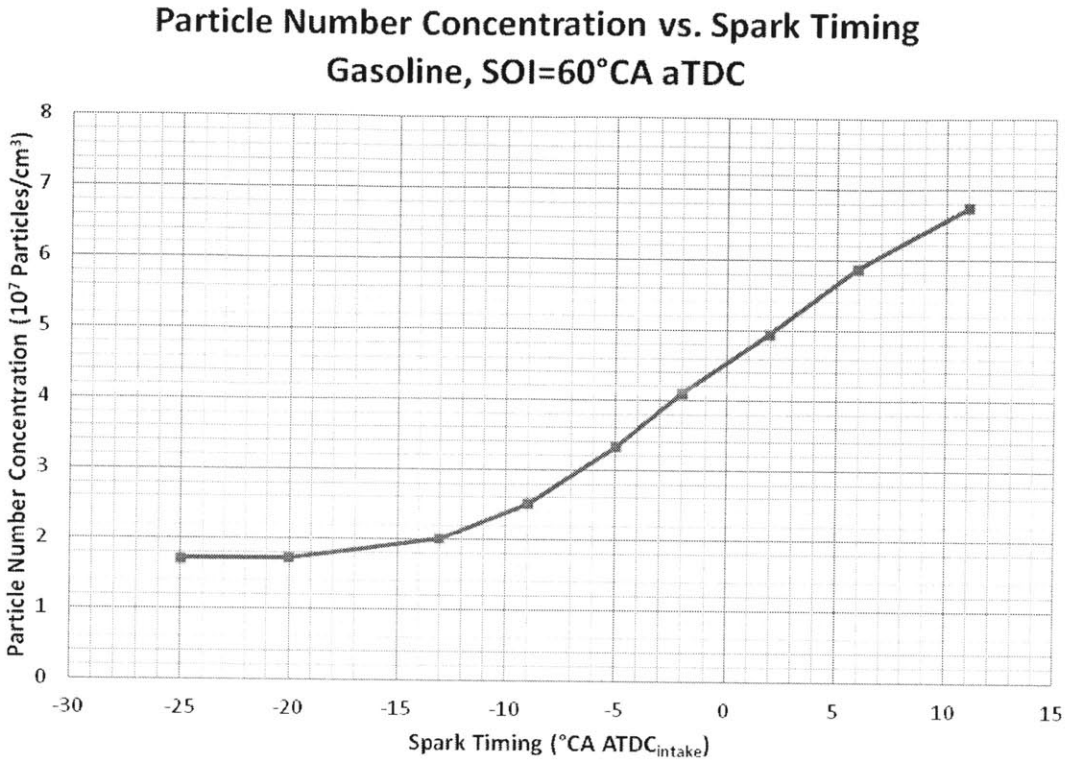

Figure 3-1: Spark timing effects on PM emissions with gasoline (ϕ=1, 1200rpm, 2 bar net IMEP)

the late ignition timing, it was necessary to increase the fuelling rate in order to maintain the net IMEP setpoint of 2 bar. The result of this is that, due to the increased fuel injection duration, it is likely that there was more fuel impingement on the piston crown and possibly on the cylinder liner. As shown in previous studies, liquid fuel films are associated with PM formation through what are often described as pool fires or diffusion flames [9, 50, 51]. Thus, it is expected that the increased fuelling rate plays a significant role in the increased PM formation, obscuring any effects from elevated temperatures and pressures. To illustrate this, figure 3-4 plots the particle number concentration and the fuelling rate versus spark timing.

Finally, by examining the size distributions of the PM emissions at the studied ignition timings (shown in figure 3-5), it was seen that while there are different magnitudes at different spark timings, the mode particle bin midpoint diameters are very

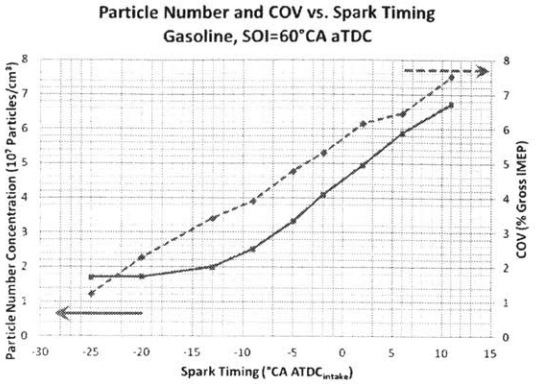

Figure 3-2: PM and COV

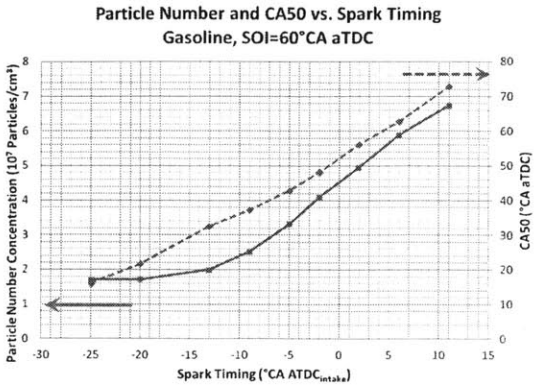

Figure 3-3: PM and CA50

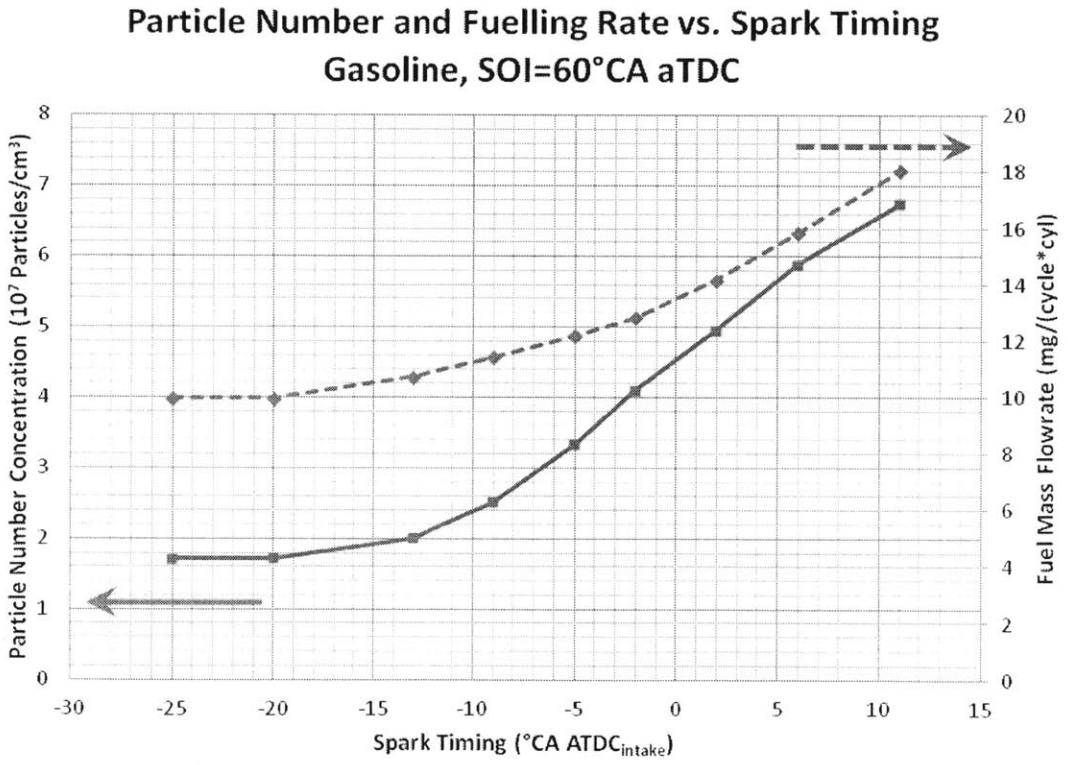

Figure 3-4: Spark timing effects on PM emissions with gasoline (ϕ=1, 1200rpm, 2 bar net IMEP)

similar as are the overall distributions. This suggests that the particles are formed through similar mechanisms regardless of ignition timing. Further experiments shed more light on these soot formation mechanisms.

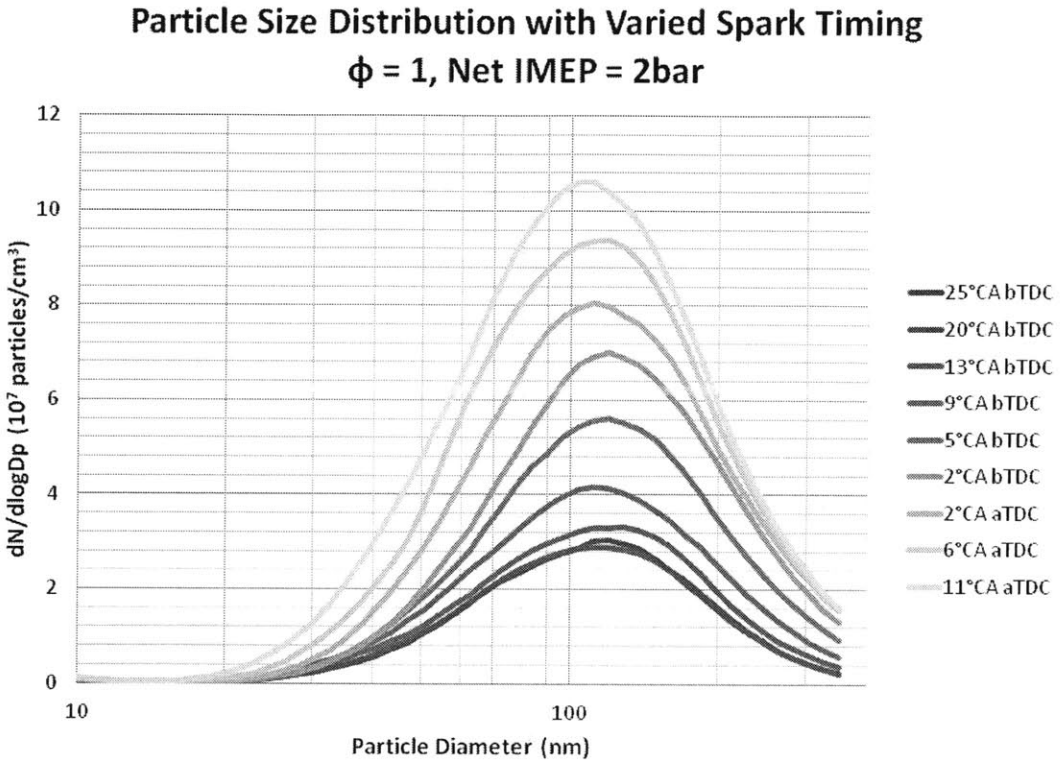

Figure 3-5: Particle Size Distributions

3.1.2 Injection Timing Investigation

Based on earlier investigations, liquid fuel films are known to give rise to PM [9, 50, 53]. The injection timing plays a large role in the formation of fuel films. The LNF engine used in these studies features side-mounted injectors, so the injection timing determines not only the amount of liquid fuel impinging on surfaces, but also the location of impingement. Very early or very late injection results in large liquid films on the piston crown due to the proximity of the piston to the injector tip during the injection event. This is illustrated in figure 3-6. Understanding the behaviour of PM emissions resulting from liquid fuel films is the key to testing the residual fuel effects hypothesis.

These experiments were conducted in order to understand the importance of the location of fuel impingement in the formation of PM in a DISI engine. Beginning

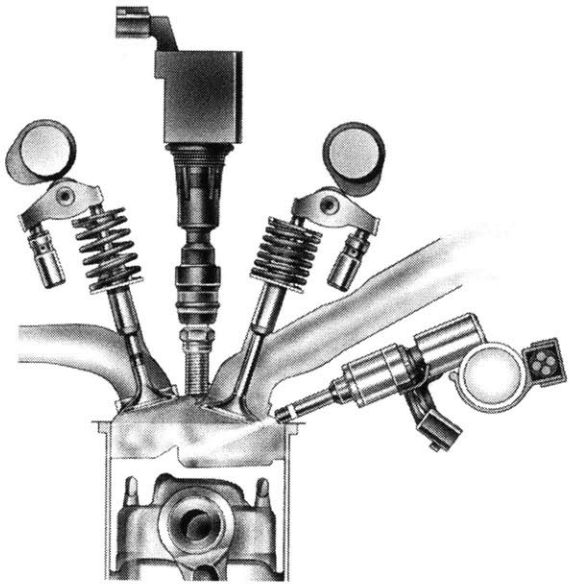

Figure 3-6: LNF engine fuel injection ©GM Company.

with an injection starting at TDC_{intake}, when the fuel stream is expected to impinge on the piston, it was found that, as the injection timing was retarded, PM emissions were reduced until the timing when the fuel is no longer expected to impinge on the piston crown. At this point, the PM emissions remain at a relatively steady concentration until, at late start of injection (SOI) timings, the PM emissions again begin to increase, corresponding to the wetting of the piston crown surface. Figure 3-7 shows the particulate number concentration in the exhaust versus the SOI timing for gasoline at a spark timing of 25°CA $BTDC_{comp}$ with the load and temperatures matching the baseline cold-idle specification. The load and speed were held constant throughout the sweep of injection timing.

The trend of increased PM emissions corresponding to impingement of fuel on piston surfaces held reasonably constant regardless of spark timing, though the increases in emissions are greater at later spark timings. In this situation it seems that the combustion instabilities associated with highly retarded spark timings couples with the formation of fuel films leading to PM emissions. This is seen in figure 3-8.

Through the plotting of particle size distributions for each of the injection timings, it becomes clear that the location and magnitude of surface impingement is an important factor in determining the magnitude of the PM concentration in engine

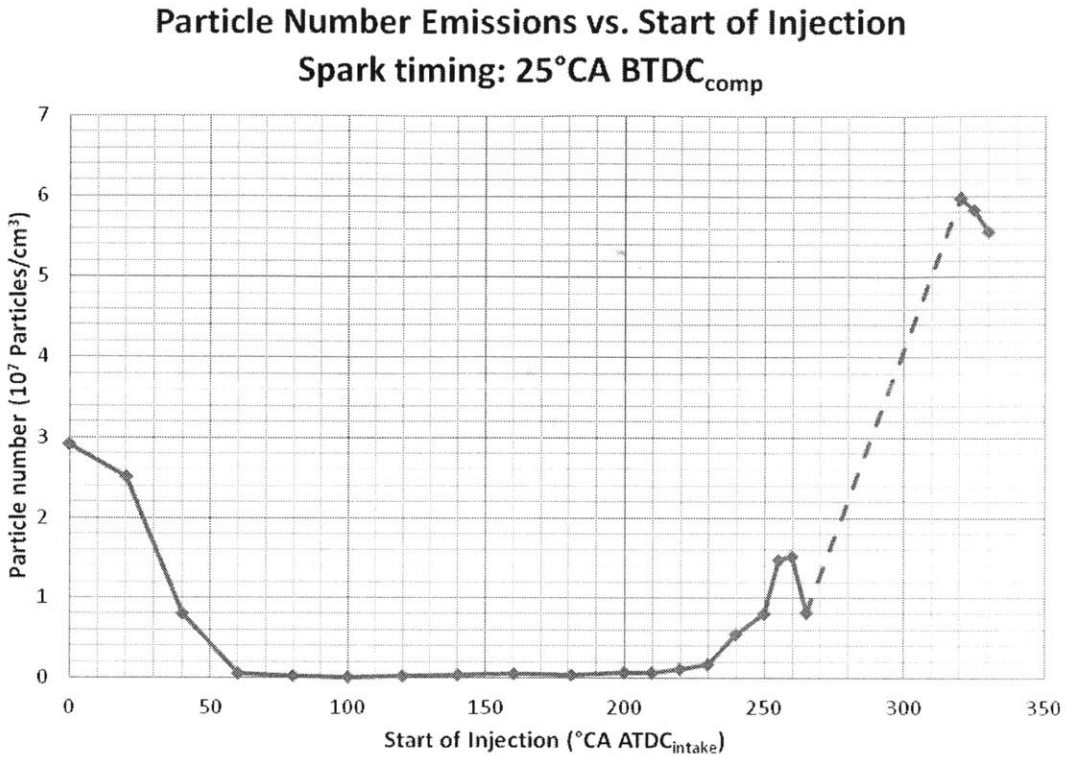

Figure 3-7: PM emissions vs. SOI timing for gasoline. The engine did not run due to combustion instability in the region represented by a dashed line.

exhaust. Figure 3-9 shows the size distributions for early injections. figure 3-10 shows the size distributions for moderately early injection timings, figure 3-11 shows the size distributions for moderately late injection timings and figure 3-12 shows particle size distributions for late injection timings.

For early injection timings, when it is expected that liquid fuel will impinge on the piston, the magnitude is larger and the mode bin mid-point diameter is significantly larger than that seen as the injection timings are retarded(see figure 3-9). At more moderate injection timings, when the fuel is sprayed into open air, there are differences of magnitude, but the particle size distribution shapes are consistent, with the mode mid-point diameter being relatively small (20-30nm). This is seen in figures 3-10 and 3-11. Differences in magnitude may be attributed in part to differences in mixing times as well as the possibiliy of fuel splashing off of liner surfaces onto the

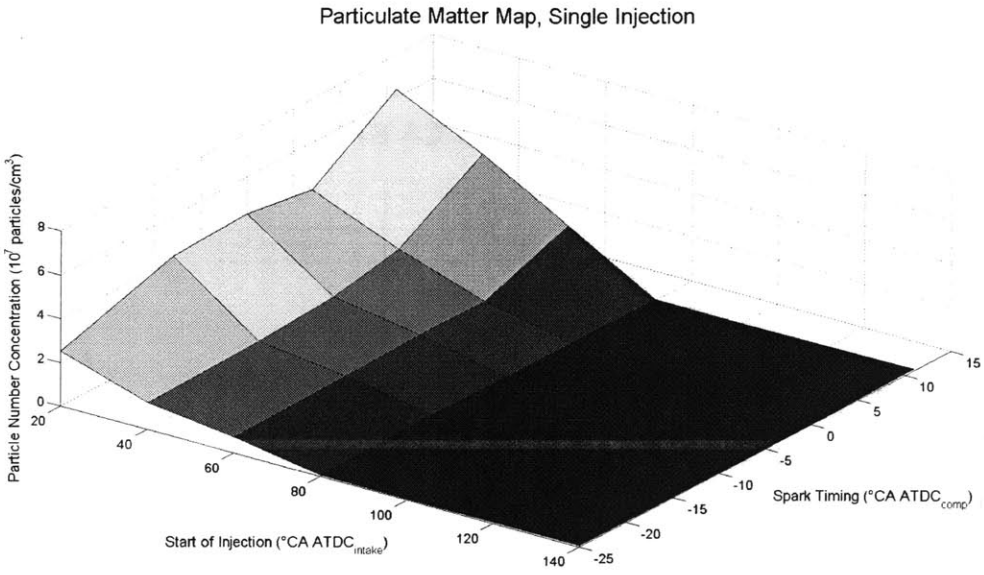

Figure 3-8: PM emissions vs. SOI timing for gasoline at various spark timings.

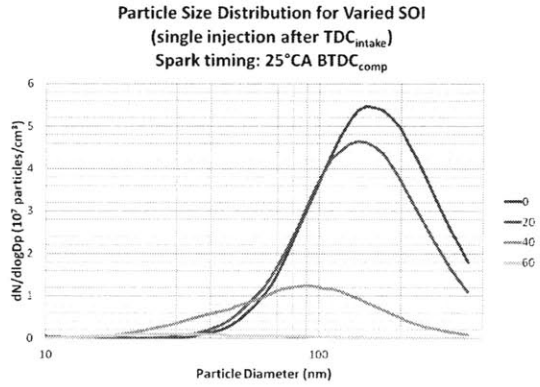

Figure 3-9: Early SOI

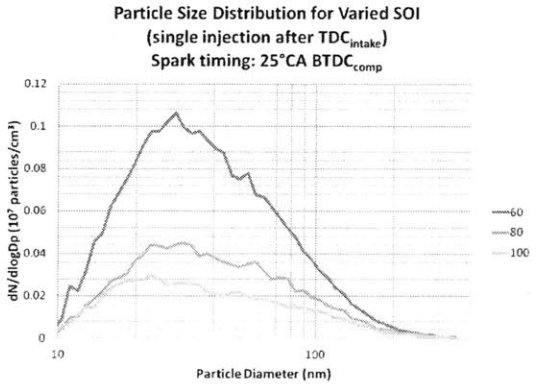

Figure 3-10: Early/moderate SOI

piston crown or cylinder head. At very late injection timings there are two major phenomena affecting PM emissions. The first is that with late injection timing, there is insufficient mixing time for complete mixing. This leads to mixture inhomogeneities which result in poor combustion stability (as is noted when the engine cannot sustain power and stalls at injection timings around 265°CA ATDC$_{intake}$), as well as regions of mixture that may be sufficiently fuel-rich to promote soot growth as there are ample hydrocarbons for particle surface growth with little oxygen for particle oxidation [57].

At very late injection timings (320-330°CA ATDC$_{intake}$), however, the engine again fires with reasonable stability. In this case, the stability is improved through the interaction of the fuel spray with the shallow piston bowl. The bowl serves to direct some of the injected fuel toward the spark plug, resulting in a fuel-rich mixture in the vicinity of the spark plug. This fuel-rich mixture supports robust combustion, but the impingement of liquid fuel on the piston crown also promotes the formation of PM, as is seen in figure 3-12.

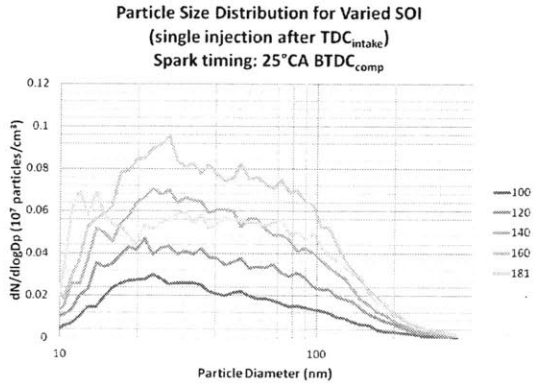

Figure 3-11: Moderate/late SOI

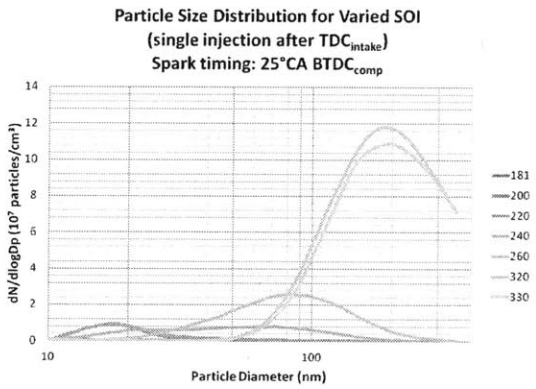

Figure 3-12: Late SOI

Impact of SOI Timing at Elevated Coolant Temperature

As has already been mentioned, the evaporation and combustion of fuel films plays an important role in the formation, oxidation and emission of particulates [9, 47, 48, 50, 92]. Thus, it should come as little surprise that the coolant temperature can have a significant impact on PM emissions [10, 78]. Generally, at higher coolant temperatures, with the associated increase in engine component temperatures, liquid fuel that impinges on cylinder surfaces will evaporate more readily, resulting in less liquid fuel being available to participate in pool fires or diffusion flames and, consequently, less PM is emitted. This is seen in figure 3-13 where it is seen that at early and moderately late SOI timings, the higher coolant temperature leads to a reduction in PM emissions.

In addition, it can be seen that the engine component temperatures affect not

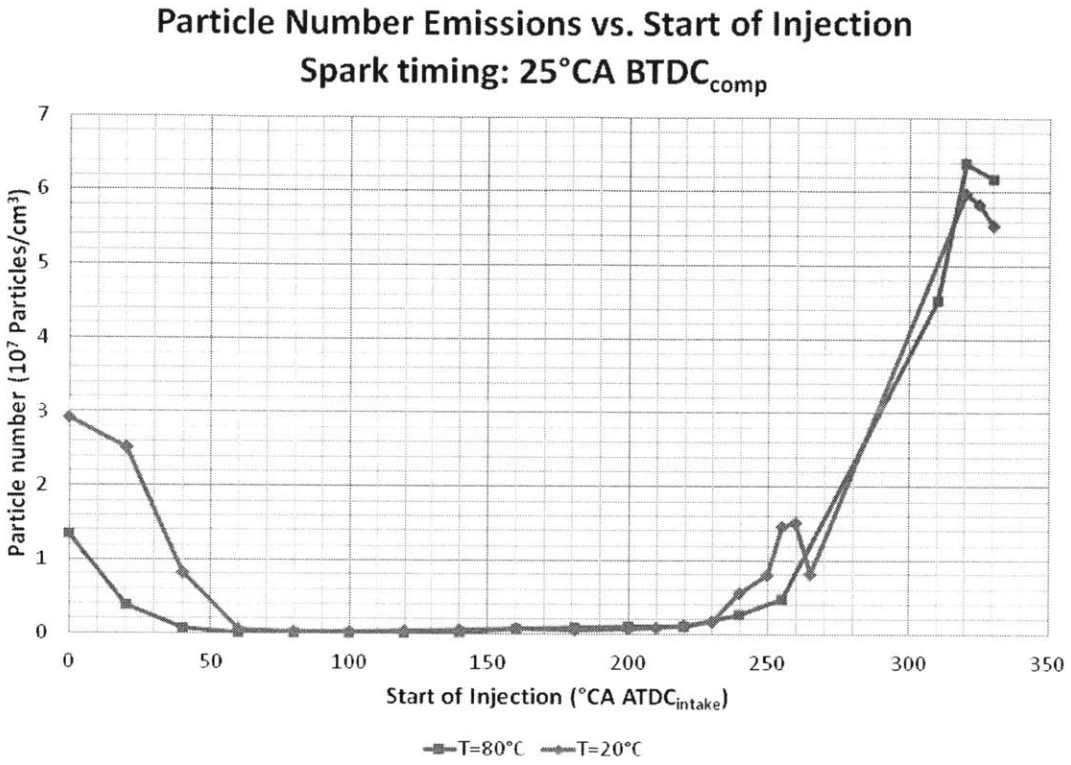

Figure 3-13: PM emissions vs. SOI timing for gasoline at cold and warm engine coolant temperatures.

only the PM concentration, but also the size distribution. Figures 3-14, 3-15 and 3-16 show the particle size distributions at injection timings of 20°CA ATDC$_{intake}$, 100°CA ATDC$_{intake}$ and 255°CA ATDC$_{intake}$, respectively. It is observed that in those situations where the injection timing leads to piston impingement, the increased temperature not only reduces the magnitude of the PM emissions, but also the mode bin midpoint diameter. This supports the idea that the mechanisms leading to soot formation depend on temperature and suggests that, at warm coolant temperatures, not only are the liquid films reduced in size, but the composition of the fuel remaining in the films may also change. For example, it is possible that a light aromatic, which does not evaporate under cold coolant operating conditions might evaporate under warm operating conditions, possibly reducing the ability of the liquid film to support the formation of soot nucleation and surface growth precursors. At moderate injection

timings, when fuel should not impinge on the piston crown, it is possible that the warm liner temperatures may allow less-volatile components which form soot surface growth precursors to slowly evaporate, taking part in combustion in rich regions. The reduced number would then be accounted for by the reduced volume of fuel forming a film on the liner and the increased mode bin mid point diameter would be accounted for by the heavier hydrocarbons able to participate in combustion. It should be noted that the piston crown is expected to be significantly hotter than the liner, so the effects of temperature on fuel film composition is, as seen here, not expected to be uniform depending on the film location.

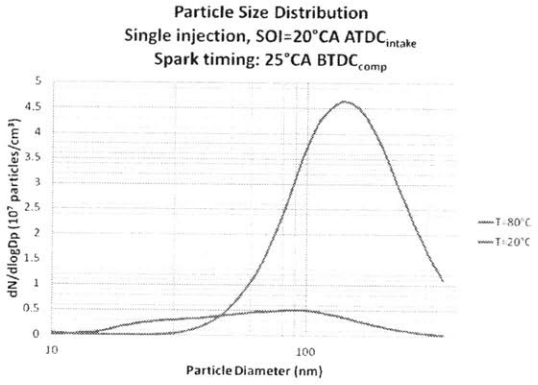

Figure 3-14: Early SOI

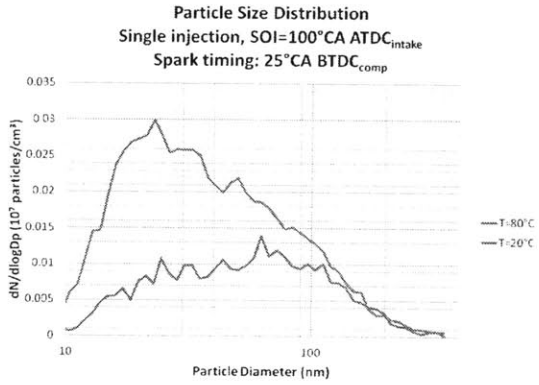

Figure 3-15: Moderate SOI

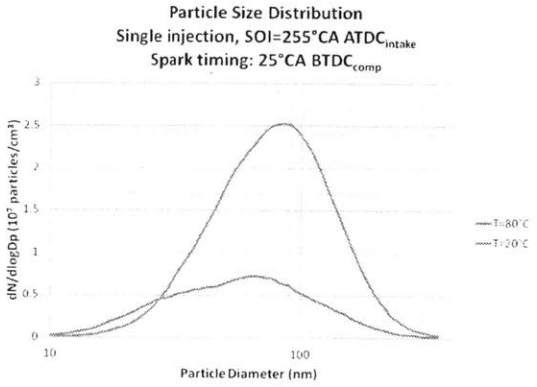

Figure 3-16: Late SOI

3.1.3 Dual Injection Investigation

The LNF engine was designed with a shallow piston bowl that enables partially stratified charge operation under cold-start conditions. This design offers an opportunity to conduct some interesting experiments designed to test the residual fuel effects hypothesis by examining the impact of fuel impingement in various regions of the combustion chamber. The partially-stratified operation is accomplished by injecting the majority of the fuel during the intake stroke with the remainder injected late during the compression stroke. The goal of this operating regime is to produce a region of fuel-rich mixture in the vicinity of the spark plug in order to enhance combustion stability at late spark timings. The PM emissions response to this operating regime is of interest due to the advantages of retarded ignition timing in terms of catalyst light-off [11], but, in this study, this operating regime is of more interest because it allows fuel films to be created on the piston crown late in the compression stroke, when there will be little time for evaporation and mixing. This allows a better inference of the location of liquid fuel films during the combustion event than was possible during the study of single injection timing. For these experiments, 70% of the fuel was injected during the main, intake stroke injection. The start of injection timing for the main injection was held constant at 80°CA $ATDC_{intake}$. This timing was chosen as it is early enough for thorough mixing, but late enough in the cycle to ensure there will be little if any impingement of the fuel spray on the piston crown (see figure 3-8). The remainder was injected during the compression stroke. The engine was operated at the cold-start conditions outlined in table 2.5, but with late spark timing. The spark timing was held at 11°CA $ATDC_{comp}$. There were two reasons for this. The first, as mentioned already, is because of the practice of retarding spark to accelerate catalyst light-off. The second is that this spark timing allows a wide range of injection timings to be studied with reasonable combustion stability. Later injections may also be of interest, but the combustion stability is not sufficient to allow SMPS data to be collected.

It was, again, observed that particulate emissions are elevated in situations where

piston-wetting is expected. Figure 3-17 graphs the PM emissions (all particle number data are total particle number between 22.08nm and 365nm) versus the timing of the start of the second injection (SOI_2). For relatively early second injections, the emissions are relatively low, since the mixing process behaves similarly to a single injection with low levels of liquid fuel impingement on cylinder surfaces. When the second injection is retarded, and the spray begins to interact with the piston crown surface, the emissions increase signifcantly. This is especially obvious in figure 3-18 which shows the same data plotted with a logarithmic y-axis. Here it is seen that there are two orders of magnitude in difference between the results of the early injections and the results of the later injections.

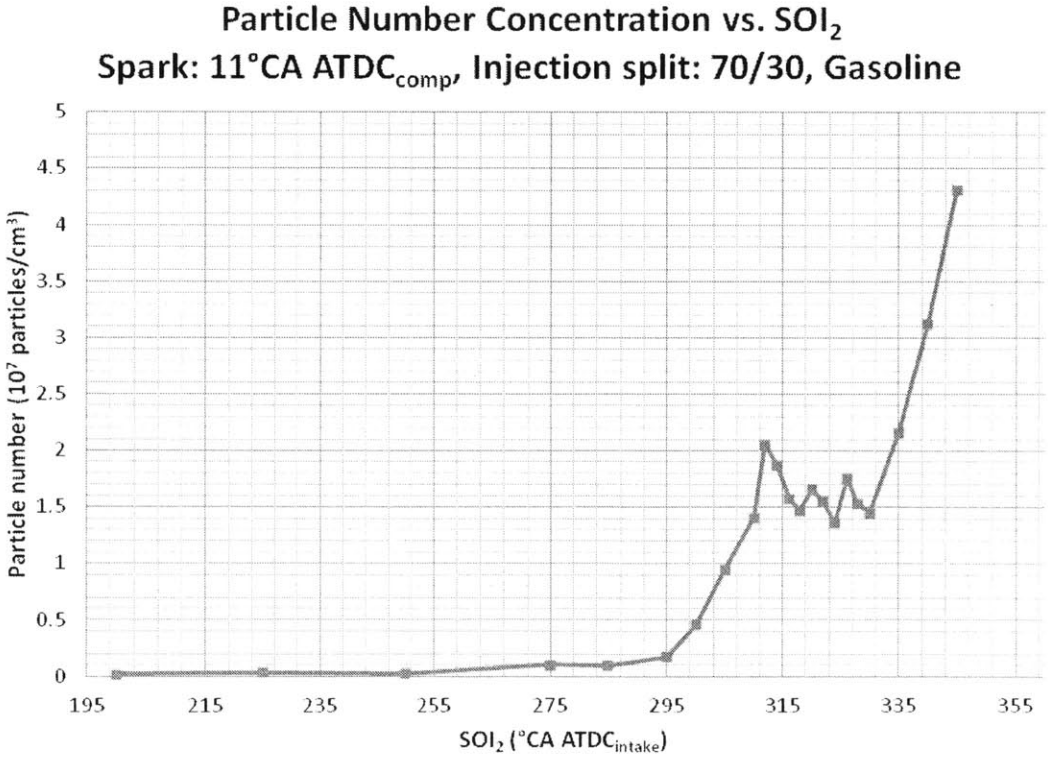

Figure 3-17: PM emissions with double injection

The decrease in emissions seen between second injection timings of 312 and 330°CA $ATDC_{intake}$ is attributed to the interaction of the fuel spray with the shallow piston bowl. In this situation, the shallow bowl directs the fuel spray toward the spark plug.

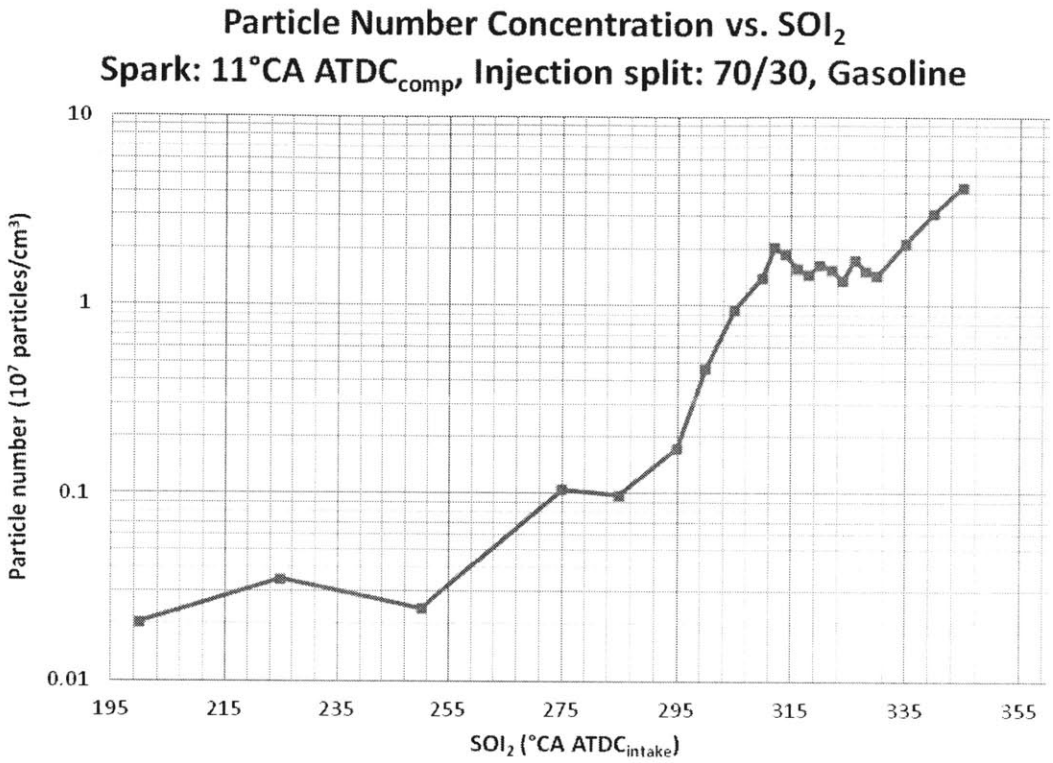

Figure 3-18: PM emissions with double injection (semi-log axes)

creating a rich region near the spark plug which enhances early combustion stability. The improved stability is accompanied by reductions in PM emissions. At very late injection timings, the bowl no longer directs the spray properly toward the spark plug, but the spray still impinges on the piston crown, creating liquid films, which are known to lead to PM emissions [9, 50, 53]. At these late injection timings, the proximity of the piston to the injector tip likely results in reduced in-flight evaporation allowing a large volume of fuel to coat the piston crown. Some fuel also may splash off of the piston crown, impinging on other surfaces.

Figure 3-19 illustrates the orientation of the piston, relative to the injector centreline at a series of start of second injection timings. It is obvious in these illustratons that as the piston rises toward the cylinder head (the piston is travelling upward in all of these images), the fuel spray will impinge more directly on the piston crown. At late injection timings, the fuel spray is expected to strike the piston very close to the

injector tip. Please note that, in this engine, the fuel spray is not perfectly parallel to the injector body. Instead, there is a downward deflection angle which is not shown here, since it has not been disclosed by the engine manufacturer. Nevertheless, the reader should be mindful of the fact that the spray is oriented in such a way that its centreline likely strikes the piston a few crank-angle degrees earlier than is illustrated here.

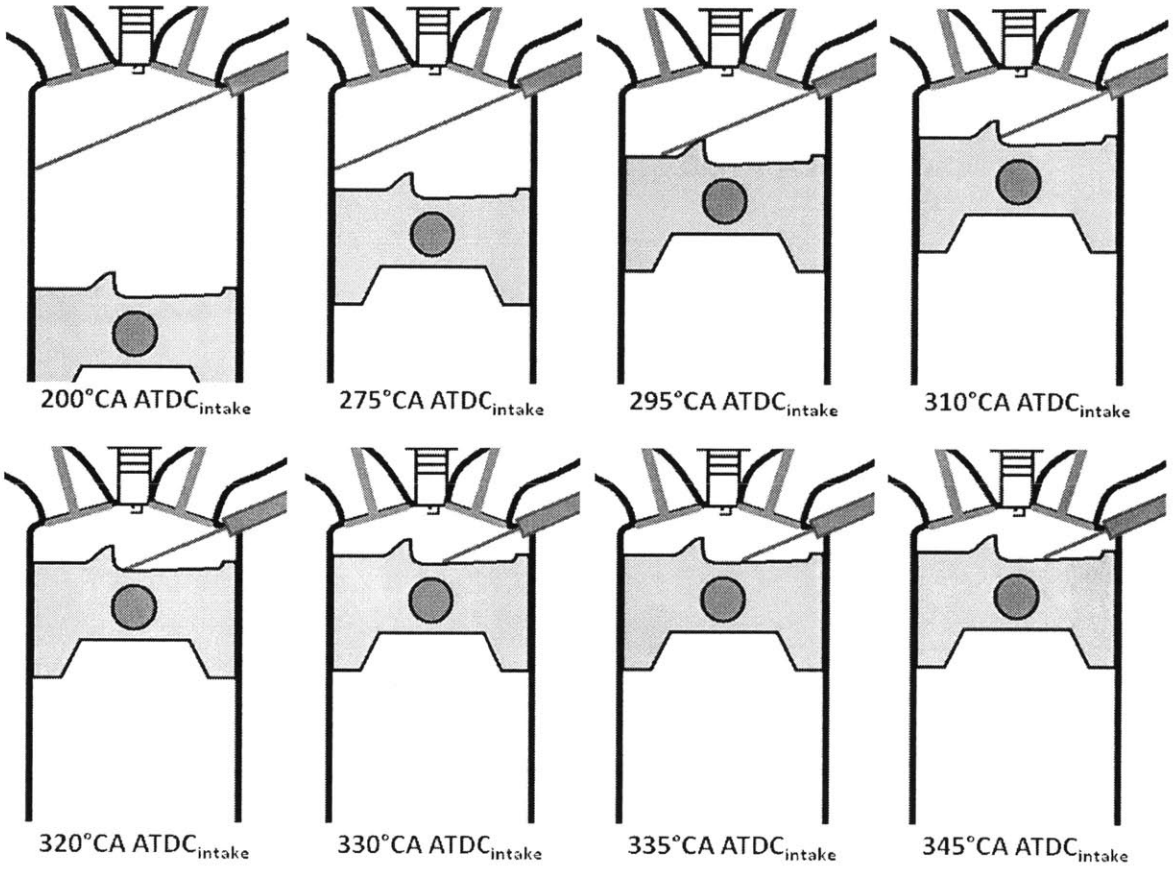

Figure 3-19: Piston positions (dimensions based on figure 3-6)

It is, again, valuable to examine the particle size distributions to gain an understanding of the mechanisms of soot formation under the different conditions. These are shown in figure 3-20. Early second injection timings result in low PM emissions, with relatively small mode bin mid-point diameters. The number and particle diameters increase as the second injection timings are retarded, but there is a decrease in the mode bin mid-point diameter apparent for those injection timings that correspond to interactions between the piston bowl and the fuel spray. At late timings there are

high numbers of large particles emitted.

It seems that there are two phenomena at play in determining the PM emissions. Firstly, the size and location of the fuel films are important. Those closer to the injector tip appear to yield larger particles. Secondly, the combustion stability is important. Operating conditions with improved stability yielded fewer and smaller particles, seeming to suggest a better efficiency at vaporizing fuel, mixing fuel and air or burning up soot particles.

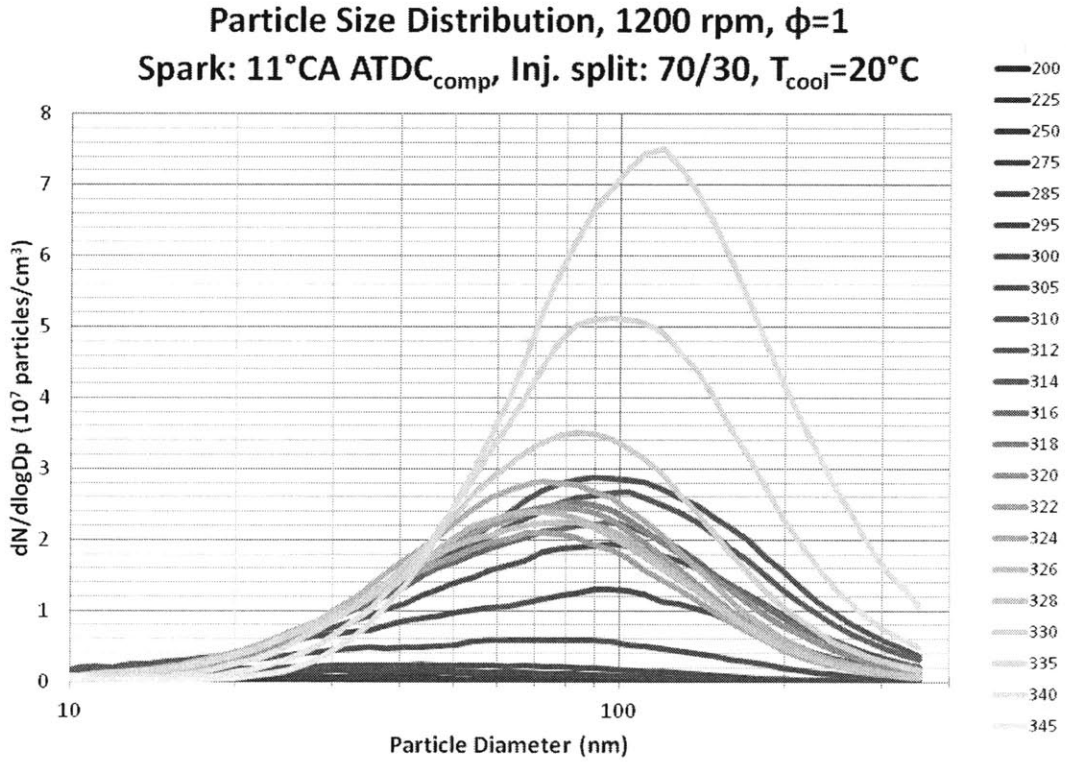

Figure 3-20: Particle size distributions for double injection.

Impact of Coolant Temperature on PM Emissions with Dual Injection

As was done in the single injection experiments, the second injection timing sweep was repeated under additional temperature conditions. The first repeated run was completed at a coolant temperature of 80°C with the operating conditions otherwise the same as those of the baseline case. This experiment allows an understanding of

the impact of increased cylinder surface temperatures. Given the ability to infer the locations of fuel impingement, the temperature change was expected to provide some valuable information about the influence of fuel films on soot formation.

The second repeat of the injection timing sweep was completed with heated inlet air, but otherwise the operating conditions were the same as those in the baseline case. In this case, the intent was to examine the effect of in-flight evaporation of fuel. Increased in-flight evaporation should enhance mixing and reduce the volume of fuel impinging on cylinder surfaces.

Figure 3-21 shows the number concentration versus second injection timing on a semi-log plot. It is seen that, apart from injection timings of 250 - 295°CA $ATDC_{intake}$ there is little change attributable to the temperature differences. For the injection timings of 250 - 295°CA $ATDC_{intake}$, a decrease was observed with increased coolant temperatures. At these injection timings, the fuel spray is likely to impinge slightly on the edge of the piston farthest from the injector. The reduction in PM emissions here is attributed to improved evaporation of the relatively small amount of liquid impinging on the piston under these conditions which is enabled by the elevated surface temperatures. There is no notable difference in PM emissions with increased inlet air temperature.

Examining the particle size distributions at the different temperature conditions provides more insight into the mechanism of soot formation beginning with liquid fuel films (see figures 3-22, 3-23, 3-24 and 3-25).

These figures show four different SOI_2 timings. The first, figure 3-22, is an early timing when there is expected to be little, if any, impingement of liquid fuel on the piston crown. In the second figure, figure 3-23, the SOI_2 timing shown is expected to result in mild impingement on the piston crown. At this point there was a decrease in emissions with increased coolant temperature. The distributions for an injection timed to interact with the piston bowl are plotted in figure 3-24 and the emissions for a very late injection resulting in severe piston crown impingement are plotted in figure 3-25. There are some differences in the magnitudes of the PM emissions seen in these distributions, but, as shown in figure 3-21 the differences in magnitude are

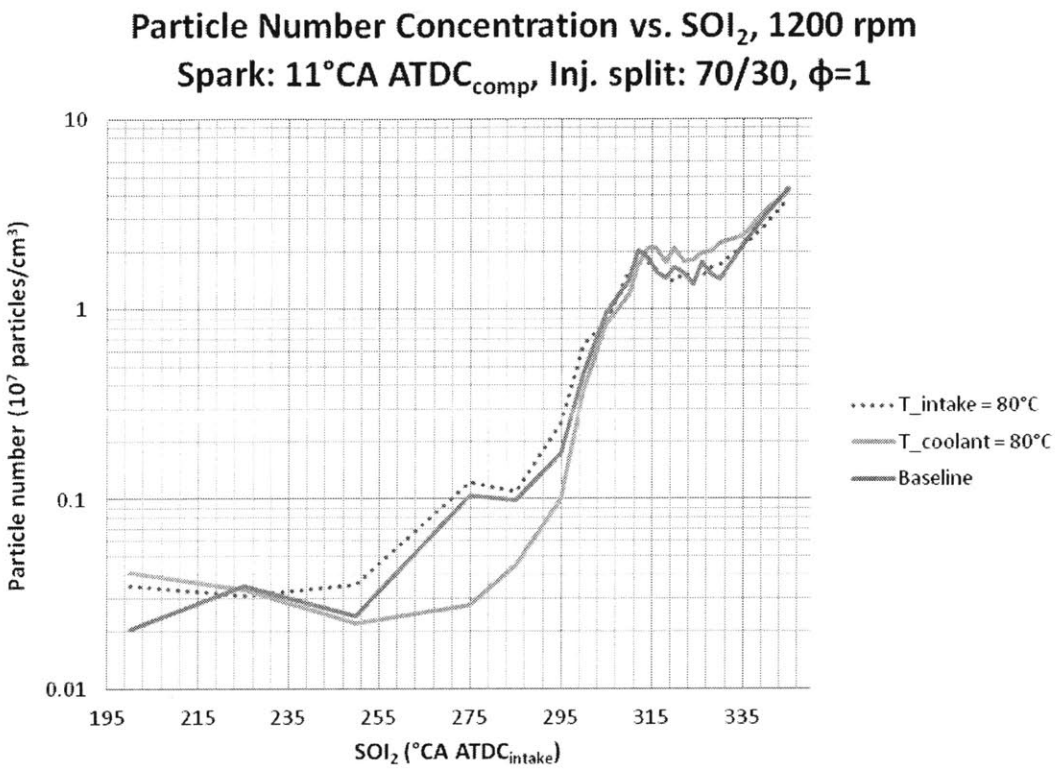

Figure 3-21: PM number concentration with second injection timing at warmed-up coolant and inlet air conditions.

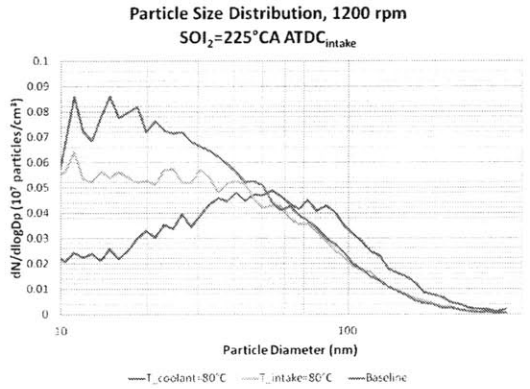

Figure 3-22: No impingement.

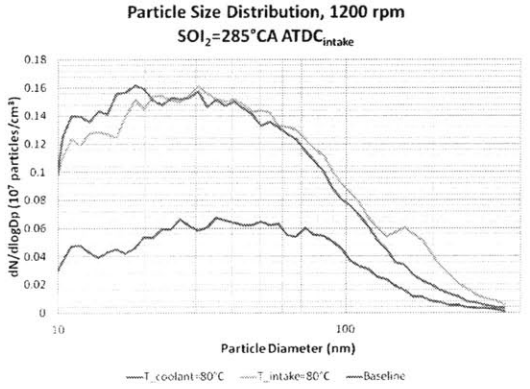

Figure 3-23: Mild impingement.

not significant except in the case of mild impingement.

Instead, of more interest is the shape of the size distributions. There appears to be little difference in the mode bin mid-point diameters or the overall distribution

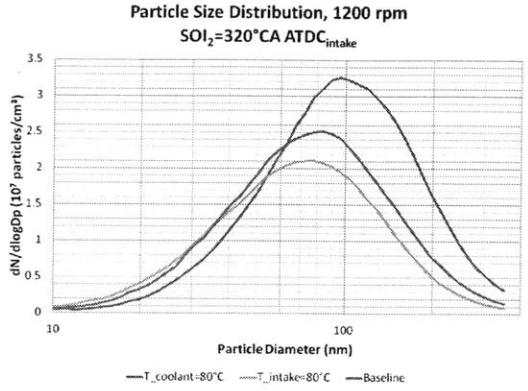

Figure 3-24: Bowl interaction.

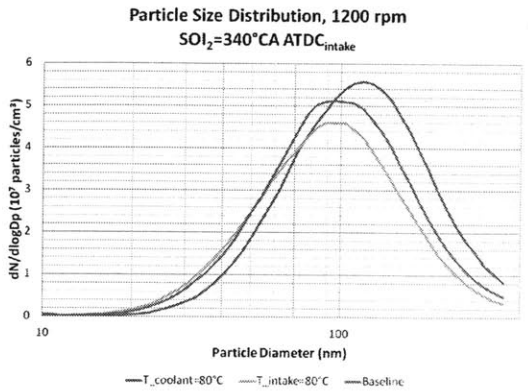

Figure 3-25: Severe impingement.

shape between the baseline case and the heated inlet air experiment. The heated coolant experiment, however, consistently appears to produce larger particles. This suggests that the increase in combustion chamber component surface temperatures supports the evaporation of the more volatile fractions of the gasoline, resulting in fuel films with higher concentrations of low-volatility compounds which may support enhanced surface growth of soot particles (though nucleation rates may not change much, or, in some cases, may actually decrease). This is apparent regardless of the presence or severity of piston impingement.

Impact of Engine Speed on PM Emissions

In order to examine the PM emissions impact of the time available for evaporation and mixing of liquid fuel from surface films, the investigation of second injection timing was repeated at engine speeds of 1500rpm and 1800rpm. The dual-injection strategy was repeated as it provides insight into several different injection/impingement regimes, thus helping to explain the mechanisms of soot formation under a variety of operating conditions. These reasonably small absolute (though reasonably large relative) increases in the engine speed should not drastically change the charge motion characteristics, but will reduce the time available for evaporation and mixing. If the residual fuel effects hypothesis is correct, reduced time for evaporation and mixing should leave more time for soot nucleation and growth.

In conducting the experiments, the load was held constant as the speed was increased. This required the throttle to be open wider as well as a slight increase in the fuelling rate. Unfortunately, this makes it somewhat difficult to fully interpret the results from this experiment. Figure 3-26 is a plot of total particle number concentration (integration of the particle size distribution from 22.08nm to 365nm). One of the most easily explained changes with increased engine speed is the narrowed region reflecting the interaction of the fuel spray with the piston crown at higher engine speeds. This occurs because, while the piston travels faster at higher engine speeds, the fuel spray does not. Thus, there are few crank angle degrees during which the fuel spray may interact with the piston bowl.

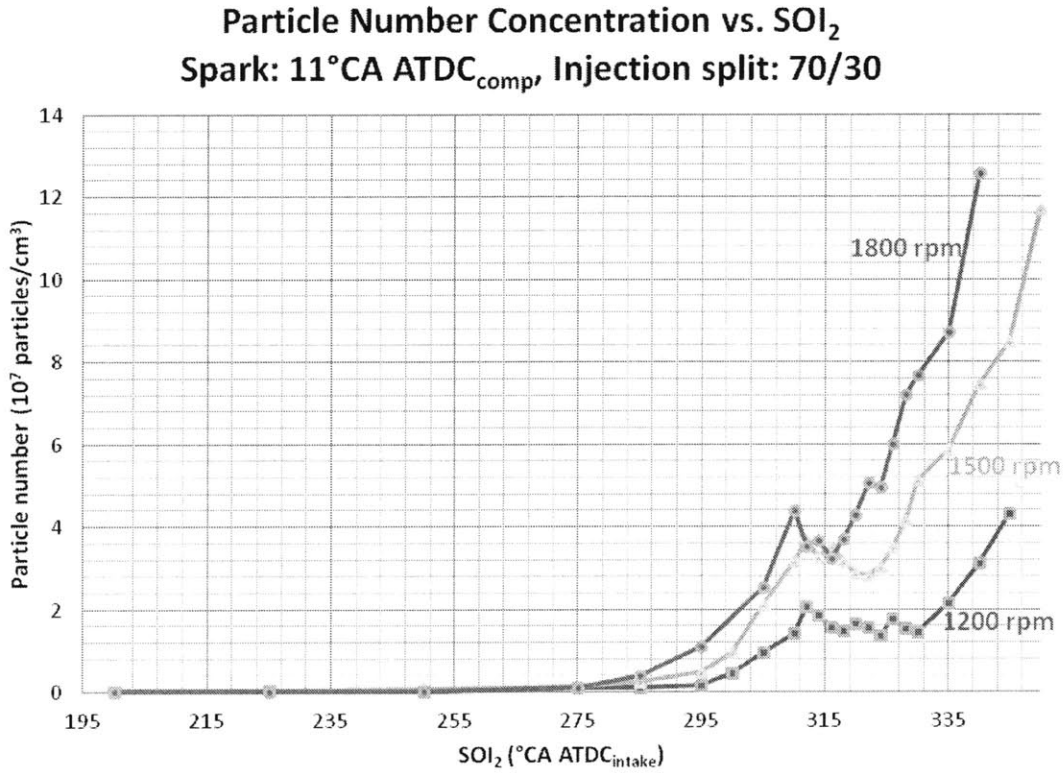

Figure 3-26: PM Emissions vs. SOI_2

In addition. it appears that the number emissions are increased at the higher engine speeds. This would appear to support the hypotheses suggesting that the evaporation of residual fuel in surface films are heavily involved in the soot formation

mechanisms, but due to the necessary increases in fuelling rate to maintain the engine load, it is not clear whether the changes in emissions are due to reduced mixing time or instead reduced to larger fuel deposits on the cylinder surfaces.

The particle sizes are also of interest as they provide further information about the soot formation process. In figure 3-27 the mode bin mid-point diameters are plotted against injection timing for second injections timed to begin between 305 and 320°CA ATDC$_{intake}$. These SOI$_2$ timings capture the fuel/bowl interaction for the 1800rpm case and for portions of the 1200rpm and 1500rpm cases. The mode particle diameter at 1200rpm is consistently larger during this range of injection timings. This suggests that the particle size is dependent on engine speed. It seems that a plausible explanation is that the lower speed provides a longer time for particle growth and agglomeration to take place, resulting in larger particles being emitted.

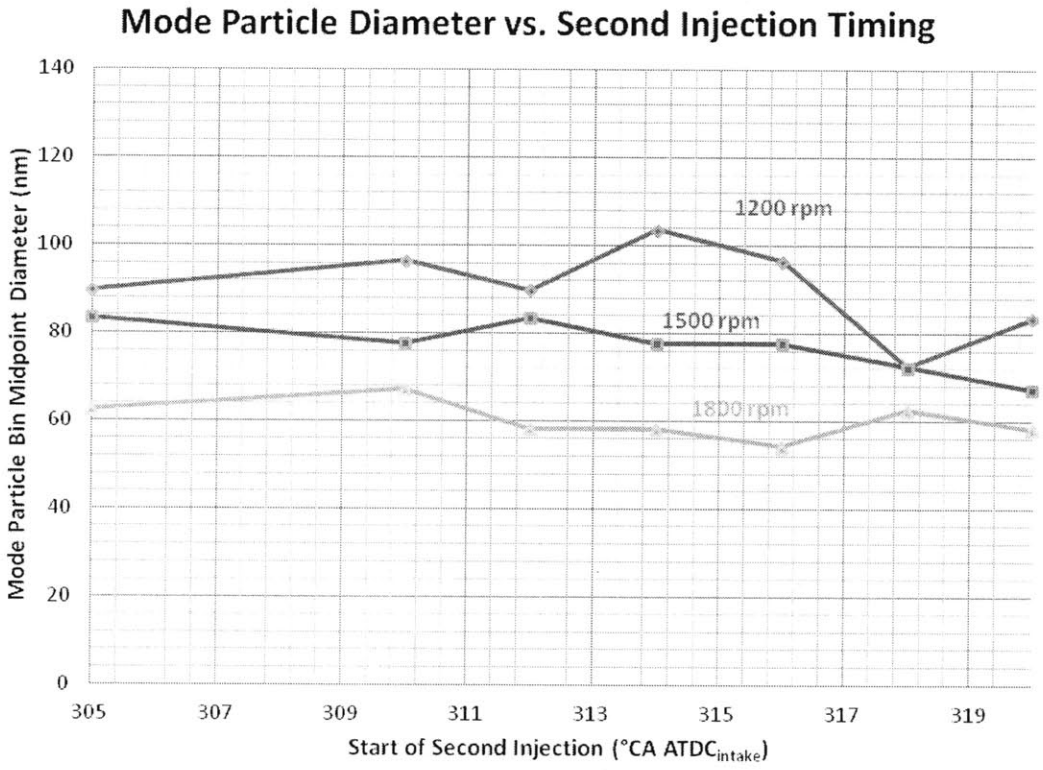

Figure 3-27: Mode Particle Diameter vs. SOI$_2$

3.1.4 Study of Fuel Effects

In order to test the fuel effects hypothesis relating to in-cylinder soot formation in DISI engines, the fuel injeection timing experiments were extended to consider additional fuels. The fuel injection timing experiments were chosen as the bases for the fuel component study because they offer a unique opportunity to examine the impact that the location and size of fuel films have on PM emissions. Blends of Haltermann HF0 437 gasoline with ethanol and toluene are considered in this series of experiments in order to examine the impact of alcohols and aromatics.

Impact of Fuel Composition on PM Emissions with Varied Single Injection Timing

To build upon the questions raised by observations of fuel film composition effects seen in the last section, experiments were performed to more carefully examine the effects of fuel composition on PM emissions in order to expand the investigation of the residual fuel effects hypotheses while also considering the fuel effects hypothesis. The sensitivity of PM emissions to aromatic and ethanol content were studied. Aromatic content is of interest as high boiling point aromatics have been shown to be a primary predictor of particulate emissions levels [67, 93] and aromatics, more generally, are widely understood as playing an important role in the formation of soot precursors [34]. Ethanol content is of wide interest due to the potential reductions in greenhouse gases associated with biomass-derived alcohol fuels, government mandates requiring ethanol to be blended in road fuels and the extended knock margins enabled by the higher octane number and enhanced charge cooling effect associated with ethanol blending in gasoline [62, 63]. Many studies of PM emissions with ethanol blending have been conducted. Some have found that poor mixing due to the high heat of vaporization of ethanol results in high carbonaceous content in soot [66], while others have identified "significant and obvious" reductions in in-cylinder soot formation attributed to ethanol content [54]. Many studies identify reduced particulate number emissions when using gasoline/ethanol blends [65, 78].

Aromatic Content In examining the sensitivity of PM emissions to fuel aromatic content, two different fuel blends were studied in addition to the baseline Haltermann HF0 437 gasoline fuel. The first is a blend of 15%, by volume, Toluene and 85% Haltermann gasoline, while the second is 30% Toluene and 70% Haltermann gasoline. The Haltermann HF0 437 fuel contains 28% aromatics, by volume.

Figure 3-28 displays the particle number concentrations measured in exhaust from the LNF engine operated at varied fuel injection timing for gasoline/toluene blends. It is seen that at early injection timings, the PN emissions with the gasoline/toluene mixtures are greater than those with the gasoline baseline, but, except at the earliest timings, there is little difference observed between the different gasoline/toluene blends. It is interesting to note that the PN emissions remain high at later injection timings than is seen with the gasoline baseline. The explanation for this is somewhat unclear, but it seems that the added aromatic content may support particle nucleation and surface growth despite smaller liquid fuel films. Also, as the SOI timing is retarded, the emissions increase at earlier SOI timings with gasoline/toluene blends than it does with neat gasoline. In these later SOI timings, more predictably, the PN emissions are seen to increase with increased toluene (aromatic) content. This should come as no surprise given the understanding of the importance of aromatics and PAH in soot nucleation and surface growth [34]. Note that there is little time for fuel to evaporate with late SOI timings.

Examining the particle size distributions with the addition of toluene, it is clearly seen that the addition of aromatic components to the fuel enhances the growth of soot particles, leading to larger mode bin mid-point particle diameters at early and late SOI timings, when piston crown fuel films are expected. This is shown in figures 3-29 and 3-31. Figure 3-30 shows the particle size distributions at a moderate injection timing, when the fuel spray is not expected to impinge on the piston crown surface. In this case, the particle number concentration increases with toluene content, but the size distribution otehrwise maintains a similar shape, though with an increased number of particles less than 20nm in diameter. This may be attributed to increased nucleation enabled by the presence of aromatic compounds, but with surface growth

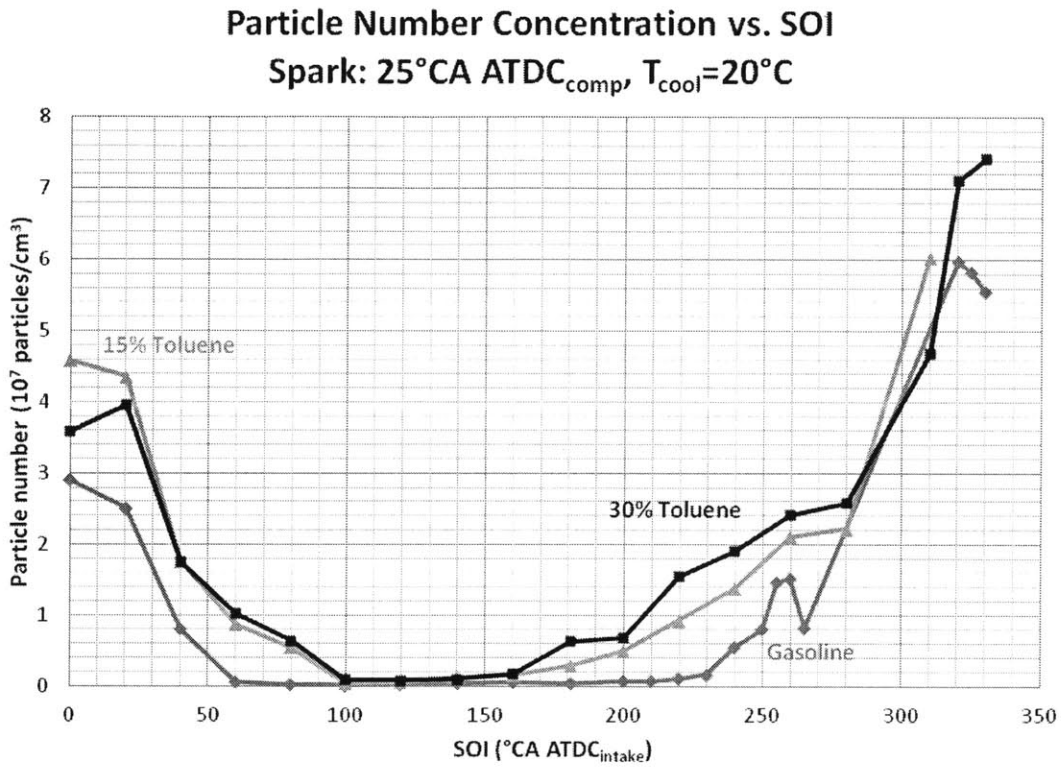

Figure 3-28: PM Emissions vs. SOI for Gasoline/Toluene blends

counter-acted by effective oxidation, since the mixture is likely more homogeneous in the situations without piston impingement.

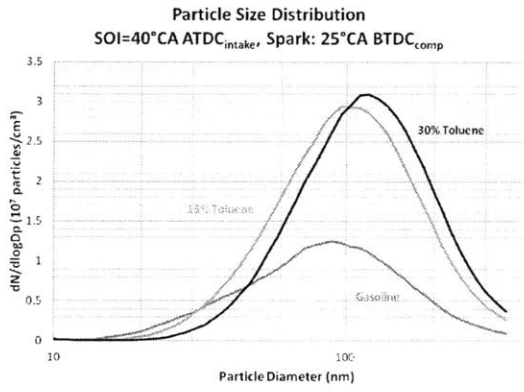

Figure 3-29: Early SOI

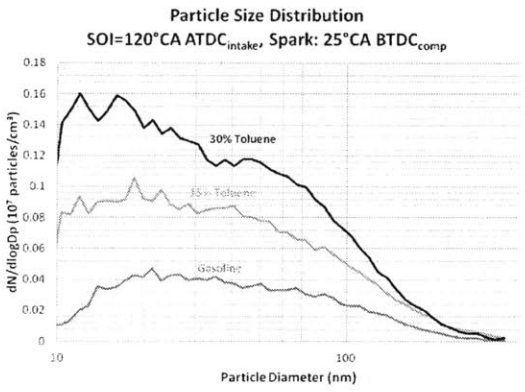

Figure 3-30: Moderate SOI

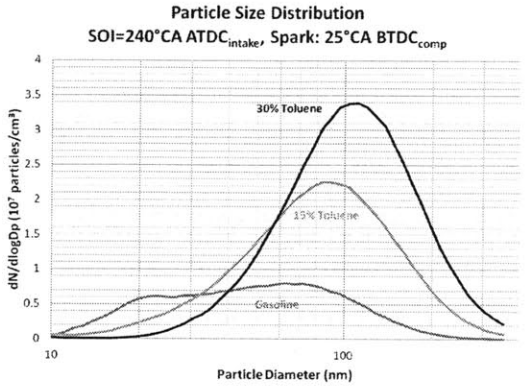

Figure 3-31: Late SOI

Ethanol Content The impact of ethanol content on PM emissions was studied in a similar way. Blends of 15% and 30% Ethanol, by volume, in Haltermann HF0 437 gasoline were considered. Figure 3-32 shows the particle number concentration in the engine exhaust versus the SOI timing.

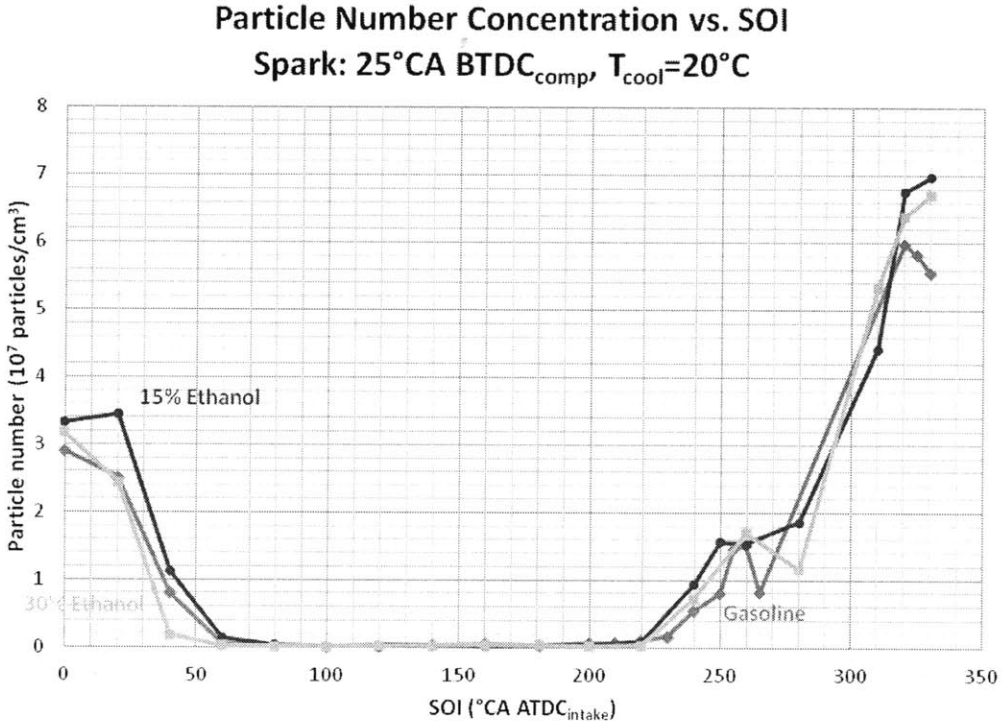

Figure 3-32: PM Emissions vs. SOI for Gasoline/Ethanol blends

The general trend is similar to that seen with neat gasoline - increased emissions at early and late SOI timings, when the fuel spray is expected to impinge on the piston crown. It is, however, difficult to make definitive statements about emissions magnitudes based on this plot, since the is some overlap in the data. Overall, there is little notable difference caused by the addition of ethanol to the fuel blend.

It is also instructive to look a the impact of ethanol content on particle sizes. Particle size distributions for the ethanol blends are plotted in figures 3-33, 3-34 and 3-35.

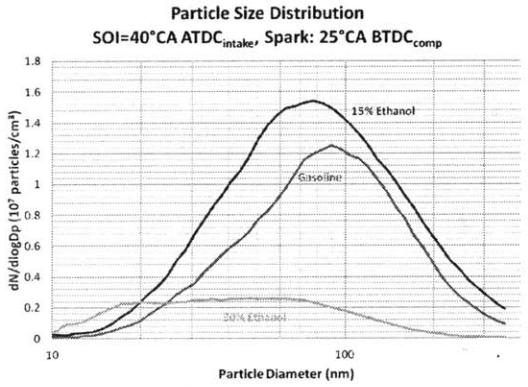

Figure 3-33: Early SOI

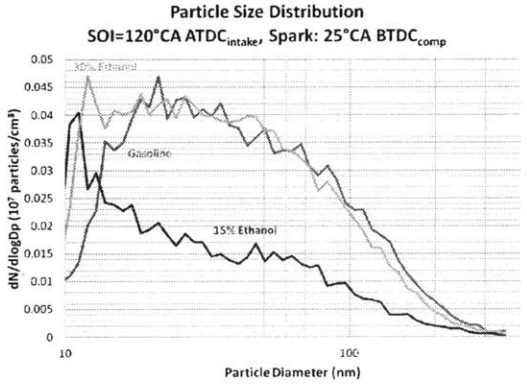

Figure 3-34: Moderate SOI

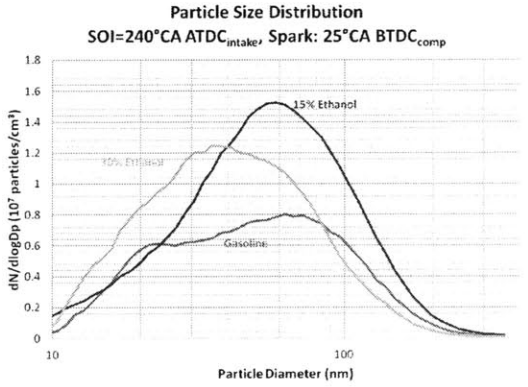

Figure 3-35: Late SOI

Examining these particle size distributions, it is difficult to draw any conclusions about the impact of ethanol content on particle number emissions, but there is some

valuable information in looking at the particle sizes. The mode bin mid-point diameter consistently decreases with increasing ethanol content. While the oxygen content is a potential culprit in smaller particles, it seems, instead, that the displacement of aromatic components from the base gasoline by ethanol likely limits the availability of soot precursors for particle surface growth, resulting in smaller particles.

Impact of Fuel Composition on PM Emissions with Dual Injection

Given the observations of increased particle size with increased coolant temperature, it seemed prudent to extend the study of second injection timing in order to test the fuel effects hypothesis in addition to the residual fuel effects hypothesis. The same fuel blends were used in this set of experiments as those used in the fuel composition investigation with a single injection. Unlike the examination of fuel effects in the single injection strategy, the sweeps of the start of second injection timing were completed at two different coolant temperatures (20°C and 80°C) for each fuel.

Aromatic Content Acetylenes and PAH are understood to play a key role in soot nucleation and surface growth [34, 35]. Since aromatic compounds provide a pathway to PAH formation during flames and pyrolysis [34], their impact on PM emissions are of interest, and the emissions sensitivity to aromatic content should be easily observed. This was, in fact, the case, especially in the 20°C coolant experiment. As is seen in figure 3-36, the particle number concentrations increase significantly with the addition of toluene in situations where low to moderate piston impingement is expected. In those cases with severe piston impingement or where the fuel spray interacts with the piston bowl, there remains only a slight increase in particle number concentration.

At early and moderate injection timings, it seems likely that the addition of aromatic content to the fuel has enabled increased particle nucleation, accounting for the increased numbers. At later injections, the severe piston wetting and anticipated large liquid films likely ensure enough liquid fuel and aromatic content in rich combustion regions arising from the films to form soot regardless of aromatic content,

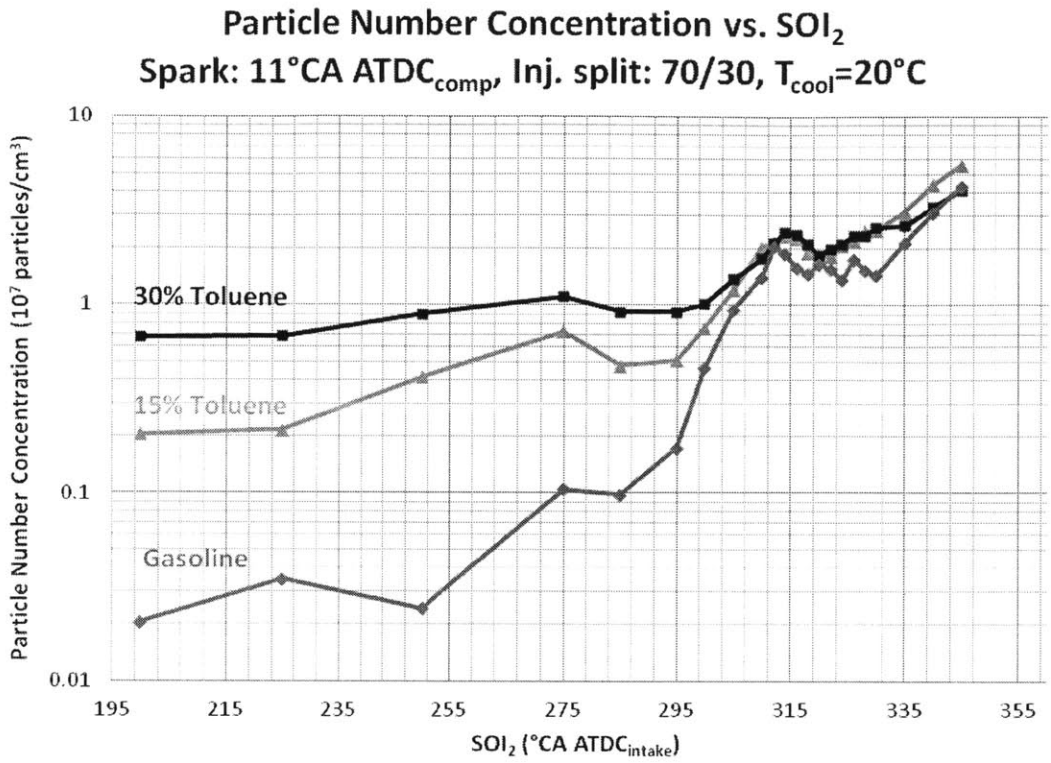

Figure 3-36: PM Emissions for Gasoline/Toluene Blends.

rendering the changes in aromatic content less consequential.

In addition to number, the size and composition of the PM emissions are of interest. For this study, the composition and morphology were not studied, but the size has been considered. These data do offer some insight into the impact of aromatic fuel components on the in-cylinder soot formation processes. Figures 3-37 and 3-38 illustrate the size distributions of PM emissions for gasoline and blends of gasoline and toluene at one early start of second injection timing and one late start of second injection timing, respectively. The early timing (200°CA ATDC$_{intake}$) plot is representative of a case with little if any fuel impingement on the piston surface and the late injection timing (330°CA ATDC$_{intake}$) plot is representative of a case with severe impingement of liquid fuel on the piston crown. In both cases, it is seen that the particle size distributions indicate that larger particles are emitted as the aromatic fraction of the fuel is increased. This is consistent with the idea that PAH can

contribute to soot particle surface growth, yielding larger particle diameters [34].

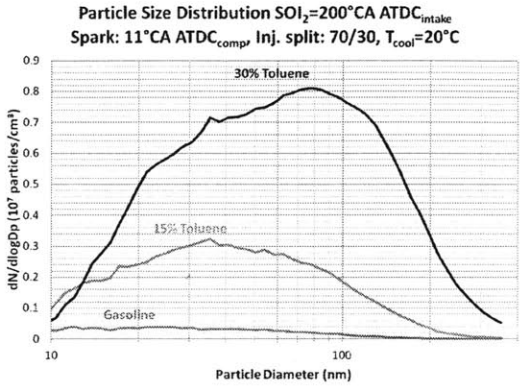

Figure 3-37: Early SOI, 20°C

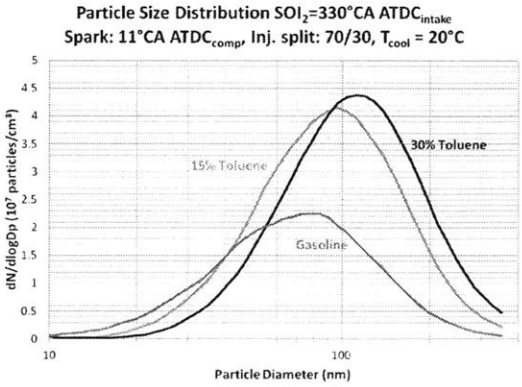

Figure 3-38: Late SOI, 20°C

At a coolant temperature of 80°C, the results look significantly different than those seen above. In the plot of particle number concentrations versus start of second injection timing shown in figure 3-39, there is a slight increase in emissions seen with the elevated aromatic content fuels at moderate SOI_2 timings, but, otherwise, there is little if any difference between the baseline gasoline emissions and the emissions for the gasoline/toluene blends. There is an explanation for this, but it is more easily outlined after examining particle size distributions associated with these data.

Figures 3-40 and 3-41 plot the size distributions for an early injection case with little expectation of piston impingement and a late injection expected to result in significant piston wetting, respectively. Here, it is seen that, unlike in the 20°C data presented above, there is very little difference in the particle size distribution based on toluene content. Instead, the size distributions are very uniform. This suggests that the same fuel components are taking place in the soot formation reactions, regardless of toluene content, indicating that the elevated coolant temperature has enhanced the evaporation of the volatile components in the gasoline blends, among which toluene is likely a part. This results in only the low-volatility fuel components remaining in liquid films or other poorly mixed regions. The implication that fuel does not evaporate uniformly comes as no surprise, but the fact that this selective evaporation related to component temperatures is reflected in the PM emissions offers strong

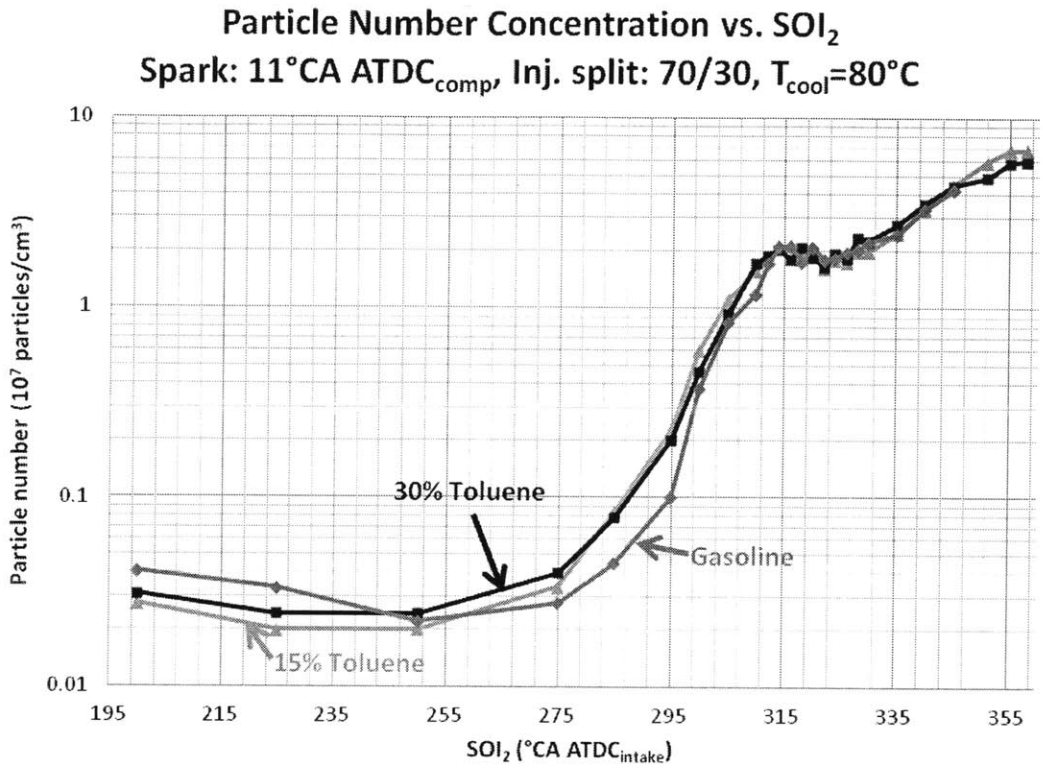

Figure 3-39: PM Emissions for Gasoline/Toluene Blends.

evidence that the engine surfaces play a key role in PM formation. This provides strong support for the residual fuel hypotheses being tested throughout this research programme.

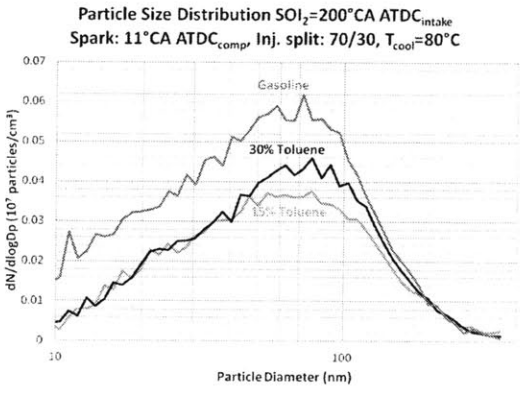

Figure 3-40: Early SOI, 80°C

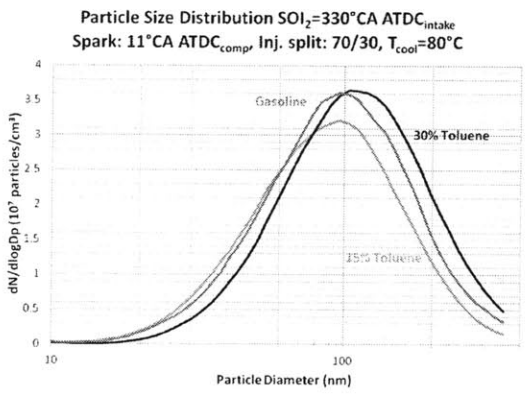

Figure 3-41: Late SOI, 80°C

Ethanol Content Studying the effects of ethanol content on PM emissions provides similar insight into the PM formation mechanisms taking place in DISI engines. Figures 3-42 and 3-43 show the total particle number emisisons (of diameters between 22.08nm and 365nm) versus second injection timing at coolant temperatures of 20°C and 80°C, respectively. It was observed that, at both operating temperatures, there was a decrease in emissions with the addition of ethanol at second injections later than 310°CA ATDC$_{intake}$. At earlier injections, the trends are unclear for the 20°C case , but, at coolant temperatures of 80°C, there is also a decrease in emissions with the addition of ethanol. The reason for the "spike" in particle number concentration for E30 blends at a second injection timing of 275°CA ATDC$_{intake}$ is not clear at this time.

The unusual behaviour at early second injection timings seen in the 20°C plot is attributed to unusual engine performance with the E15 blend at the low engine coolant temperature. The engine suffered from severe combustion instability at these injection timings and it was, thus, not possible to collect PM emissions data. No mechanical faults were identified with the engine to explain the unusual engine behaviour with E15 but not with E30.

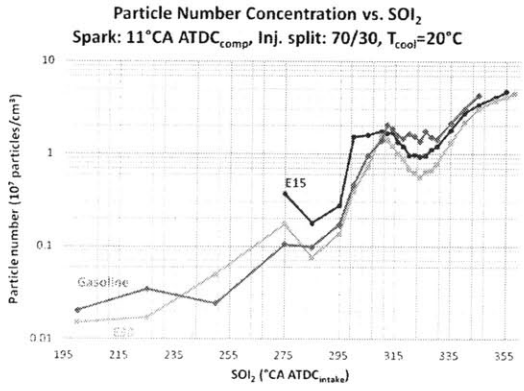

Figure 3-42: PM emissions at 20°C (Gasoline/ethanol blends)

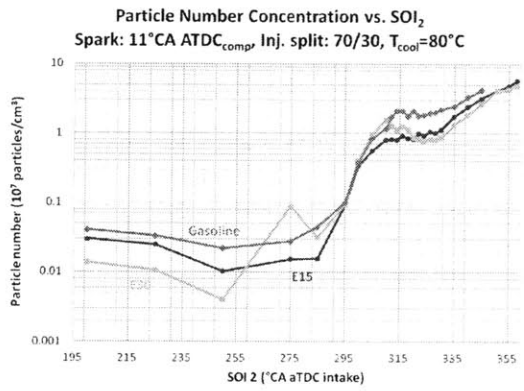

Figure 3-43: PM emissions at 80°C (Gasoline/ethanol blends)

In comparing the particle size distributions for the gasoline base fuel, E15 and E30 at an injection timing of 320°CA ATDC$_{intake}$ it is seen that the mode bin mid-point particle diameter decreases when ethanol is added to the fuel, though the difference

in size depending on the volume of ethanol blended is less clear (see figures 3-44 and 3-45). This is observation is consistent at coolant temperatures of 20°C and at 80°C. The addition of ethanol displaces a certain volume of gasoline including those highly-sooting compounds such as aromatics. Since ethanol has less propensity to soot than, for example, toluene or benzene [43], it is expected that the PM resulting from a blend of ethanol and gasoline will experience less efficient surface growth processes leading to smaller primary particles. The smaller size of primary particles would then lead to smaller agglomerates.

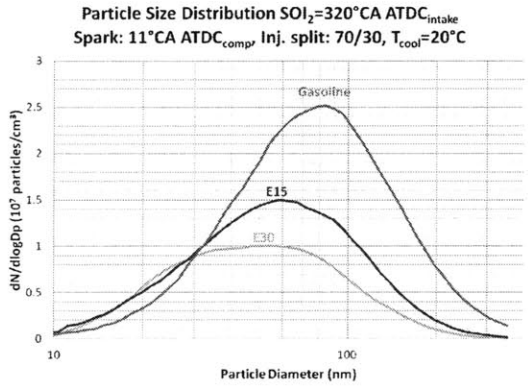

Figure 3-44: PM emissions at 20°C (Gasoline/ethanol blends)

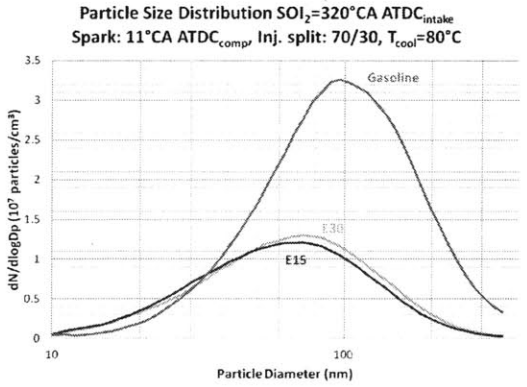

Figure 3-45: PM emissions at 80°C (Gasoline/ethanol blends)

It is also instructive to compare the size distributions for the individual ethanol blends at the two different operating temperatures. First, figures 3-46 and 3-47 show the particle number concentrations in the emissions with E15 and E30, respectively. In both figures, the data for 20°C and 80°C are plotted on the same axes. Apart from the strange response seen with E15 at early and moderate injection timings, there are few differences obvious when examining the plots. At late second injection timings, when significant piston wetting is expected, the plots are nearly identical.

The uniformity of the plots in figures 3-46 and 3-47 is somewhat surprising after examining the particle size distributions for the same data. For E15, size distributions are plotted at second injection timings of 320°CA ATDC$_{intake}$ and 345°CA ATDC$_{intake}$. These represent injection strategies with spray interaction with the piston bowl, and severe piston impingement, respectively. The data are plotted in figures

3-48 and 3-49.

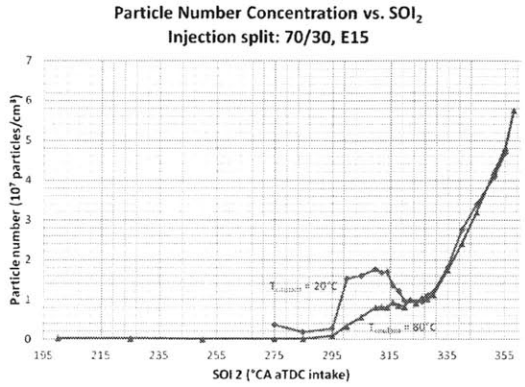

Figure 3-46: E15 PM Emissions

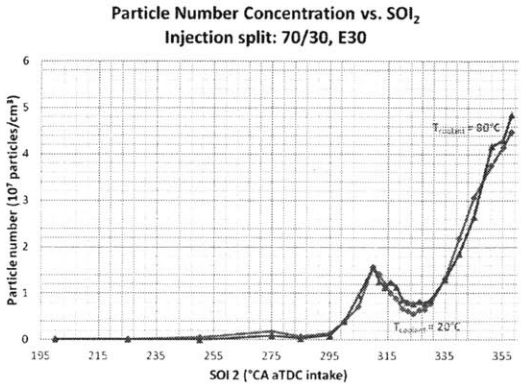

Figure 3-47: E30 PM Emissions

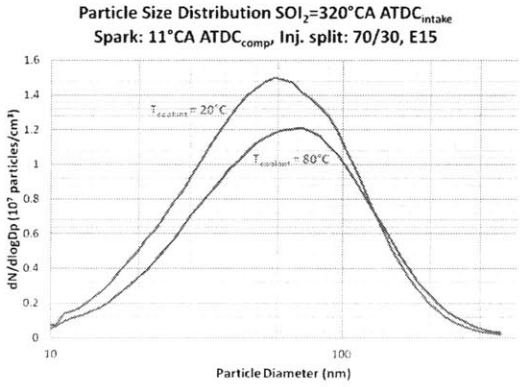

Figure 3-48: E15, SOI2=320°CA ATDC$_{intake}$

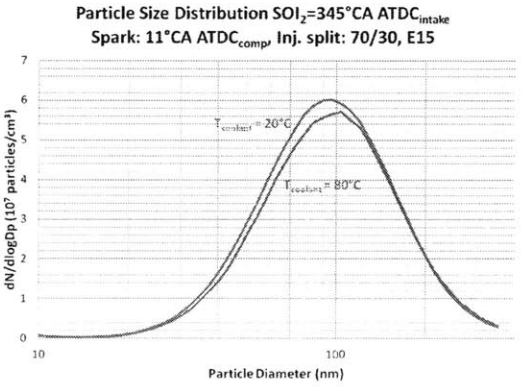

Figure 3-49: E15, SOI2=345°CA ATDC$_{intake}$

For E30, size distributions are plotted at second injection timings of 225°CA ATDC$_{intake}$, 320°CA ATDC$_{intake}$ and 345°CA ATDC$_{intake}$. These represent injection strategies with little or no piston crown impingement, spray interaction with the piston bowl, and severe piston impingement, respectively. Data at 225°CA ATDC$_{intake}$ were unfortunately not available for E15 fuels due to the unexpected poor combustion stability at cold coolant temperatures discussed earlier. The data for E30 are plotted in figures 3-50, 3-51 and 3-52.

The results shown in these size distributions may at first seem counter-intuitive. Eariler it was observed that particle diameters were smaller for ethanol blends com-

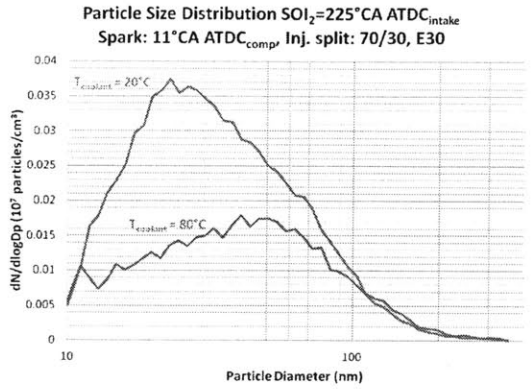

Figure 3-50: E30, SOI2=225°CA ATDC$_{intake}$

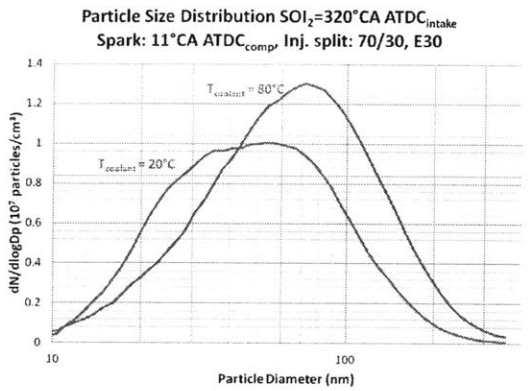

Figure 3-51: E30, SOI2=320°CA ATDC$_{intake}$

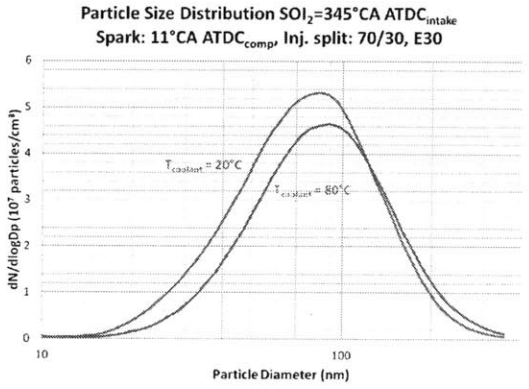

Figure 3-52: E30, SOI2=345°CA ATDC$_{intake}$

pared to the base gasoline. Further to this, one may expect that with increased coolant temperature, the mass of liquid fuel in-cylinder would decrease, leading to fewer particles and less mass for particle growth. However, when comparing the emissions for a particular ethanol blend at different operating temperatures, it was observed that the particle size actually increased with warmer coolant temperatures. The differences are. in some cases, slight, but it is clear that the mode bin mid-point diameters are higher at temperatures of 80°C than they are at 20°C. This observation was seen consistently across all ethanol blends and injection timings.

The explanation for this is really quite simple and provides strong support for the hypothesis that liquid fuel is responsible for PM emissions. As was seen with

toluene blending, at the elevated coolant temperatures, it is likely that ethanol is among the volatile components that evaporate quickly in-flight, or upon contact with cylinder surfaces. The result is that less volatile components, that may have a greater sooting propensity, are left behind. Thus, highly sooting components make up a larger fraction of the liquid fuel at coolant temperatures of 80°C than they do at coolant temperatures of 20°C. It has also been suggested that the evaporation of ethanol in this manner may actually inhibit the evaporation of the low-volatility, highly-sooting fuel components since ethanol's high latent heat of vaporization will lower the temperatures in the vicinity of the fuel films [67].

3.1.5 Fuel Volatility Investigation

Based on the study of the effects of fuel composition on PM emissions from DISI engines under a dual-injection, late spark timing operating condition, which revealed notable changes in emissions based on fuel composition that could be related to cylinder surface phenomena, it was decided that further study of fuel composition should be completed with a focus on volatility. In these experiments, the goal is not so much to identify the sooting propensity of fuels, but rather to further test the residual fuel effects hypothesis. In these experiments, a fuel mixture is created that possesses only two components: isooctane and isopentane. Isooctane represents the "low-volatility" component of the fuel while isopentane represents the "high-volatility" component. By increasing the isopentane fraction, the volatile fraction is increased. Relative to Isooctane, Isopentane is a very volatile hydrocarbon [94, 95] and it was expected that it would vaporize readily under typical in-cylinder conditions. By using a fuel made up of this very volatile fraction and a less volatile fraction, it was possible to modify the mass of liquid fuel participating in soot-producing phenomena. By conducting a simplified sweep of injection timing with a dual injection strategy, with varied volatile fractions (and, consequently, varied liquid masses) a straightforward test of the hypothesis of fuel films giving rise to soot formation was achieved. In addition to their volatilities, isooctane and isopentane were chosen because isooctane is a heavily-used fuel in internal combustion engine research and isopentane has a

similar sooting tendency with a significantly higher volatility [44].

A baseline experiment was conducted with neat isooctane to verify the PM emissions response to second injection timing with the single-component fuel. As always, the first injection was timed to start at 80°CA $ATDC_{intake}$ with the engine loaded to 2bar net IMEP at 1200rpm. The coolant was chilled to 20°C for all tests in the volatility investigation. As seen in figure 3-53, the trend observed for isooctane is very similar to that seen with gasoline, though the magnitude of the particle number concentration is significantly lower, except at extremely late injection timings.

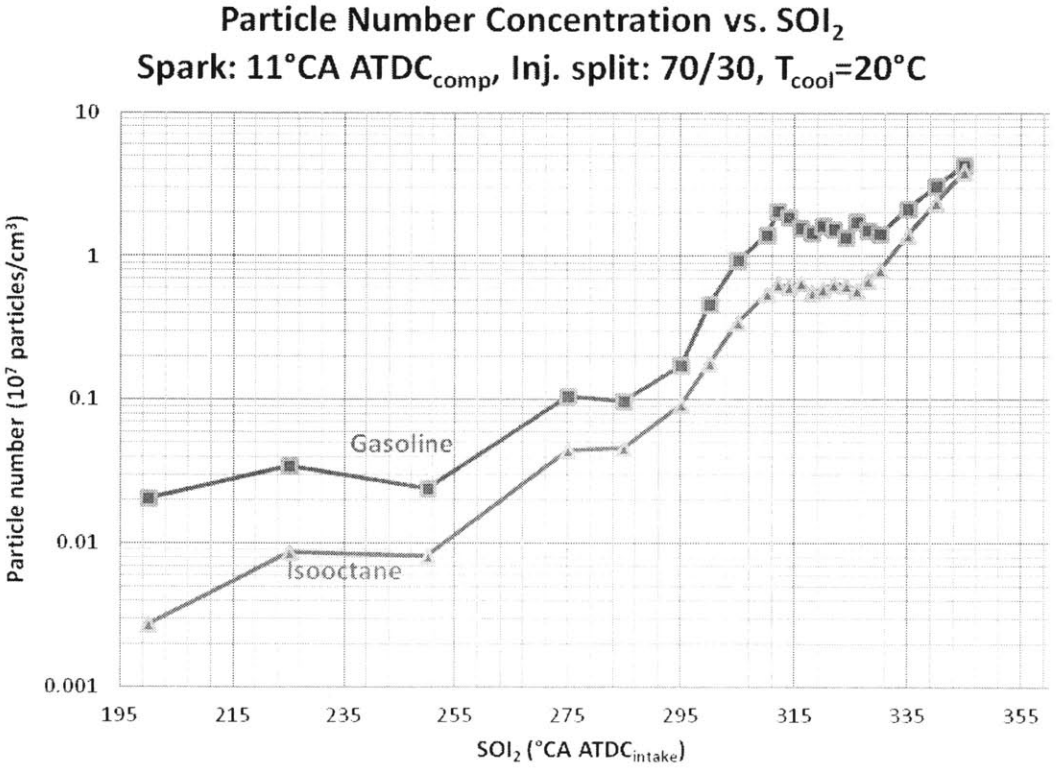

Figure 3-53: PN vs. SOI2 for Isooctane

Since it is a single component fuel, the size distributions for isooctane are more uniform with second injection timing than was seen for gasoline. The size distributions for isooctane are shown in figure 3-54, but the differences in the response to second injection timing between isooctane and gasoline are more clearly seen in figures 3-55 and 3-56, where extremely late SOI_2 timings are omitted. Here it is

observed, firstly, that the particle diameters with isooctane are substantially smaller than those seen for gasoline fuel. This is not surprising considering the paraffinic nature of issoctane. The pathway to producing acetylene and PAH (and, consequently, soot) is more complicated beginning with a paraffin than it is beginning with a fuel containing aromatic components [6]. Secondly, it is seen that while there is some increase in diameter with moderate injection timings, and a slight decrease again when the injection timing leads to interactions between the fuel spray and the piston bowl, the changes in mode bin mid-point diameter are less pronounced than they are with gasoline.

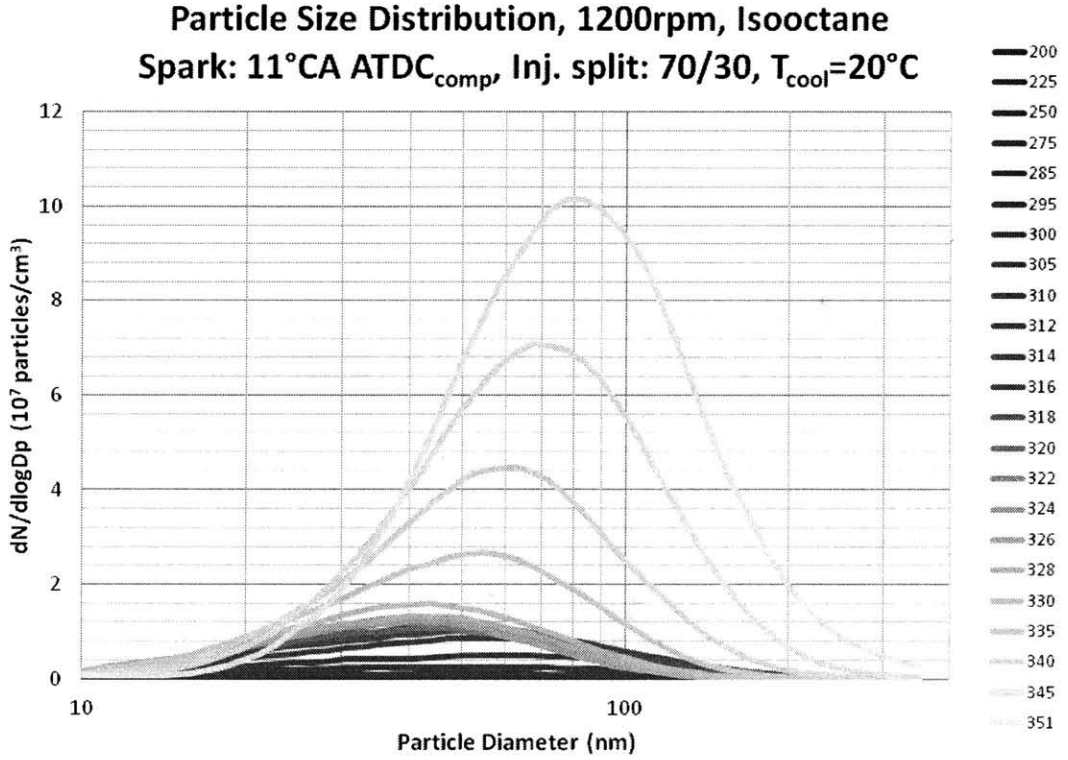

Figure 3-54: Particle Size Distributions for Isooctane

Using the isooctane emissions measurements as a baseline, particle number and size data were collected for blends of 10%, 20%, 30% and 40% isopentane, by volume. If the hypothesis of soot formation originating form liquid fuel on cylinder surfaces (primarily the piston crown) holds, then it stands to reason that the particulate

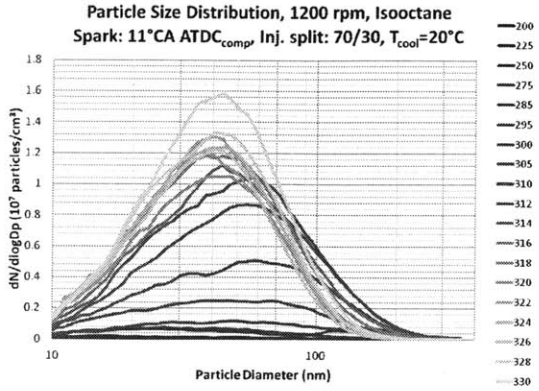

Figure 3-55: Isooctane
(Late SOI_2 omitted)

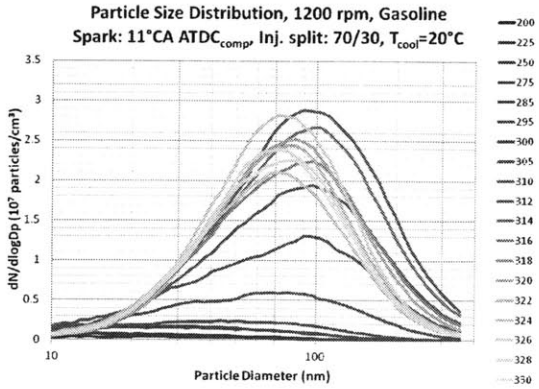

Figure 3-56: Haltermann HF0 437
(Late SOI_2 omitted)

number emissions should decrease corresponding to decreased fuel film mass and size, as caused by the evaporation of ispoentane. Data were collected for a single injection at 80°CA $ATDC_{intake}$ and under dual-injection conditions with the first injection timed to begin at 80°CA $ATDC_{intake}$ and the start of the second injection at 225, 295, 310, 320, 330 and 340°CA $ATDC_{intake}$. This set of second injection timings provides data points in each of the fuel wetting configurations of interest. As shown in figure 3-57, the typical trend for particle number concentration versus second injection timing is still captured in this simplified sweep of second injection timing. The differences in emissions are not exceptionally stark, but it should, nevertheless be apparent that, especially during those conditions with piston impingement, the particle number concentration decreases with the addition of isopentane.

To more clearly illustrate the changes in emissions with increasing isopentane fraction, in figures 3-58, 3-59 and 3-60 the particle number concentration in the engine emissions are plotted against the isopentane fraction for each injection timing. For a single injection, or dual injection strategy with early second injection, the decrease in emissions is fairly rapid with the addition of isopentane. At these injection timings, there may be some impingement on the liner (as evidenced by observed oil dilution with fuel), but it seems unlikely that there would be significant impingement on other surfaces such as the piston crown, which tends to produce elevated PM emissions. In this case, instead of relying on reduced film sizes, it may be that the bulk of the

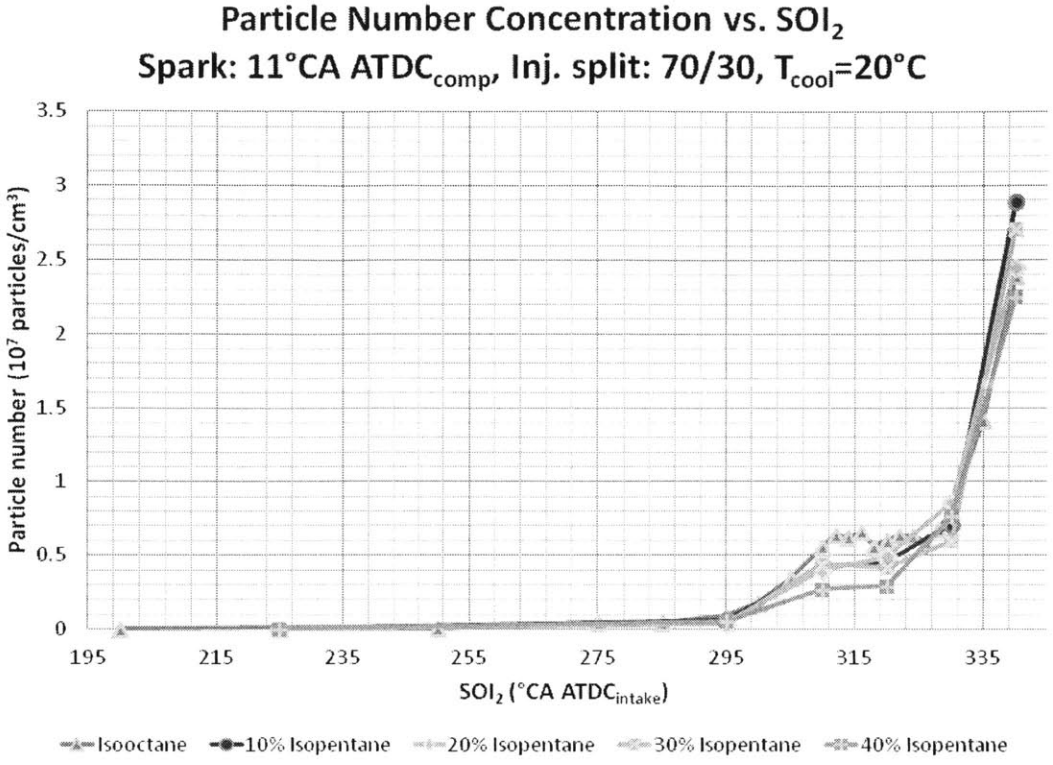

Figure 3-57: Particle Number Emissions for Isopentane/Isooctane Mixtures

soot is formed in rich (or droplet-containing) regions in the bulk cylinder gases. The differential in volatility between isopentane and isooctane may enhance evaporation of the entire mixture since the evaporation of isopentane may cause fuel droplets to break-up more quickly, further enhancing evaporation.

At moderate second injection timings, when the fuel spray is expected to interact with the piston bowl, it seems that the main fuel effects hypothesis holds. The reductions in particle number concentrations track reasonably closely with the isopentane fraction in the fuel mixtures. To reiterate, in this situation, isopentane should evaporate readily, either in-flight or after contacting the relatively hot piston crown surface, leaving behind only isooctane in the liquid state. Thus, the volume of liquid fuel in piston crown films will decrease in proportion to the isopentane fraction. This is best illustrated for the injection timing of 320°CA ATDC_{intake}, where there is a 50% decrease in emisisons with a 40%, by volume, mixture of isopentane and isooctane.

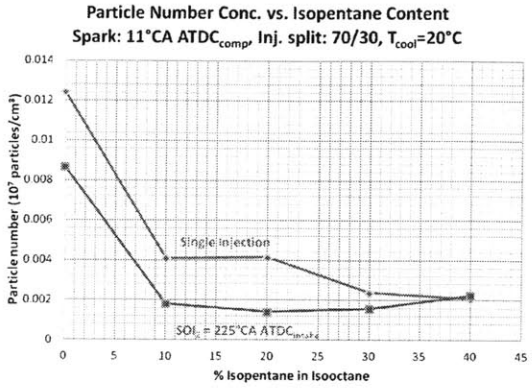

Figure 3-58: Early Injection

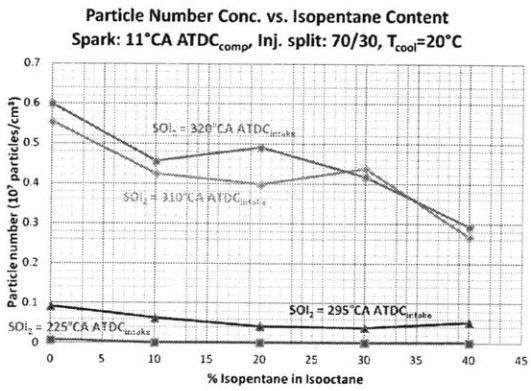

Figure 3-59: Moderately Late Injection

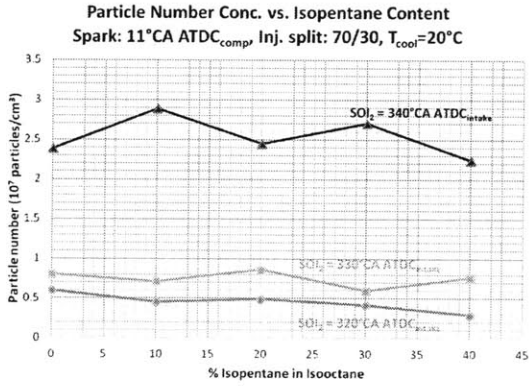

Figure 3-60: Late Injection

Examining the particle size distributions, with varied fuel content at each injection timing studied, shown in figures 3-61 through 3-67, it is observed that, with the exception of the second injection timing of 225°CA ATDC$_{intake}$, the particle size distributions are remarkably consistent in shape, with reasonably uniform mode bin mid-point diameters among fuel blends at each injection timing point. This suggests that the particulates being emitted have a common fuel origin. In this case, given the evaporation properties of the fuel, it is known that the particles are originating from isooctane. At an injection timing of 225°CA ATDC$_{intake}$, for neat isooctane, the particle size distribution displays a shape different from the isopentane/isooctane blends. The cause of this is not immediately clear. It seems that there may have been a measurement fault, perhaps an unobserved change in dilution ratio during the

SMPS scan.

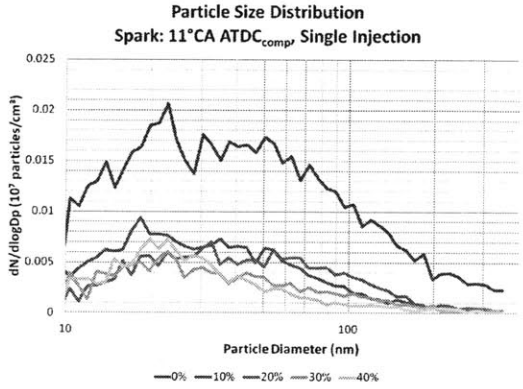

Figure 3-61: Single Injection

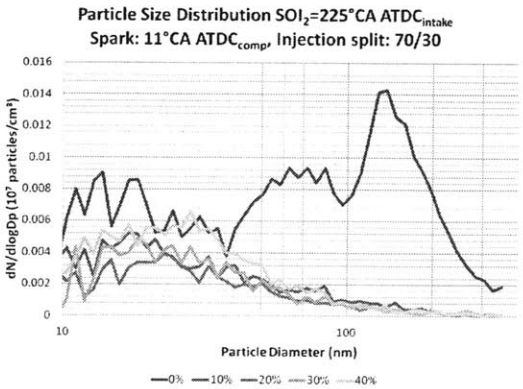

Figure 3-62: SOI_2=225°CA $ATDC_{intake}$

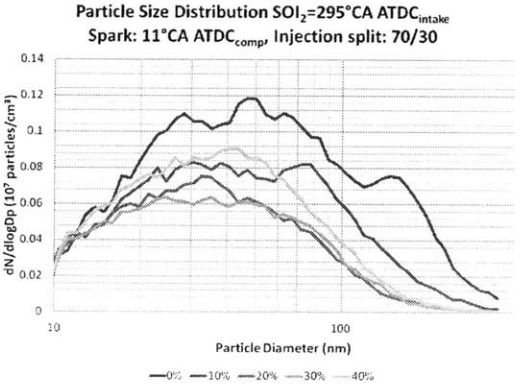

Figure 3-63: SOI_2=295°CA $ATDC_{intake}$

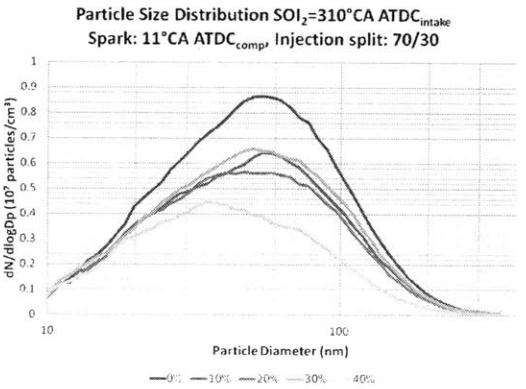

Figure 3-64: SOI_2=310°CA $ATDC_{intake}$

This study of fuel volatility, in a situation where there is expected to be a stratification of fuel composition, meaning that the liquid fuel is expected to be of a single component, provides further evidence in support of the residual fuel effects hypothesis. These data demonstrate the reduction in PM emissions associated with a decreased presence of liquid fuel in-cylinder. They further confirm the more general hypothesis that liquid films on cylinder surfaces are important in the formation of particulate matter.

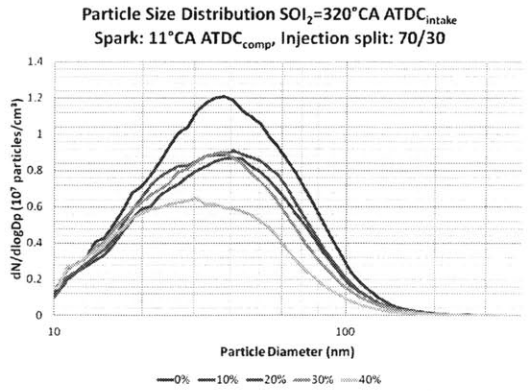

Figure 3-65: SOI_2=320°CA $ATDC_{intake}$

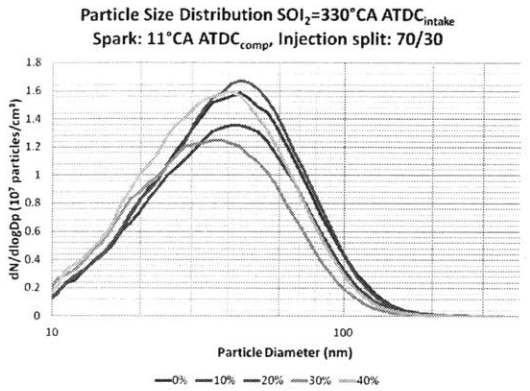

Figure 3-66: SOI_2=330°CA $ATDC_{intake}$

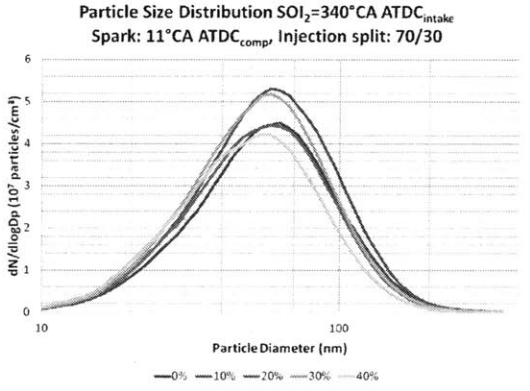

Figure 3-67: SOI_2=340°CA $ATDC_{intake}$

3.1.6 Effects of Burned Gas Oxygen Content

The results presented thus far affirm the basic statement outlined in the residual fuel effects hypothesis suggesting that PM originates in combustion events involving liquid fuel present on cylinder surfaces. The hypothesis, however, also proposes some details of the physical characteristics of soot-producing reactions. Specifically, it was suggested that the soot-producing reactions do not take place in a pool fire or diffusion flame as these concepts are traditionally understood. The term "diffusion flame" describes a flame in which the rate of fuel consumption is determined by the rate at which fuel and oxygen are brought together in proportions that support a reaction [43]. The term "pool fire" simply describes a diffusion flame in which the fuel is in a pool of liquid. Generally, when discussing diffusion combustion, the

combustion reactions occur in an interface between air and fuel where the fuel mixes with fresh air (or another oxygen-rich oxidizer) as the reaction is taking place. Since it can be demonstrated that liquid fuel films are supplying the fuel for soot-forming reactions, it seems likely that a mixing process between oxidizer and the evaporating fuel largely determines the rate of the reaction. The nature of the oxidizer is where it is hypothesized that the soot-producing reactions in a DISI engine depart from the traditional understanding of diffusion combustion. The combustion of fuel films, as demonstrated by Costanzo et al. [52] occurs after the main combustion event. This is a critical observation, as it indicates that the "oxidizer" is likely made up of burned gases with very low oxygen concentrations. This idea forms the second part of the residual fuel effects hypothesis, suggesting that soot is formed in reactions between fuel vaporizing from films and burned gases.

In order to test this aspect of the residual fuel effects hypothesis, the burned gas oxygen content experiment was completed. In this experiment, the engine was primarily fuelled with liquid gasoline (Haltermann HF0 437), but the mixture was further enriched through the addition of propane to the inlet air. By running the engine with a constant rate of liquid fuel injection, then enriching the mixture with propane, it was possible to observe the impact of burned gas oxygen content on the formation of particulate matter, with the goal of testing the hypothesis that soot formation occurs in a reaction between fuel and oxygen from burned gases. Maintaining a constant rate of liquid fuel injection ensures that the liquid fuel phenomena do not change with the equivalence ratio and, thus, the size of liquid films and mass of liquid in-cylinder should remain constant, providing a true measure of the impacts of residual oxygen rather than results confounded by changes in fuel impingement. Propane was used as the enriching fuel for two reasons. Firstly, as a gaseous fuel injected upstream of the compressor, it will be well-mixed, ensuring there is no stratification producing regions rich in propane. Secondly, propane has a low sooting propensity [43], so any changes in PM emissions can be attributed to changes in the reactions involving gasoline components.

The experiment was repeated twice, once with a fuel-lean baseline operating condi-

tion and once with a stoichiometric baseline operating condition. For each of these experimental methods, the experiment was repeated at three different injection timings: a single injection at 40°CA ATDC$_{intake}$, a single injection at 100°CA ATDC$_{intake}$ and a dual injection strategy with the 70% of the liquid fuel injected at 80°CA ATDC$_{intake}$ and 30% of the liquid fuel injected at 320°CA ATDC$_{intake}$. The fraction of the total fuel that was liquid, in terms of the heating value, is outlined for the various experiments in table 3.1. The maximum value of the liquid fuel contribution to the total heating value corresponds to the baseline case with no propane enrichment. The minimum value corresponds to the maximum propane enrichment case.

Table 3.1: Liquid Fuel Contribution to Mixture Heating Value (%)

	Lean Baseline		**Stoichiometric Baseline**	
	Max	Min	Max	Min
SOI = 40°CA ATDCintake	100	84	100	85
SOI = 100°CA ATDCintake	100	84	100	85
SOI = 80/320°CA ATDCintake	100	83	100	87

The single injection at 100°CA ATDC$_{intake}$ case represents an operating condition with good mixing and little, if any, liquid fuel impingement. The early single injection case represents an operating condition with severe pison impingement. It is expected that the volume of fuel hitting the piston will be quite large, but there is some time for evaporation and mixing. The dual injection case represents operating conditions with the fuel spray interacting with the piston bowl, as would be the case in a partially-stratified, late spark timing catalyst light-off operating condition. In this case, fuel is injected with the piston very close to the injector tip, with little time for evaporation and mixing before ignition.

The data for the lean baseline experiment are shown in figure 3-68. Here it is seen that the particle number concentration increases as the mixture is enriched by propane. This is especially obvious for the cases with piston impingement. There is an increase with equivalence ratio for the moderate single injection case as well, but it is not very pronounced on this plot due to the relatively low magnitude of the particle number concentrations. These observations suggest that the reduction in oxygen in

the burned gases does indeed increase the rate of soot production. The fact that there are no abrupt changes in the soot formation rate (for example, at the stoichiometric condition) suggests that, as hypothesized, soot formation is not determined by the global cylinder equivalence ratio, but rather by the local equivalence ratio in regions surrounding fuel films.

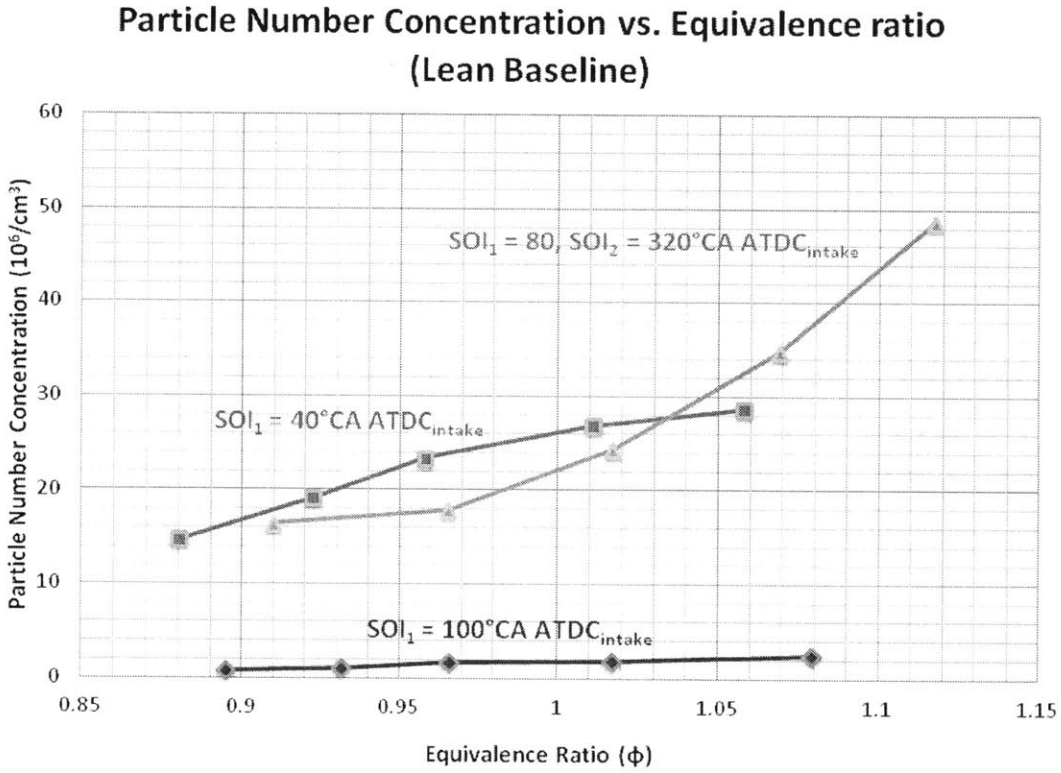

Figure 3-68: PN vs. ϕ (Lean Baseline)

Figure 3-69 plots the data from the stoichiometric baseline experiments. Similar to the results from the lean baseline experiment, it was found that PM emissions tend to increase with increasing equivalence ratio. The single injection timing at 100°CA ATDC$_{intake}$ again produces emissions at a much lower magnitude than those seen in the cases with piston wetting. The single injection timing at 40°CA ATDC$_{intake}$, in this experiment, did not display the increase in emissions seen in the lean baseline experiment. Here, instead, it is not possible to identify a significant trend. If anything, it seems that the emissions remain relatively stable. On its own, this ex-

periment offers no insight beyond that derived from the lean baseline experiment. When plotted on the same axes as the results from the lean baseline case (see figure 3-70), however, these data provide further support for the idea that local (not global) mixture properties determine the likelihood of soot formation. This is because, even beginning with a different baseline (though the same rate of liquid fuel injection) the trends remain reasonably consistent, with no abrupt changes when transitioning from lean to rich combustion.

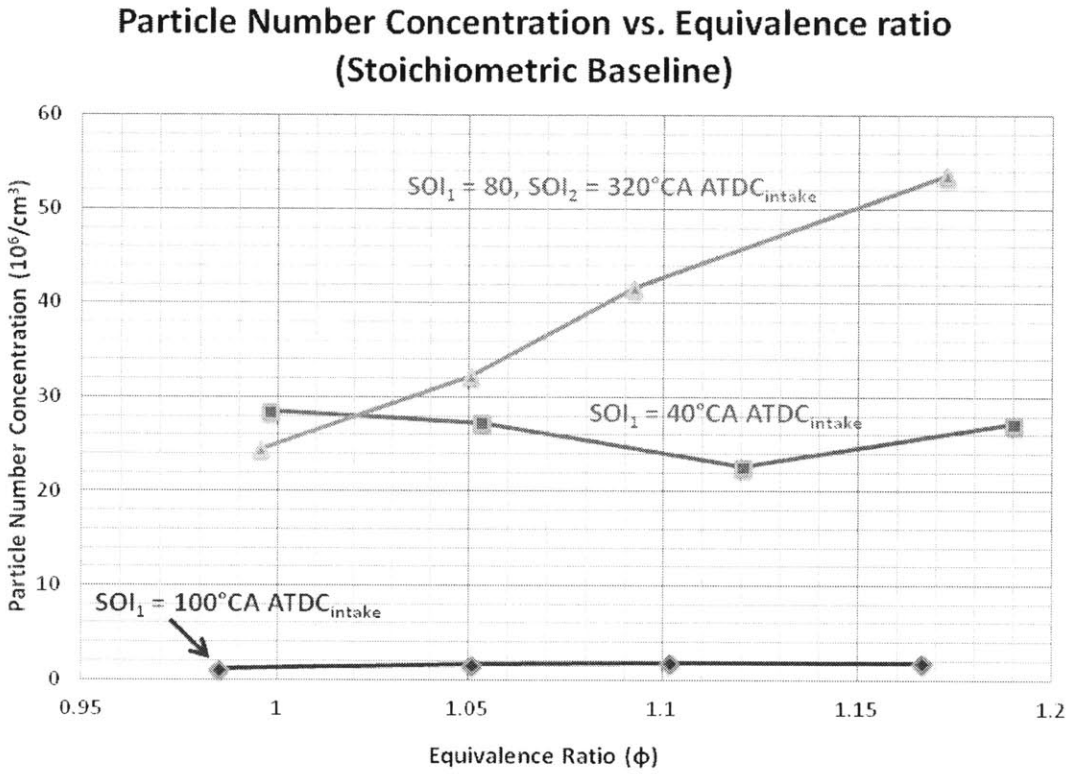

Figure 3-69: PN vs. ϕ (Stoichiometric Baseline)

The particle size distributions for the lean baseline case are plotted in figures 3-71, 3-72 and 3-73. It is seen in all three of these plots that the size distributions remain uniform, with consistent mode bin mid-point diameters and overall shapes. Of course, the particle number emissions do increase in magnitude, extending the size distribuiton upward as the mixture is enriched. The implication from these data is that the particles all form following the same process, involving the same fuel

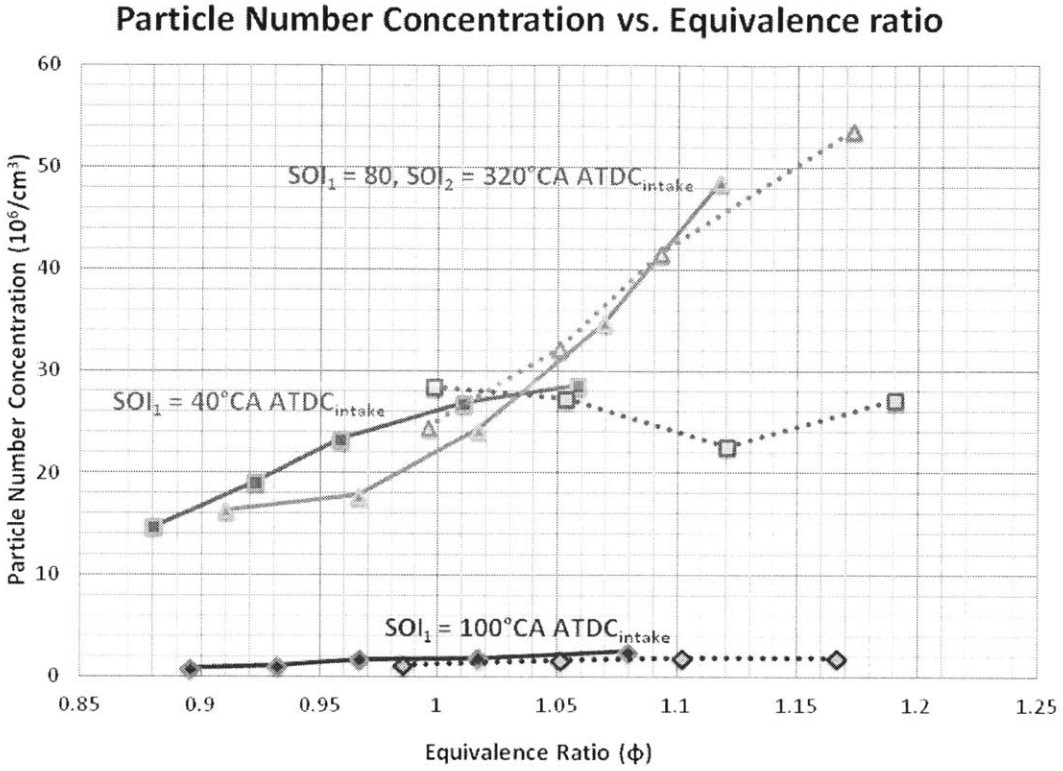

Figure 3-70: PN vs. ϕ (Overview)

components. This means that the PM emissions are affected by the change in oxygen content, not by changes in evaporation and mixing processes. This suggests that this experiment was successfully implemented and that the reactions leading forming soot do indeed occur with residual gases.

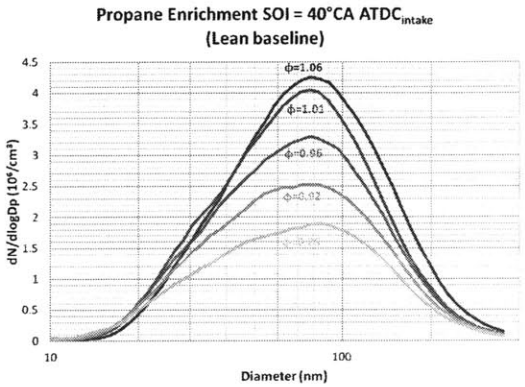

Figure 3-71: SOI=40°CA ATDC$_{intake}$

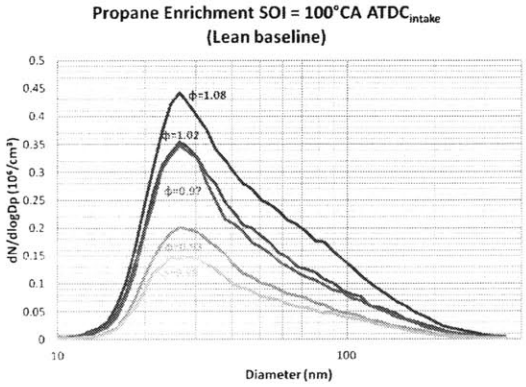

Figure 3-72: SOI=100°CA ATDC$_{intake}$

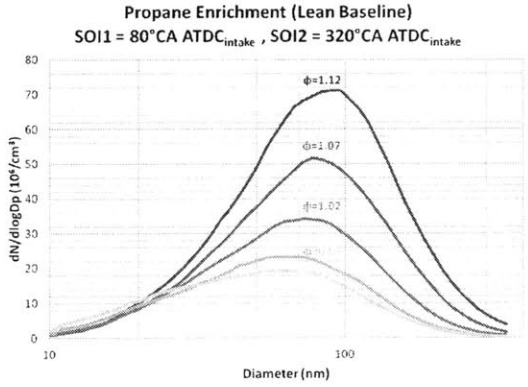

Figure 3-73: SOI$_2$=320°CA ATDC$_{intake}$

3.1.7 RCM Study of Fuel Effects

In the engine-based experiments, there were a number of investigations involving fuel composition. It was observed that with added aromatic content and a cold engine, particulate matter emissions increased and particle sizes increased. It was also found that smaller particles were emitted with blends of ethanol and gasoline. The most instructive aspect of the engine-based fuel composition investigations, however, came along with the combination study of blended fuels and warmed-up coolant temperatures. In this case, it was possible to attribute changes in emissions to the interaction of fuel and cylinder surfaces. This provided strong support for the residual fuel effects hypothesis, but it did little to strengthen support for the fuel effects hypothesis.

Existing studies have done a good job of quantifying the sooting propensity of fuels in the form of a PM index, so, the idea that different fuels will result in soot formation at different equivalence ratios already enjoys reasonably strong support [68, 69, 93]. It was, however, desired to conduct a simple experiment to verify the broad trends seen in the engine studies, while avoiding the complications associated with surface temperatures and injection properties. If, as outlined in the residual fuel effects hypothesis, the PM is formed in regions of rich mixture surrounding fuel films, using the RCM with rich mixtures was seen as a possible method of examining soot formation under rich combustion without the complications associated with engine combustion.

In order to ensure the results from the RCM were relevant to engines, an attempt was made to match the temperatures and pressures at the end of the RCM compression event with values that might realistically be seen by the end-gas in a modern DISI engine. The conditions of the end-gas are of interest because, if the residual fuel effects hypotheses are correct, then the soot-producing reactions in an engine will occur near the cylinder walls or piston-crown, likely toward the end of the combustion event. A simple first-law model was used to estimate the temperature and pressure of the unburned gas toward the end of the combustion event. For a 1200rpm, 2bar

gross IMEP operating condition, it was estimated that pressures of 8bar and temperatures of 720K would be experienced by the end-gas. This value was used as a rough starting point for the RCM study. As described in Chapter 2, the temperatures and pressures after compression were specified by tuning the argon to nitrogen ratio in the synthetic air mixture.

The cylinder pressure and light intensity are the only data recorded during the RCM experiment. From the light intensity data, the soot volume fraction and soot yield can be calculated. The pressure data can be used to estimate the cylinder temperatures and volume using the adiabatic core hypothesis of isentropic compression in the mixture outside the boundary layer which surrounds the RCM surfaces [96]. Before further calculations were completed, both the pressure and the light intensity data were filtered to eliminate the high-frequency noise associated with the mechanical vibrations generated during the firing sequence. As an example, pressure and light transmission data are plotted in figures 3-74 and 3-75, respectively. These data were collected for a fuel blend of 20% (by volume) toluene in Haltermann HF0 437 with an equivalence ratio of 2.7, a target compression temperature of 750K and a target mixture density of 0.14kmol/m^3.

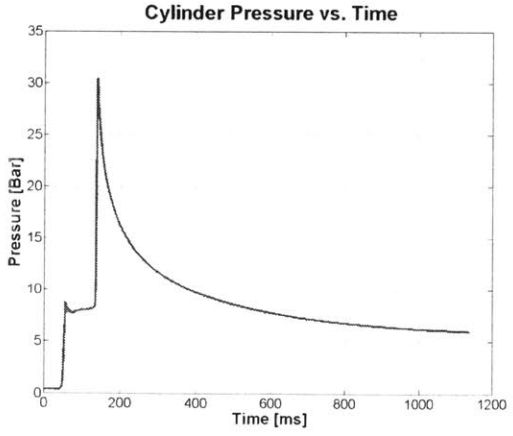

Figure 3-74: Cylinder Pressure

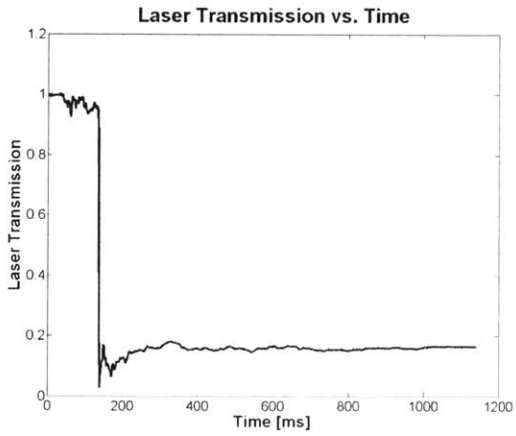

Figure 3-75: LASER Transmission

As is seen in figure 3-74, after the initial compression, there is a short ignition delay, followed by a steep increase in pressure corresponding to the combustion event. The decrease in pressure in the remainder of the recorded data is due to heat transfer to

the RCM walls and likely some leakage past the piston seals. The light intensity data shown in figure 3-75 show a steep decrease in intensity coinciding with the combustion event. This indicates that soot has formed in-cylinder. Following the steep decrease is a very modest rebound in intensity. This corresponds to the oxidation of a fraction of the soot that was initially formed. The intensity data plotted here are normalized by the average of the first 100 data points.

From the light intensity data, the soot yield was calculated. Figure 3-76 plots the soot yield versus experiment time for this example case. The shape is essentially the inverse of the light intensity chart. The soot yield increases rapidly coinciding with the combustion process. This is then followed by a decrease, corresponding to soot oxidation, before reaching a steady value. For the purposes of these experiments, it is this steady-state value that is of interest. For each experimental point, the steady-state attenuation is measured and is used in the determination of the equivalence ratio threshold for soot formation, which was defined as the equivalence ratio at which the attenuation is equal to or greater than 50%.

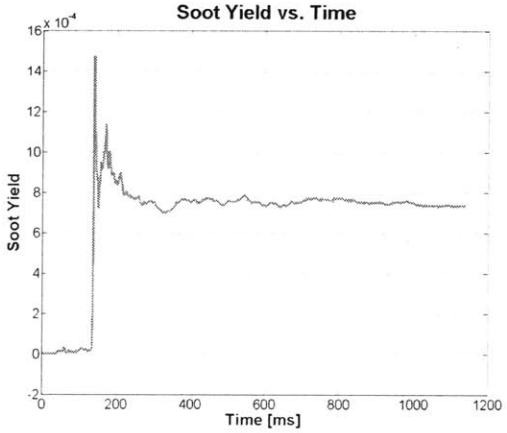

Figure 3-76: Soot Yield

By recording the attenuation percentage as the equivalence ratio is gradually enriched, an s-shaped attenuation curve can be plotted. The curve asymptotically approaches unity as the mixture is enriched. It is on this curve that the threshold may be identified. Interpolation is used to estimate the equivalence ratio at an attenuation of 50%. Figure 3-77 plots the attenuation curve for the baseline gasoline

fuel at a target compression temperature of 695K and a target mixture density of 0.14 kmol/m^3. In this case, the threshold equivalence ratio, following the simplified definition, is found to be approximately 2.65.

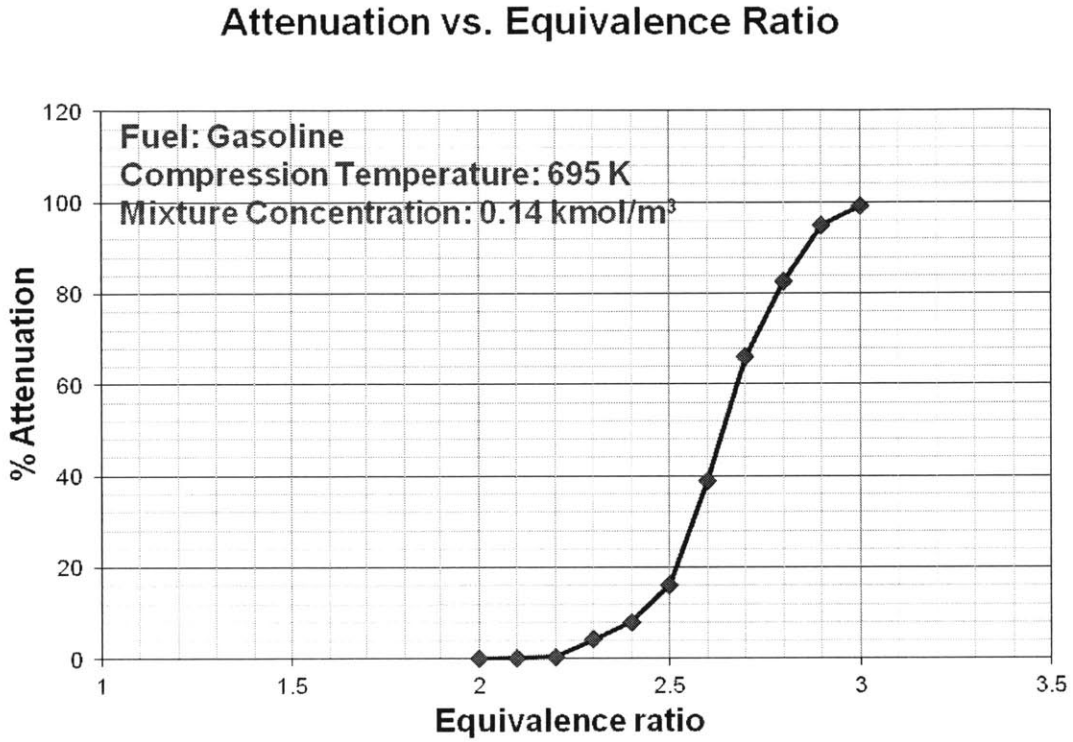

Figure 3-77: Light Attenuation vs. Equivalence Ratio

The attenuation data are useful for identifying trends in fuel PM formation characteristics, but they are not particularly useful in actually understanding the more fundamental ideas behind soot formation. In that case, calculating the soot yield based on the attenuation data provides a more valuable measure of soot formation. Figure 3-78 plots the soot yield versus the equivalence ratio for the same data as those shown in figure 3-77. These data offer a better representation of the impact of equivalence ratio on PM emissions. Here, there is no asymptotic approach toward a saturation value. Instead, the soot yield appears to continue increasing with increased equivalence ratio. In the context of a real engine, this is important to note, since poor mixing may result in regions of mixture that are significantly more rich than the global

cylinder equivalence ratio. Given that the soot formation potential increases quite significantly as the mixture is enriched, it is important to avoid such regions, be they caused by evaporating liquid films, or stratification due to poor charge motion and mixing.

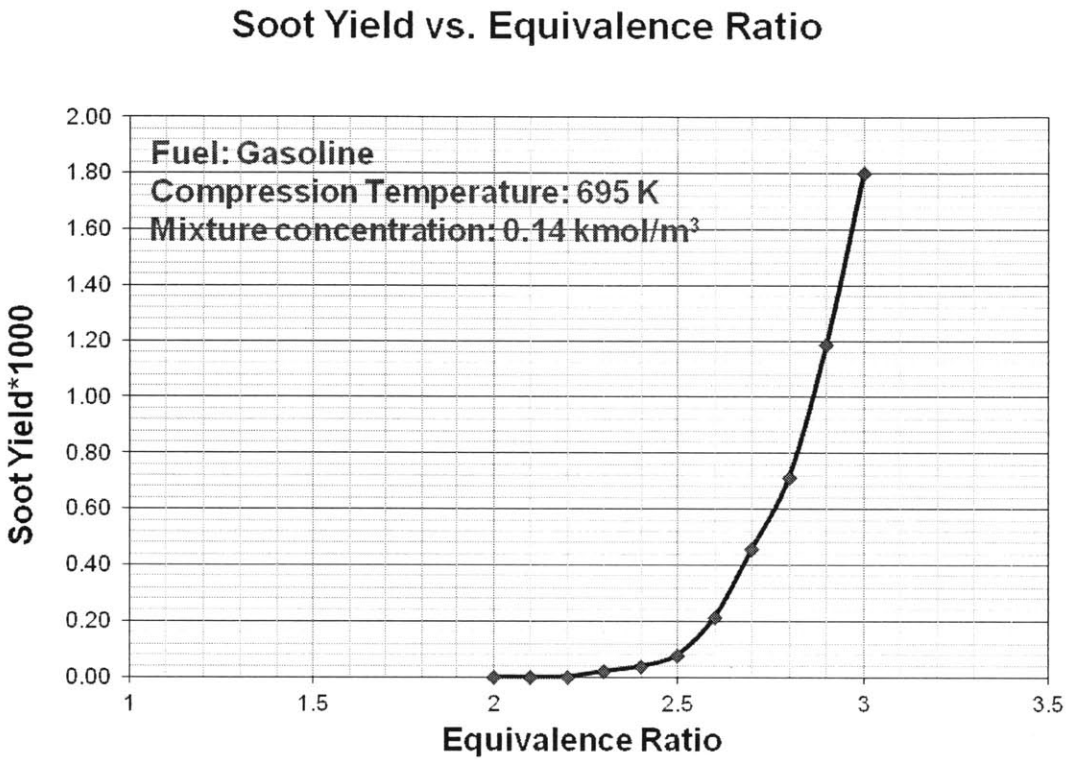

Figure 3-78: Soot Yield vs. Equivalence Ratio

With these basic analytic techniques. the effects of three parameters on PM formation were examined using RCM data. The first is the impact of fuel composition. The second is the impact of compression temperature and the third is the impact of mixture density.

Fuel Effects As was done in the engine experiments, it was planned to examine the effects of aromatic content and ethanol content. Unfortunately, due to the auto-ignition resistance of ethanol, it was not possible to collect data for ethanol/gasoline blends as these mixtures would not ignite with a reasonable ignition delay. Data were

collected for a blend of 20% toluene in gasoline as well as for the baseline gasoline. Figure 3-79 plots the soot yield curves for gasoline at three different mixture densities and the gasoline/toluene blend at two different mixture densities. The mixture density is, essentially, the pressure. A higher density results in a higher pressure upon compression. With the toluene blend, it was not possible to reach the desired temperatures at a mixture density of 0.12kmol/m^3, so that point was excluded for the blended fuel.

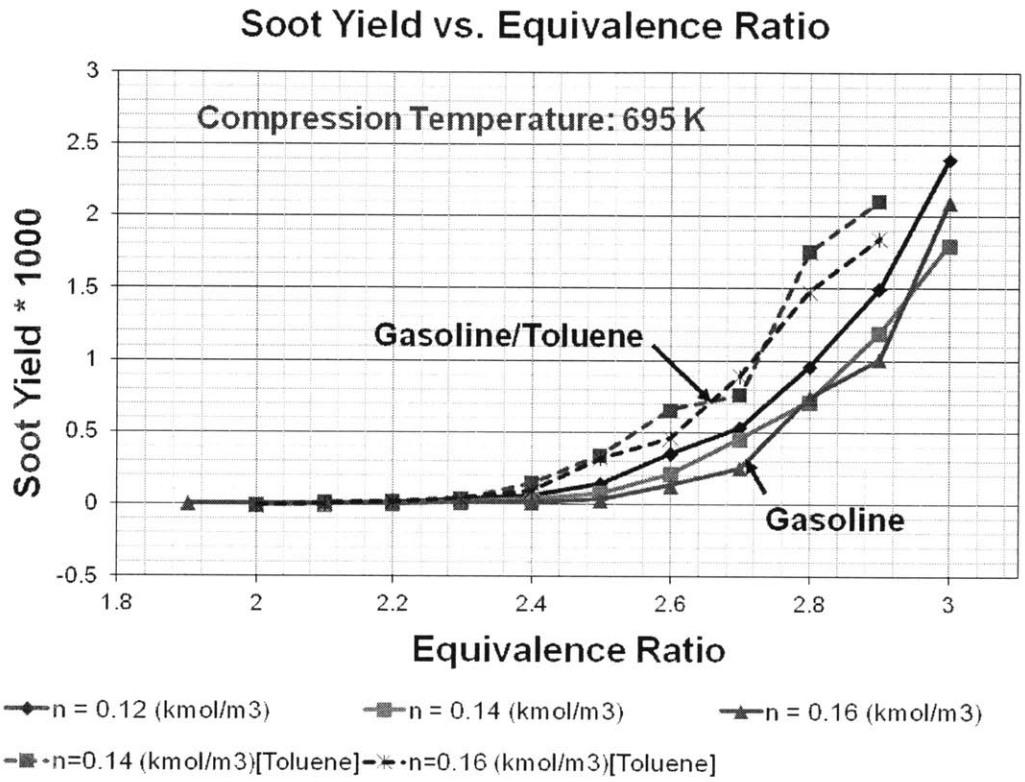

Figure 3-79: Soot Yield vs. Equivalence Ratio

There are noticeable, though not entirely consistent changes in soot yield with the change in mixture density, but the most obvious observation from this plot is the increase in the soot yield with the addition of toluene to the fuel. Effectively, by adding toluene, the soot yield curves are shifted toward lower equivalence ratios. This supports the hypothesis that different fuels possess different equivalence ratio thresholds for soot formation. It is consistent with the observations from the engine

experiments, which, under cold operation, when fuel films were expected to evaporate slowly, resulting in fuel-rich regions in their vicinity, resulted in increased PM emissions associated with the addition of toluene to the fuel.

Compression Temperature The impact of the compression temperature, that is, the temperature at which ignition begins, is interesting. The change in equivalence ratio threshold for soot formation versus the compression temperature is plotted for gasoline at three different mixture densities in figure 3-80.

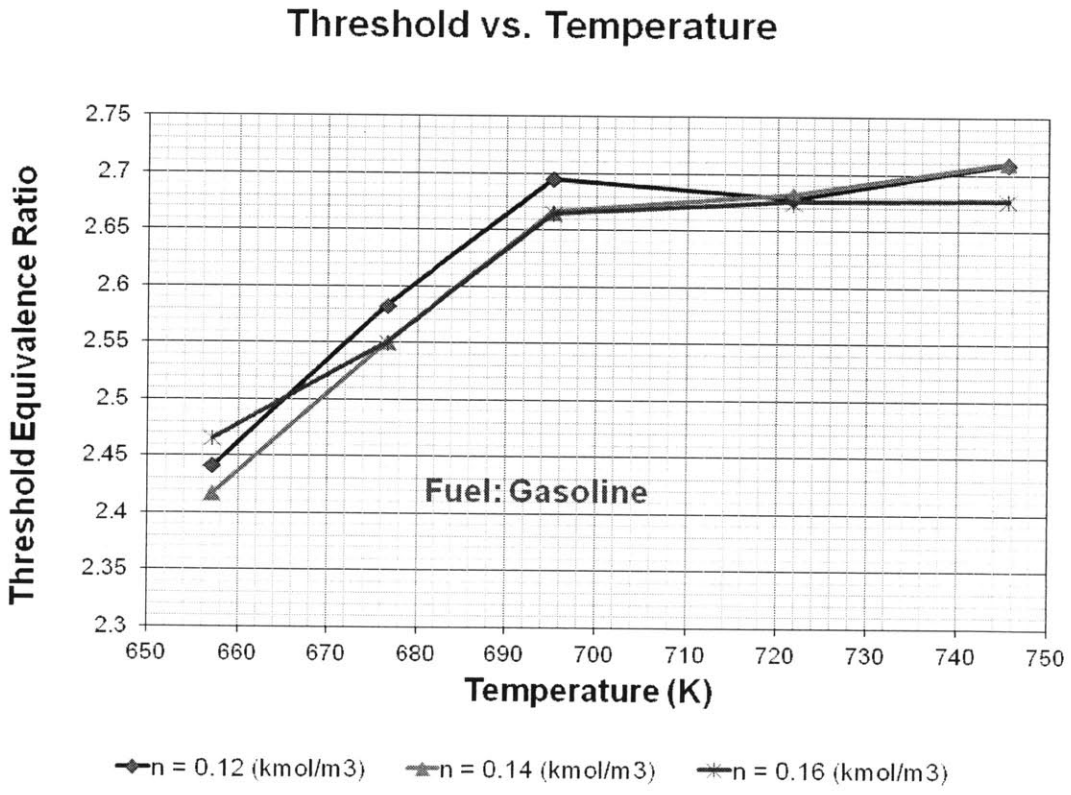

Figure 3-80: Threshold vs. Compression Temperature

These data are interesting because there appears to be different behaviour in different temperature regimes. At lower temperatures, the threshold equivalence ratio increases (i.e. the sooting propensity decreases) with increasing temperature. This is not surprising, as the rate of soot oxidation generally increases faster with temperature than the rate of soot formation, resulting in less soot formation at high temperatures

[43]. At higher temperatures, however, the threshold equivalence ratio remains constant. This is a valuable result as it may open the door to future engine experiments in which the soot formation in the bulk charge can be distinguished from those created due to fuel films. This is because the soot arising from fuel films is strongly dependent on evaporation processes, dependent on the engine surface temperatures, which determines the amount of fuel participating in soot-producing reactions. For soot formed in the bulk charge, however, the combustion temperature may still play a role in the soot formation at lower temperatures, but it may be independent of the flame temperatures at higher temperatures. These observations are consistent across all of the mixture densities studied. It may be of interest to extend this study to examine additional fuels.

Mixture Density Finally, the impact of mixture density was examined. This gives some insight into what effects might be expected based on engine load or operating conditions, when the cylinder pressures are changed. At high loads, it seems intuitive that the cylinder pressures will increase. There are other operating conditions, however, which are also accompanied by changes in cylinder pressure. One example is changes in spark timing. Retarding the spark timing will result in lower peak pressures.

The equivalence ratio threshold for soot formation is plotted versus the mixture density in figure 3-81. The lack of change in the threshold is quite remarkable. Here is shown only one example for the baseline gasoline case, but data at other temperatures showed consistent results. These may be useful data as they suggest that, under similar fuelling and mixing rates, the rate of PM formation in a DISI engine should not vary significantly with load. Engine experiments to explore this question might prove interesting, though difficult, since it would be hard to change the engine load without changing the amount of fuel and, consequently, the mixing process.

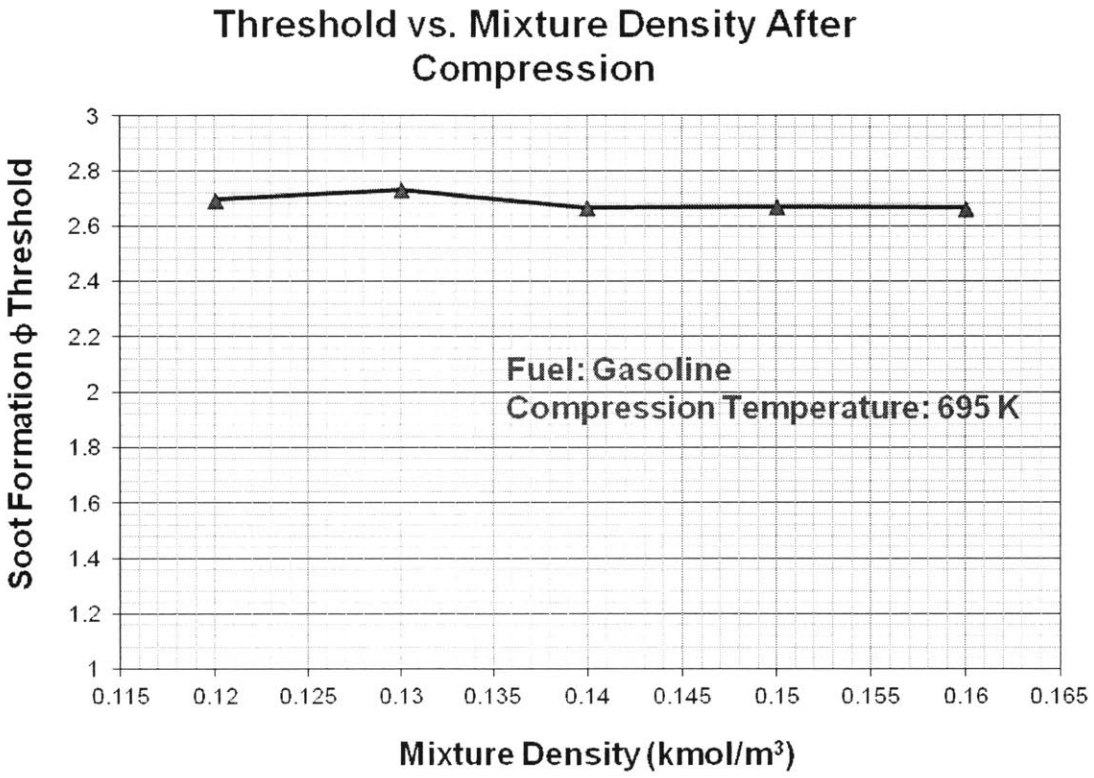

Figure 3-81: Threshold vs. Mixture Density

This page intentionally left blank

Chapter 4

Discussion

In Chapter 3, the data obtained from the engine and RCM experiments were outlined and an attempt was made to relate the results to physical processes occurring in-cylinder. In this chapter, the results will be further analyzed and discussed, first in the context of testing the hypotheses laid out in the first chapter of this thesis, then in the context of a coherent conceptual model explaining the physical processes leading to soot formation in a modern DISI engine, under cold-idle operating conditions.

4.1 Support for Hypotheses

At the beginning of this programme of study, two hypotheses detailing soot formation in DISI engines were outlined. The first, termed the residual fuel effects hypothesis, suggested that the sooting propensity under cold-idle operating conditions may be attributed mainly to the presence of residual liquid fuel on cylinder surfaces, which reacts with residual oxygen in the burned gases at the end of the combustion event. It was hypothesized that the combination of liquid fuel and low oxygen concentrations would result in reactions resembling very rich combustion, with the associated soot formation potential.

The second hypothesis, the fuel effects hypothesis, is more straightforward, but it was necessary in order to complete the story of soot formation in DISI engines since the residual fuel effects hypothesis does not really address chemical effects, rather it

focuses on mechanical processes. The fuel properties, however, are expected to play an important role in the soot formation process. Since there is more than one chemical pathway to soot formation, some of which are more efficient than others, it should come as no surprise that some fuels generate more soot than others. Considering the residual fuel effects hypothesis, however, some further explanation may be possible. If the residual fuel effects hypothesis holds, then, under identical mixing conditions, a fuel which forms soot at lower equivalence ratios will result in greater PM emissions than a fuel requiring a very rich mixture in order to form soot. Thus, it is hypothesized that the equivalence ratio threshold for soot formation plays an important role in determining engine-out PM emissions. This hypothesis is coupled to the residual fuel effects hypothesis via the evaporation properties of the fuel, which play a role in determining the mass of residual fuel and the mixing processes.

This section examines the ways in which the data presented in chapter 3 support or refute these hypotheses. Where applicable, refinements to the original hypotheses may be included.

4.1.1 Residual Fuel Effects

The residual fuel effects hypothesis can be divided into two distinct components. The first is the hypothesis that, during cold engine operation, soot is primarily produced in regions of fuel vapour which form surrounding liquid fuel films on cylinder surfaces. The second is the hypothesis that the combustion of these fuel vapours takes place with residual oxygen from the burned gases after the main combustion event.

Evaporation of Fuel Films The first question that is raised by the assertion that soot forms in regions surrounding liquid fuel films is whether or not it can be confirmed that fuel films are indeed formed during these operating conditions. This question is not whether or not fuel films can form in a DISI engine; it is already known that they can and do [9, 47]. The question is, instead, whether or not they form in this specific engine under these operating conditions. This question must be answered since if there were not fuel films forming on piston or liner surfaces, then

the residual fuel effects hypothesis was not actually being tested by the experiments that were completed.

Based on the data presented in chapter 3, it is clear that, at the very least, there is, indeed, fuel impingement on the piston crown, and likely on the cylinder liner. Looking at the injection and cylinder geometries, it is clear that impingement on the piston crown and on the liner is possible, depending on the fuel spray penetration characteristics. Using emissions data, however, it was possible to relate emissions levels to likely impingement on the piston crown. This was clear in both the studies of single injection timing as well as the study of second injection timing in a dual-injection strategy. The increases in emissions corresponding to piston positions that enable wetting of the piston crown with fuel indicate quite clearly that liquid films are formed on cylinder surfaces, creating at least the most basic conditions needed for soot formation to occur following the process suggested by the residual fuel effects hypothesis. As for fuel impingement on the liner, there was evidence during experiments that fuel was striking the liner, resulting in dilution of the lubricating oil in the crankcase. This was especially obvious when ethanol blends were used. In this case, when the oil was drained, it appeared as a frothy, milky emulsion. To verify that it was fuel dilution and not another problem with the engine operation, a sample of the oil was heated and the oil quickly returned to the typical dark colour of used engine oil once the diluent was evaporated.

With this question settled, it is possible to address the main question in this component of the hypothesis. That is, whether or not the soot is formed in regions of fuel vapour which has evaporated from liquid films. Here, the consideration of the data presented in chapter 3 must be more careful as the support for soot formation in regions of fuel vapour is more subtle than is the support for film formation. The variation of the coolant temperature provides the strongest support for the suggestion that the fuel films evaporate during the cycle, and that soot forms through reactions involving these vapours. This is especially true when the base gasoline was blended with ethanol or toluene. In both of these cases, changing the coolant temperature, while maintaining the other operating temperatures at constant levels, results in changes

not only in particle number concentrations, but also in the particle size distributions. This suggests that, depending on coolant temperatures (and the related engine component temperatures), the fuel components participating in soot-producing reactions may change. The implication of this observation is that fuels do not evaporate uniformly. Instead, there may be stratification of the fuel components. Importantly, however, this suggests that the fuels do, indeed, evaporate after contacting cylinder surfaces and before participating in soot-producing reactions. It would appear that soot-producing reactions are initiated with the fuel components that evaporate slowly. As an example, when toluene was added to the fuel, at cold coolant temperatures, the particle number concentrations increased dramatically with the addition of toluene and the particle sizes were increased, presumably due to the added aromatic content. At warm coolant temperatures, however, the number concentrations did not change markedly and, interestingly, the particle size distributions remained consistent, indicating that the toluene added to the fuel was among the volatile portions of the fuel that evaporated and burned in the bulk charge before the soot-forming reactions were initiated. In this case, regardless of toluene content, the same fuel components were left behind in evaporating fuel films to produce PM.

Combustion with Residual Gases Having offered support for the hypothesis that the evaporation of fuel films leads to soot formation, the details of the soot formation reactions can be clarified by considering the hypothesis that the combustion of the fuel vapours occurs in residual gases. The study of burned gas oxygen content, performed by enriching the charge with propane, seems to refute the hypothesis that combustion occurs. By adding propane to the inlet air, enriching the mixture while maintaining constant liquid fuel characteristics, it was observed that reducing the burned gas oxygen content leads to an increased particle number concentration, but it does not change the general shape of the particle size distributions. The fact that the emissions change at all with the change in burned gas oxygen content is encouraging as it supports the idea that the condition of the burned gases does impact soot formation, meaning that the soot that is emitted is formed near the end of

the combustion event. The observation that the number changes but that the size distributions don't change suggests, however, that the soot formation mechanism does not change with the changing oxygen content. Instead, it seems that a reduction in oxygen concentration results in larger fuel-rich regions supporting PM formation.

In light of these observations, it seems that the use of the term "combustion" in the formulation of the residual fuel effects hypothesis may not be accurate. Were combustion taking place, one would expect the changing oxygen content to lead to more pronounced changes in PM emissions than was observed. This is not only true for number concentrations, but also for size distributions, since the different flame temperatures expected at different oxygen concentrations should lead to larger changes in soot characteristics in a true combustion reaction. Instead, it seems possible that soot is formed in reactions more closely resembling pyrolysis using the heat conducted from the hot burned gases, without the presence of a reacting flame. While the observations do not explicitly confirm this, given the very low burned-gas oxygen concentrations seen with propane-enriched combustion, it seems likely that the soot-forming reactions are a sort of oxidative-pyrolysis rather than a typical fuel-rich combustion reaction. This would suggest that the luminosity observed in optical engine studies [9, 52] may have simply been radiation from the hot particulates formed in the pyrolysis reactions.

4.1.2 Fuel Effects

The fuel effects hypothesis can also be divided into two distinct components. The first is the hypothesis that the evaporation properies of the fuel are at least partly responsible for the amount of liquid fuel forming films on cylinder surfaces. This point couples the fuel effects hypothesis to the residual fuel effects hypothesis. The second component of the fuel effects hypothesis is the suggestion that, under the same mixing rate. fuel stoichiometry may affect the soot formation. Related to this is the suggestion that different fuels experience different soot formation chemistry. These are related since the mixture stoichiometry is decided by the fuel chemical composition, as is the equivalence ratio at which soot forms, which is really the key point in

considering the soot formation chemistry. Knowing the actual chemical mechanism of soot formation is not critical. Instead, it is desired to know the likelihood of soot formation given a particular fuel composition.

Evaporation Properties In order to test the hypothesis that fuel evaporation properties may be responsible for the ultimate size of fuel films, the fuel volatility study was completed. By creating a two-component fuel with known volatile and relatively non-volatile fractions (isopentane and isooctane, respectively), it was possible to examine the impact of fuel volatility on emissions. The reductions in PM emissions with increasing isopentane fraction under operating conditions with identifiable piston impingement were of the same order as the increases in isopentane fraction. This indicates that the addition of volatile fuel components decreased the size of the piston crown fuel films. This offers reasonable support to this aspect of the fuel effects hypothesis.

Fuel Chemical Composition It was possible to relate PM emissions to fuel chemistry, but it is difficult to quantify, in a useful way, the sooting tendencies of fuels from engine experiments. The studies of ethanol and toluene content provided support for the idea that different fuel compositions will result in different PM characteristics. This is not, however, a novel discovery. A number of studies have established PM indices which may be used to examine the sooting tendencies of fuels based on their chemical characteristics [68, 69, 93].

The more salient question to be answered for this hypothesis is whether or not the mixture stoichiometry, specifically, may affect soot formation. In order to test this hypothesis, the RCM experiments were conducted. While the experiments were not completely representative of what might be expected in a real engine, they were, nevertheless useful for ranking fuels based on their equivalence ratio threshold for soot formation. It was found that different fuels do, indeed, require different equivalence ratios for soot to form. The implication from these data is that while one fuel may not produce soot under the mixing conditions in the cold-idle operation, another

fuel, with a lower threshold equivalence ratio may result in substantial PM emissions. These observations do not prove this hypothesis, but they do, at least, suggest that it is plausible.

4.2 Conceptual Model of Soot Formation in DISI Engines

The engine and RCM experiments discussed in this study offer support for and allow refinement of the residual fuel effects hypothesis and the fuel effects hypothesis. These hypotheses are, however, quite general, and their implications in a real engine may not be immediately obvious. In this section, the basic hypotheses will be refined to describe a conceptual model of PM formation in DISI engines under cold-idle operating conditions. The intent is to outline the mechanisms of PM formation in DISI engines in a similar way to what was accomplished by Dec for Diesel combustion [97]. As was done in the discussion of the hypotheses, above, the conceptual model will refer back to the results from engine and RCM experiments for support.

The model presented here outlines the physical processes leading to soot formation, following the formation of fuel films, in a DISI engine operating with a dual-injection strategy and late spark timing. The dual injection strategy was chosen because it illustrates two different fuel sources for soot formation - liner impingement and piston crown impingement. This conceptual model can, however, be adapted to apply to soot formation from fuel films on any surface.

The model is composed of four main events. These are the fuel injection and establishment of liquid films, the formation of fuel vapour plumes, the soot-producing reactions, and the exhaust process.

4.2.1 Fuel Injection and Film Formation

The first steps in this model of soot formation is for fuel to be introduced to the cylinder and for the impingement of liquid fuel on cylinder surfaces to form liquid films.

The location of films depends largely on the injection timing. Generally speaking, very early and very late injections are likely to impinge on the piston crown. Moderate injection timings may or may not result in liquid impingement on the cylinder liner depending on the spray penetration (this, in turn, depends on several factors, including the fuel pressures, temperatures and the injection duration). The first injection, in the modelled case is at a moderate timing in the intake stroke, while the second injection is at a late timing in the compression stroke. Illustrations are included in order to help explain the conceptual model. Please note, however, that these are merely illustrations, they are not based on optical data, so, while instructive, they may not accurately represent the geometry of the processes taking place.

First Injection In this description of soot formation, the first injection is at a moderate timing of 80°CA $ATDC_{intake}$. At this injection timing, the fuel spray is not expected to impinge on the piston crown. This idea is supported by the data shown in figure 3-7, which shows elevated particle number concentrations at very early and very late injection timings, coinciding with conditions where the fuel spray is expected to impinge on the piston crown. The first injection is illustrated in figure 4-1. Here, the piston is drawn at its location at the end of the first injection. It is seen that the spray, even with a modest downward deflection, should not strike the piston crown.

During the injection process, a large fraction of the fuel should evaporate in-flight, mixing with the incoming air and forming the bulk mixture. Some of the fuel, however, will not evaporate and may strike the cylinder liner. Of this fuel, some may splash off of the liner to be mixed in the main charge or to impinge on other cylinder surfaces, some may evaporate from the liner surface and mix with the main charge, and some may form a film on the liner surface. Of this last fraction, some may mix with the oil film, eventually flowing to the crankcase, resulting in oil dilution. The remaining fuel likely remains on the liner surface, possibly mixed with lubricating oil, where it may slowly evaporate or be scraped off of the liner by the top piston ring before taking part in soot-forming reactions.

The idea that some fuel escapes the combustion event is well-estblished based

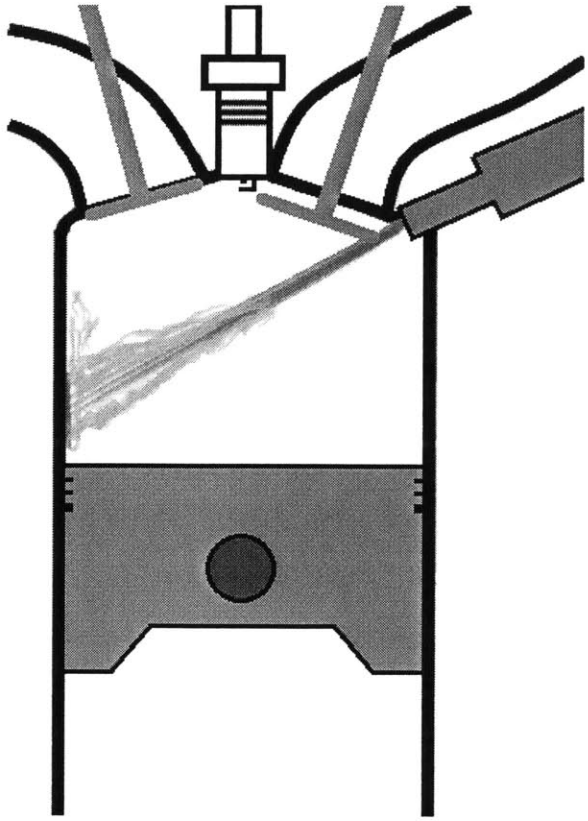

Figure 4-1: Illustration of First Injection

on observations of severe oil dilution under cold operating conditions. This was especially obvious with ethanol blends. This oil dilution confirms that fuel does impinge on the liner walls. Observations from experiments at cold and warm coolant temperatures suggest that some of the liquid fuel in liner films (that does not end up in the crankcase) will, as suggested, lead to soot formation. This is seen looking at the data included in figures 3-19, 3-36, 3-37, 3-39 and 3-40.

If one examines the PM emissions from gasoline/toluene blends with a first injection timed at 80°CA ATDC$_{intake}$ and a second injection timed at 200°CA ATDC$_{intake}$, it can be determined that PM emissions do form in reactions involving fuel from liquid films on the cylinder liner. This dual injection scenario closely approximates the conditions at a single injection at a moderate injection timing. Both 80°CA ATDC$_{intake}$ and 200°CA ATDC$_{intake}$ result in sprays that do not impinge on the piston but may impinge on the liner. This is illustrated in figure 3-19. Figure 3-36 shows the PM emissions for gasoline/toluene blends versus the start of second injection timing at

a coolant temperature of 20°C. It is clearly seen that the emissions increase with the addition of toluene. At a coolant temperature of 80°C, however, there is little, if any, difference in emissions based on toluene content. This is seen in figure 3-39. Clearly, since the coolant temperature is the only variable that was changed, the soot formation process is related to the interaction between the fuel and the liner. To further understand what is happening, figures 3-37 and 3-40 are also instructive. These figures indicate that, at cold temperatures, the addition of toluene results in significant incrsases in the diameters of emitted particles, but that, at warm temperatures, the particle size distributions maintain the same general profile regardless of toluene content. This suggests that the more volatile fraction of the fuel evaporates upon contact with the liner. In this case, at engine coolant temperatures of 80°C, the added toluene is among the more-volatile components of the fuel.

The implication of all of this is that, in the first injection, some liquid fuel does impinge on the liner, and that some of that fuel mixes with the oil (oil dilution), some evaporates quickly (the volatile fraction - including toluene at 80°C coolant temperatures) and some will participate in late, soot-producing reactions. These observations are reflected in the description of the first injection in this conceptual model.

Second Injection The second injection in this description was timed to begin at 320°CA $ATDC_{intake}$. This is a late injection during the compression stroke which results in the impingement of liquid fuel on the piston crown. Impingement is expected at this injection timing based on the data presented in figure 3-17, where the injection at 320°CA $ATDC_{intake}$ coincides with fuel spray interaction with the piston bowl. The second injection process is illustrated in figure 4-2. Here, the piston position is drawn at its location at the end of the second injection. It is clear from the illustration that, given the proximity of the piston to the injector tip, fuel impingement on the piston crown is highly likely.

During the second injection process, some of the fuel will evaporate in-flight, with the remainder striking the piston crown. Of the fuel that strikes the piston, some will

splash off of the piston crown to evaporate and mix in the main charge or to impinge on other surfaces. The volatile fraction of the fuel may evaporate quickly after contacting the relatively warm piston crown and mix with the bulk charge. The remainder of this fuel should form a slowly evaporating fuel film that later participates in soot-producing reactions. It should be noted that the fuel remaining in piston-crown films has significantly less time to evaporate before ignition than do liner films.

In addition to the mixture dynamics of the fuel delivered in the second injection, the fuel from the first injection is still undergoing evaporation and mixing processes. Most of the fuel from the first injection should be mixed in the bulk charge, which, at the start of the second injection is lean of stoichiometric. Also, at this point, the piston is travelling upward, approaching the cylinder head. Thus, some of the fuel vapours, which surround liquid liner films, may be forced upward by the piston motion. Some liquid fuel (or mixture of liquid fuel and lubricating oil) may also be scraped off of the liner by the upward motion of the piston top ring. This scraped fuel may be entrained in the bulk charge where it may evaporate and mix. Alternatively, it may remain as free-flowing droplets which may also lead to soot formation. This process involving liner liquid fuel films and vapour plumes has not been confirmed experimentally, so it will not be discussed further in this thesis beyond noting that it seems likely that the piston ring/liner interactions do influence the behaviour of liquid films on the liner and the fuel vapours formed surrounding them prior to soot formation.

The link between piston wetting and PM emissions is well-established based on exisiting studies [9, 50, 51]. While piston impingement is not directly observed in this study, it may be inferred quite reliably from emissions measurements. For example, looking at the emissions data for dual injection with isooctane fuelling, plotted in figure 3-53, it is seen that there is a significant increase in PM emissions, accelerating at a start of second injection timing of approximately 295°CA $ATDC_{intake}$. As shown in figure 3-19, at injection timings later than this, it would appear that piston wetting is likely. The increase in PM emissions coinciding with this likelihood of piston wetting strongly suggests that piston fuel films produce favourable conditions for

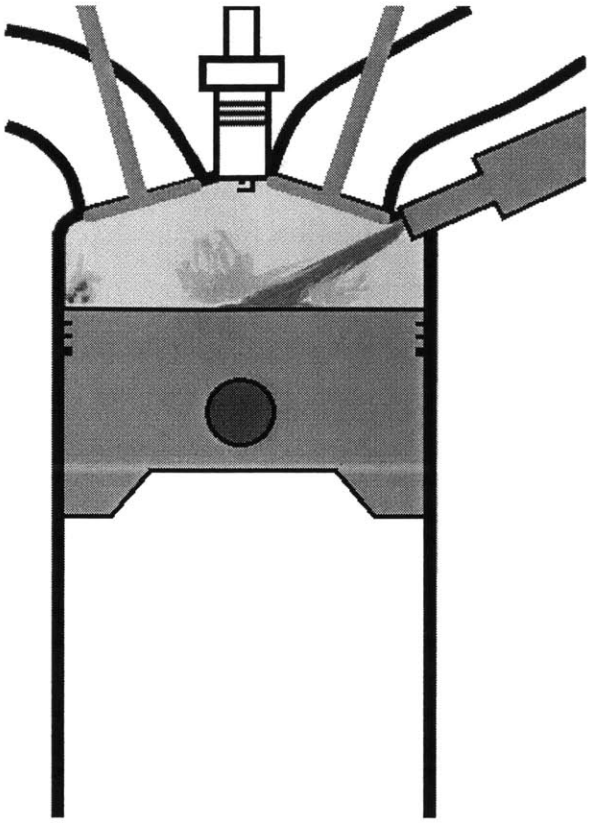

Figure 4-2: Illustration of Second Injection

soot formation.

Furthermore, the study of fuel volatility offers further support for the suggestion that fuel films are responsible for soot formation since the particle number concentrations decrease roughly in proportion to the increase in the volatile fraction of the fuel (see figure 3-59). The decrease in emissions with increased isopentane fraction is understood to be a result of the evaporation of isopentane resulting in smaller films of isooctane remaining on the piston crown. At the injection timing of 320°CA ATDC_{intake}, figure 3-65 shows that, regardless of isopentane fraction, the size distribution maintains a uniform shape (though the particle number magnitude changes). This confirms that isooctane produces the bulk of the soot and that the isopentane fraction evaporates and mixes with the bulk charge. The close correlation between isopentane fraction (and, thus, the amount of liquid fuel in-cylinder) and PM emissions provides strong support for the idea that fuel films do form, and that they are a major contributor to PM emissions.

Similar to the first injection, the study of coolant temperatures also offers support for the behaviour of the second injection, as described in this conceptual model. As seen in figures 3-46 and 3-47, there is little difference in the particle number concentrations at warm or cold engine coolant for both E15 and E30 blends. It is interesting, therefore, to note that, at a second injection timing of 320°CA $ATDC_{intake}$, for both E15 and E30, the particle size distributions shift toward larger diameters with increased temperature (see figures 3-48 and 3-51). Despite being somewhat counter-intuitive, these data suggest that piston films are important sources of PM since the coolant and, thus, piston temperature influences the PM composition. This means that the composition of piston fuel films influences the PM emissions (in this case, the temperatures are high enough for the ethanol content to evaporate, leaving behind components that are more likely to enable soot surface growth) and, more fundamentally that piston films exist and support soot formation.

4.2.2 Fuel Vapour Plume Formation

After the injection events have been completed, the mixture will continue to develop. Most of the fuel will be reasonably well-mixed in the bulk charge. Surrounding the fuel films, however, plumes of fuel vapour will form as the films evaporate. This process continues from the end of injection until the flame front from the main combustion event meets the plume.

Plume Formation Before Ignition Before ignition, most of the mixture is uniform and near-stoichiometric. Fuel plumes, which are regions of fuel vapour (or very rich mixtures of fuel vapour and air) form surrounding the liquid fuel films as the fuel evaporates. The energy for evaporation is likely drawn primarily from the component surfaces. The mixture temperature should also be quite high following compression, but without knowing the thermodynamic condition of the liquid fuel, it is difficult to predict the influence of the gas pressures on the fuel evaporation [98]. A prediction of the early plume formation is illustrated in figure 4-3, which displays the plume formation near TDC of the compression stroke. Apart from the developing plume,

the shape of which is not well-known, the mixture is expected to be mostly uniform.

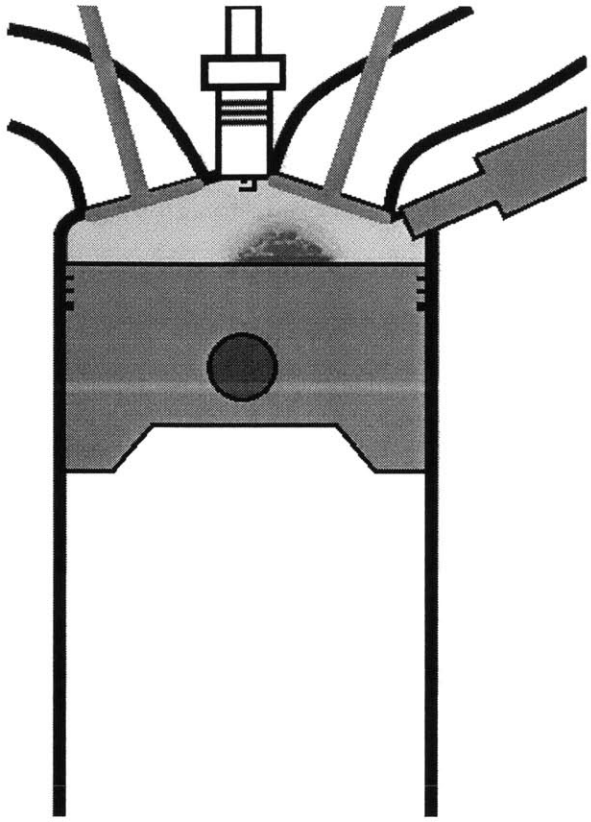

Figure 4-3: Illustration of Early Plume Formation

Plume Formation During the Early Flame Development Immediately after ignition, the fuel vapour plume is not strongly impacted by the developing flame front. At this time, only the uniform mixture is consumed by the flame front. The fuel vapour plumes will continue to develop in the regions surrounding the fuel films. In the very early stages of combustion, the flame should not have much influence on the shape or size of the fuel vapour plumes as little expansion should have taken place.

The periphery of the fuel vapour plumes will approach the equivalence ratio of the bulk, uniform charge, but the equivalence ratio will increase progressively toward the centreline of the plume, as well as toward the film surface. The core of the plume should be quite quite rich at this time. The plume formation during the early flame development is illustrated in figure 4-4. The illustrated time corresponds to

approximately 10% mass-fraction burned. Again, the actual shape of the plume is not known.

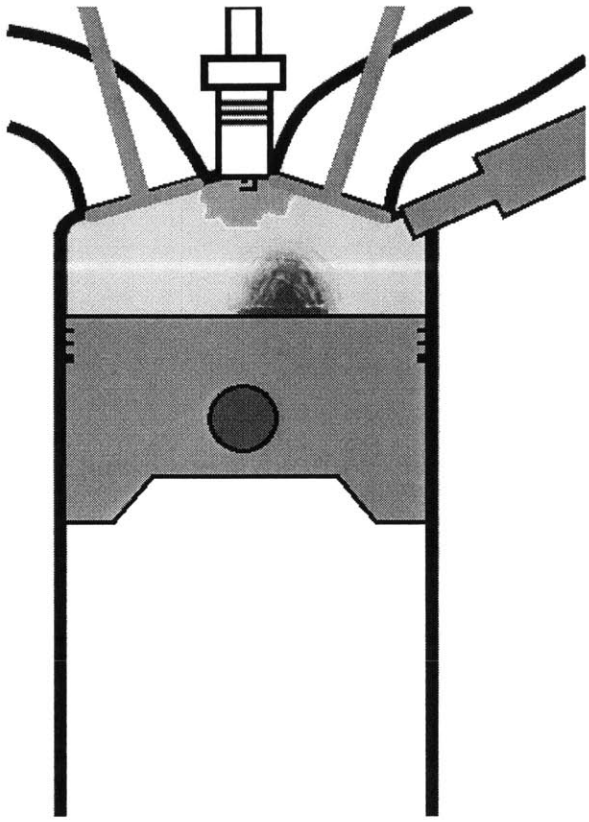

Figure 4-4: Illustration of Early Flame Development

The main source of support for this plume formation process comes from the work of Costanzo et al. [52]. The primary focus of this work was to study the impact of liquid fuel films on the emissions of unburned hydrocarbons, but the experiments also offered valuable insight into the formation of particulate matter. The experiments included videos of the combustion process obtained in MIT's square piston optical engine. In these videos, it was possible to see luminosity directly above a piston fuel film. The luminosity was visible immediately as the main flame front passed by. The shape of the luminous region suggests that a very fuel-rich region of fuel vapour was present before the main flame reached the area. In this study, this fuel-rich region is understood to be the fuel vapour plume.

4.2.3 Soot-Producing Reactions

The formation of fuel vapour plumes continues throughout the main combustion event. As shown in figure 4-4, above, it seems likely that, during the main combustion event, the plume growth process would continue in a similar fashion to the process prior to ignition. Once the main flame front reaches the fuel vapour plume, however, the process becomes more complicated. The plume growth should continue, likely accelerated by the heat transfer from the flame, but reactions will also be initiated within the plume.

Early Interaction Between the Vapour Plume and the Main Flame Front
As mentioned earlier, as the fuel vapour plume grows, near the centreline and film surface, the mixture will be very fuel-rich, but the periphery of the plume should approach the equivalence ratio of the bulk mixture - generally close to stoichiometric. Since the periphery of the plume is reasonably well mixed, as the flame front passes through it, the near-stoichiometric, though rich, periphery should burn in a rich pre-mixed flame. Portions of such flames may be sufficiently fuel-rich to support soot formation, but their contribution to the total PM emissions should be relatively small.

In the richer portions of the plume, however, the equivalence ratio is expected to be far too rich to burn. Instead, it is suggested that the low oxygen concentration in the fuel vapour plume, in conjunction with heat transfer from burned gases (from the main flame and the rich pre-mixed combustion) create an environment supporting pyrolysis reactions in which soot is formed. Due to the high temperatures of the burned gases and the heat release from pyrolysis, those soot particles formed in these regions will also be very hot. As a result of these high temperatures, soot particles will emit visible radiation [99]. As shown in figure 4-5, these soot-forming reactions (and soot incandescence) should begin as the flame front and burned gases first meet the fuel vapour plume. This incandescence is likely the luminosity typically identified as diffusion flames or pool fires.

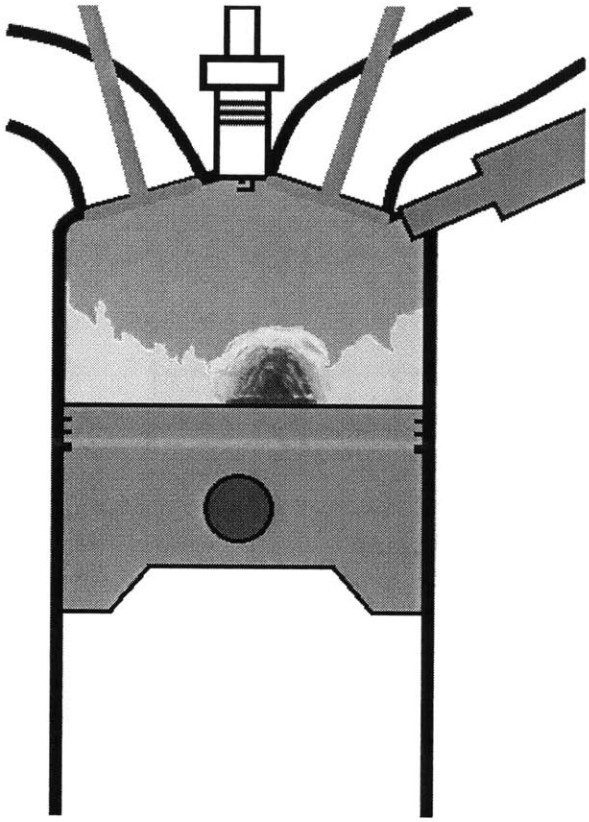

Figure 4-5: Illustration of Early Plume Ignition

After the Completion of the Main Combustion Event At the end of the main flame front, the bulk mixture has been consumed in the main combustion event, but the soot-forming reactions continue in the fuel vapour plume. It must be reiterated that this is not a typical diffusion flame as there is not a diffusion of air (or another oxygen-rich gas) into the fuel vapour plume. Instead, there may be a diffusion of burned gases (with very low oxygen content) into fuel vapours. This process does not supply sufficient oxygen for combustion. The luminosity visible immediately after the main flame is complete, typically identified as a flame, is more likely soot incandescence at the interface between the fuel vapours (in which pyrolysis is leading to soot formation) and hot burned gases. This process is illustrated in figure 4-6, where the rich core of the plume is seen, with luminous soot particles at the periphery of the fuel vapour plume.

As was the case for the general hypothesis of plume formation, support for the soot formation process is drawn partly from the work of Costanzo et al. [52]. In

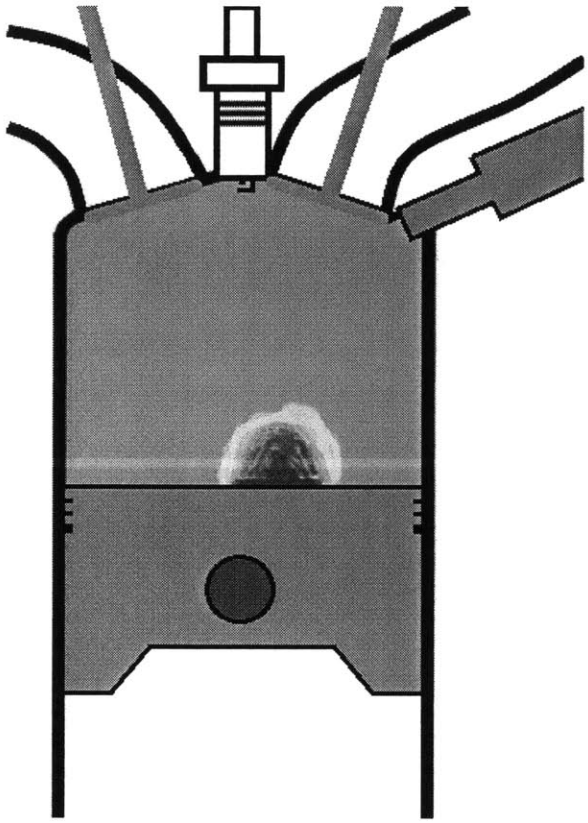

Figure 4-6: Illustration of Early Soot-Producing Reactions with Luminosity

the engine combustion videos seen in the square piston optical engine study, it is observed that as the flame front passes over the fuel films, a luminous region appears in the location of an apparently pre-existing fuel vapour plume. This region remains luminous well after the completion of the main combustion event.

In a typical diffusion flame, such as a candle flame or a co-flow diffusion flame, luminous soot is also visible, but most of the particles are oxidized before being emitted. In this case, however, there is very little oxygen in the surrounding gases, so it is unlikely that much oxidation will take place. In fact, due to the lack of oxygen, the luminosity (and, thus, the particles) persists into the exhaust process. These videos provide strong evidence for the presence of a fuel vapour plume and the formation of soot in these regions despite the lack of oxygen.

In addition to these data, the study of engine speed on PM emissions, outlined in figure 3-26, offers some support for the ideas presented here. The increased emissions at higher engine speeds might be partly explained by the decreased time for the

fuel vapour plume to evaporate and mix with the bulk charge. The result of less evaporation and mixing is that more fuel will be left behind to form the very rich core of the fuel vapour plume, which is expected to be the major source of PM emissions.

Reactions Involving the Core of the Vapour Plume The core of the fuel vapour plume is also far too rich to burn since there is effectively no oxygen in the plume and insufficient oxygen in the burned gases to support combustion. It is still, however, suspected that some of the PM emissions originate from these fuel components.

It seems likely that, in a similar way to the early soot-producing reactions, heat conduction from the burned gases in the bulk charge is sufficient to enable pyrolysis of the fuel vapours even at the core of the fuel vapour plume (though it is not clear exactly how far into the plume heat conduction is sufficient to enable pyrolysis). Under these conditions, soot precursors such as acetylene and PAH can be readily formed from the hydrocarbons in the fuel vapours. With the temperatures high enough, these precursors are able to support the nucleation and surface growth of soot particles [34, 36, 38, 39]. Due to the lack of oxygen in the burned gases and within the fuel vapour plume, there is little, if any, surface oxidation of soot particles to compete with surface growth, allowing the particles to grow rapidly. This process, in which pyrolysis occurs in the core of the fuel vapour plume, enabled by the high temperatures of the burned gases is illustrated in figure 4-7. The presence (or intensity) of luminous soot particles in the core of the plume is not clear from this work or from previous studies since the luminosity of the outer shell of the plume, where most of the soot should form, obscures the core. In this figure, the core is shown as being dark to illustrate the presence of soot, but it is possible that the soot in this region may also be radiating in the visible spectrum. As in all of the illustrations, the plume shapes described here are for instructive purposes only. The actual appearance of these processes (in this engine) is not known.

The propane enrichment experiment discussed in Chapter 3 offers justification for

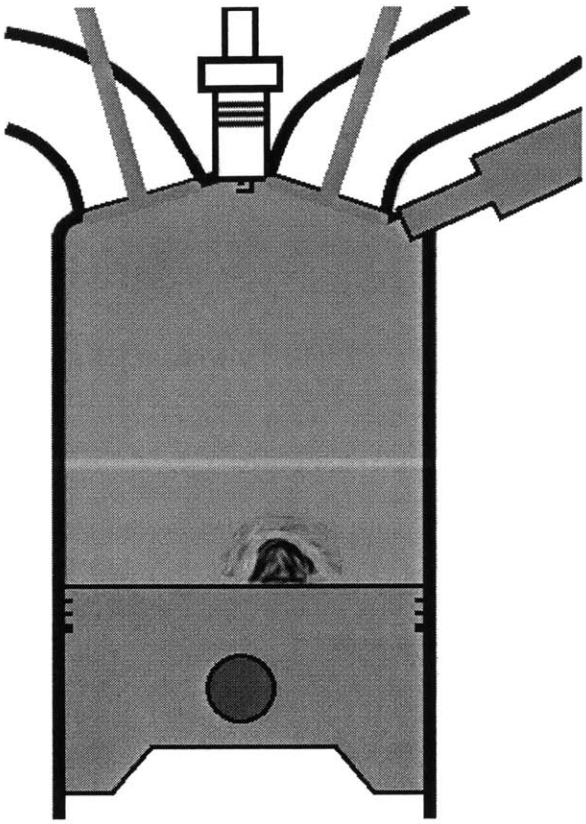

Figure 4-7: Illustration of Late Soot-Producing Reactions

the assertions above regarding soot formation in the core of the fuel vapour plume via pyrolysis reactions. This experiment varies the burned gas oxygen concentration by using propane to enrich the charge. The use of propane to enrich the mixture allows the liquid fuelling rate to remain constant while still changing the equivalence ratio. This means that the evaporation properties should remain relatively constant. Propane should not contribute to additional soot formation for two reasons. Firstly, it has a relatively low sooting propensity [43]. Secondly, it is added to the inlet air upstream of the compressor, so it should be well-mixed and should take part in the main combustion, in which little soot should be formed.

Figures 3-68 and 3-69 plot the particle number concentrations versus the equivalence ratio for mixtures enriched with propane beginning with a lean baseline or a stoichiometric baseline condition, respectively. Figure 3-70 offers a summary of both the lean and stoichiometric baseline experiments. Viewing these figures, it is clear that, for the late dual injection case, as described in this conceptual model,

the particulate emissions increase monotonically with propane enrichment, that is, with a decreased burned gas oxygen concentration. This information, alone, doesn't offer much insight since the idea that soot emissions increase with equivalence ratio is nothing new. Looking at figures 3-71, 3-72 and 3-73, however, makes it clear that, with decreasing burned gas oxygen content, the soot formation mechanism likely doesn't change. In a rich pre-mixed flame, or a rich conventional diffusion flame, one would expect the increased equivalence ratio to lead to increased particle sizes due to the additional fuel taking part in the soot formation process and the changes in the formation process (different temperature profiles, for example). In this case, however, the number concentration changes, but the sizes do not. The size distributions remain remarkably uniform regardless of equivalence ratio. This suggests that the soot is formed following the same mechanism in each case with only the volume of fuel vapour participating in the soot-formation reactions increasing with decreasing burned gas oxygen content.

The basic idea is that, as the burned gas oxygen concentration decreases, the fraction of the fuel plume that is too rich to support combustion increases. The result is that a larger volume of fuel vapour is contained within the core of the plume, where the equivalence ratio is far too rich to burn. While combustion cannot be sustained, the high temperatures of the burned gases from the main flame and the rich pre-mixed combustion of the plume periphery are still high enough to initiate pyrolysis reactions in the core of the plume. As the plume core enlarges, both the surface area and the volume of the plume core increase. Since the actual shape of the fuel vapour plume is not known, it is not possible to determine which dimension determines the soot formation characteristics. It may be related primarily to the surface area of the plume core, since it is the outer periphery of the plume that will be in thermal contact with the hot burned gases. With effective enough heat transfer, however, it could also be related to the volume of the vapour plume, as there will be fuel vapour contained within the entire volume. It is likely that the relation between emissions and plume dimensions lies somewhere between surface area and volume.

In addition to the propane enrichment study, the study of engine speed also offers

some support for the soot formation reactions described in this model. Figure 3-27 plots the mode bin mid-point particle diameter, that is, the diameter with the largest particle number concentration, versus the start of second injection timing during the regime in which the fuel spray interacts with the piston bowl on the LNF engine. It is seen that, during this regime, the peak particle diameter is consistently larger for slower engine speeds. This is true even though the particle number decreases at slower engine speeds, as shown in figure 3-26. The implication of these observations is that, at slower speeds, there is more time for soot particle surface growth in the absence of oxygen, resulting in larger particles. Nucleation occurs relatively quickly [100], so the engine speed should not have a tremendous impact on nucleation, but surface growth, oxidation and agglomeration are ongoing. Under most conditions, oxidation and particle growth are competing processes, making it difficult to identify the impacts of time. In this case, however, there is very little, if any, oxygen present in the plume pyrolysis reaction zone. Thus, the increased time at slower engine speeds is correlated to increased particle sizes.

4.2.4 Exhaust Process

Finally, to complete this conceptual model, there is the exhaust process. This is illustrated in figure 4-8. In the exhaust stroke, the soot, which could not be oxidized in-cylinder due to the lack of oxygen in the burned gases is emitted with the bulk charge. During the blowdown process, the plume(s), now containing a high concentration of PM, expand toward the exhaust valve due to the pressure drop. This process causes some mixing of the particulates with the bulk charge, but oxidation still does not take place due to the lack of oxygen remaining in the bulk charge. The illustration of this process is largely based on observations from the videos produced by Costanzo et al. [52].

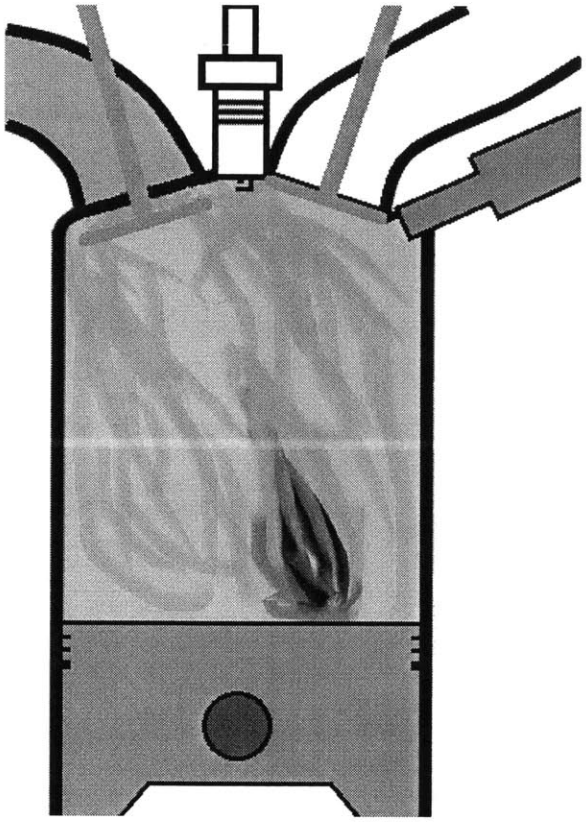

Figure 4-8: Illustration of the Exhaust Process

4.2.5 Soot Formation Pathways

To summarize the physical processes leading to PM emissions, the conceptual model is presented in this section as a flowchart mapping the soot formation process from injected fuel to soot. The flowchart is seen in figure 4-9. This flowchart shows the paths that liquid fuel can follow before the exhaust process. Those termini that are grey and labelled "combustion" refers to non-sooting combustion in the main combustion event. The black termini labelled "soot" refers to fuel which is involved in the soot-producing reactions.

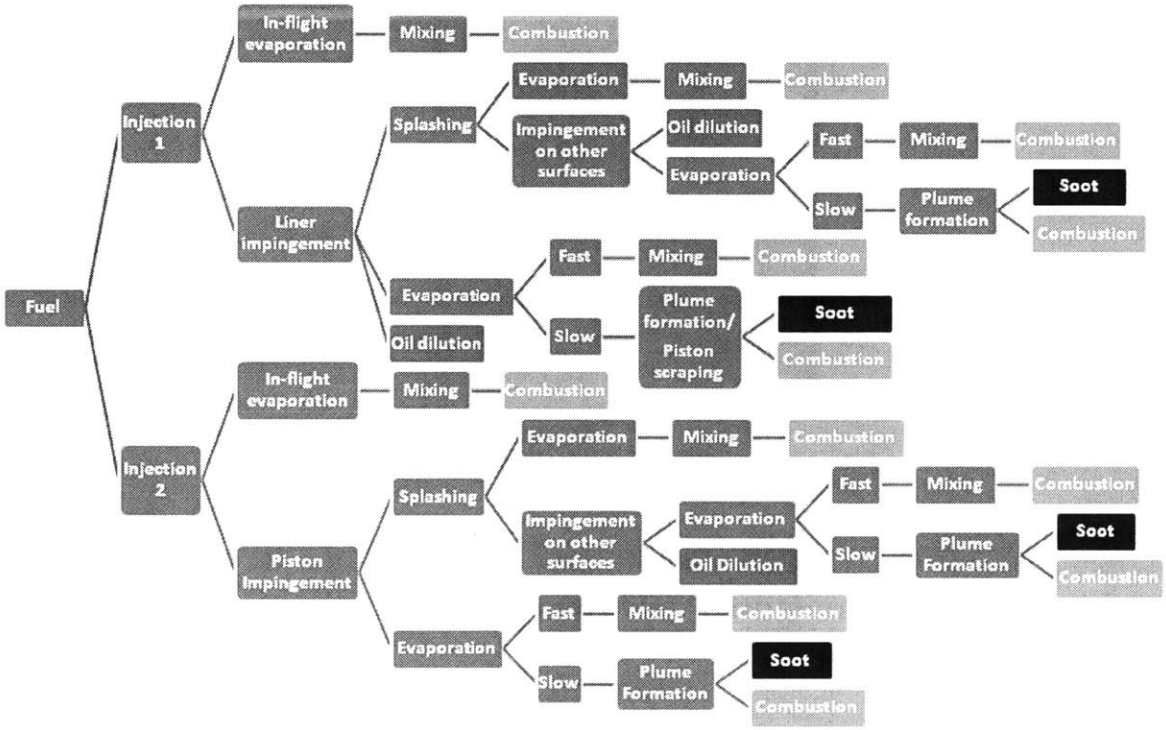

Figure 4-9: Summary of Soot Formation Processes

Chapter 5

Conclusions and Recommendations

This chapter offers a summary of the experiments completed in this study, the results of these experiments and their significance. This includes a summary of the conceptual model developed based on a refinement of the study hypotheses in light of the data collected in this study. The conceptual model offers an explanation of soot formation in DISI engines under cold-idle operating conditions. Following this, some concluding remarks are made regarding the study findings and their significance to the field of internal combustion engines. Finally, recommendations are made to help orient future academic studies of particulate matter formation in DISI engines.

5.1 Research Summary

This study of PM emissions in DISI engines involved a large number of engine and RCM experiments designed to test two hypotheses regarding the formation and emission of PM from these engines. This section will offer a brief summary of the experiments conducted during this study and their significance to the questions raised in the hypotheses. The two hypotheses considered during this study were the residual fuel effects hypothesis and the fuel effects hypothesis.

Residual Fuel Effects Hypothesis The residual fuel effects hypothesis predicted that, in cold engines, PM forms in reactions involving residual fuel (fuel not partici-

pating in the main, pre-mixed combustion event) resulting from the impingement of liquid fuel on cylinder surfaces. More specifically, it was suggested that regions of fuel vapour form surrounding the residual fuel films and that fuel-rich combustion occurs in these regions with residual oxygen from burned gases.

Fuel Effects Hypothesis The fuel effects hypothesis predicted that the differences in PM emissions observed for different fuels can be related to differences in fuel evaporation properties, mixture stoichiometry under identical mixing rates and soot formation chemistry. The evaporation properties of fuels couples the fuel effects hypothesis to the residual fuel effects hypothesis, since fuel evaporation should play a role in determining the mass of residual liquid fuel.

5.1.1 Experiments

The bulk of the data used to test the hypotheses and to develop the conceptual model of soot formation were collected from engine experiments. Some data used to test the fuel effects hypothesis were collected using RCM experiments. Here, the key insights from the experiments are summarized.

Spark Timing Investigation The study of the effects of spark timing on PM emissions was conducted by varying the spark timing while holding the engine speed, load, equivalence ratio and operating coolant temperatures constant. The result was that the PM emissions increased with retarded spark timing. This was attributed largely to reduced combustion stability and the retarded combustion phasing, but the increased fuelling rate needed to maintain a constant load may also contribute to the increased emissions by increasing the mass of residual fuel. The size distributions were uniform regardless of ignition timing, suggesting a common formation mechanism. This offers some, albeit weak, support for the idea that soot forms in secondary combustion events, since it would appear that the soot formation process is not fully dependent on the behaviour of the main combustion event.

Injection Timing Investigation The injection timing investigation was composed of a sweep of injection timing while maintaining constant engine load, speed, equivalence ratio and temperatures. The measured particle number concentrations were significantly higher for very early, or very late injection timings. It was at these timings that the fuel spray was expected to impinge on the piston crown, considering the proximity of the piston to the injector tip during the injection process. In addition to the increased number concentration, larger diameters were observed in the PM emissions produced when piston impingement was expected. These data provided good support for the residual fuel effects hypothesis, demonstrating that the soot characteristics can be correlated to the locations and nature of fuel films.

Repeating the same experiment at a higher coolant temperature resulted in reduced PM emission concentrations as well as reduced particle diameters. It seems that the increased coolant temperature, which should correspond to increased cylinder component temperatures, enabled better evaporation of the fuels from cylinder and piston surfaces, resulting in less residual liquid fuel and different fuel components remaining in those films. This provides support for both of the hypotheses.

Dual Injection Investigation The study of injection timing for a dual injection strategy was conducted to further understand the impact of film locations on PM emissions. The experiments were conducted with 70% of the liquid fuel injected during the first injection (timed to avoid piston impingement), creating a reasonably uniform mixture in the bulk of the cylinder. The remainder of the liquid fuel was injected during a second injection during the compression stroke. The timing of the start of this second injection was varied while maintaining a constant engine speed and load. Similar to the results of the single injection timing study, it was found that the particle number concentrations were as much as two orders of magnitude higher for those injection timings where severe piston wetting is expected. Further to that, the particle sizes are increased as well. There is a range of injection timings through which the fuel spray interacts with the piston bowl; here, the particle emissions remain relatively uniform.

Upon repeating the experiments, once with increased coolant temperatures and once with increased inlet air temperatures, it was found that there was little difference in total particle number concentrations. In the case of the heated inlet air, the goal of which was to examine the impacts of in-flight evaporation, there was also no change in the particle diameters. With heated coolant, however, the particle diameters increased noticeably. This suggests that the volatile fraction of the fuel evaporates more readily, leaving heavier, more highly-sooting components behind. Together, these experiments show that in-flight evaporation has little impact on soot formation, while surface temperatures prove to be very important, thus confirming the hypothesis that fuel films are the main source of particulates at these cold operating conditions.

Fuel Composition Effects Interesting results were obtained when the dual injection timing experiments were repeated using different fuel blends. Blends of 15% and 30% toluene (by volume) in gasoline, as well as 15% and 30% ethanol in gasoline were studied. The emissions trends with injection timing were the same as those seen with the gasoline baseline, but the addition of toluene resulted in higher particle number concentrations with 20°C engine coolant, especially when piston wetting was unlikely. The addition of ethanol did not lead to significant differences in total particle number concentrations. The most interesting results were observed when comparing the particle sizes for each fuel at the two different coolant temperatures studied.

In the case of ethanol addition, increasing ethanol content resulted in smaller particles, at both temperatures. Comparing the emissions from a single fuel at the two temperatures, however, showed that the particle sizes actually increase at higher coolant temperatures, suggesting that the fuel components with low soot formation potential evaporate readily at the higher coolant temperatures. In the case of toluene addition, it was seen that, at coolant temperatures of 20°C, the particle diameters increased with toluene content, but, at coolant temperatures of 80°C, the particle sizes were uniform regardless of toluene content. This suggests, again, that the fuel volatility is important, since it appears that, in the warmed-up engine case, the same fuel components are participating in the soot-producing reactions regardless of toluene

content.

These observations offer further support for the residual fuel effects hypothesis, but offers strong support for the assertion that fuel evaproation characteristics are important for soot formation. Similar results were obtained from the fuel variation study with single injection.

RCM Experiments In addition to the fuel injection studies, RCM experiments were used to study the equivalence ratio threshold for soot formation for gasoline and gasoline/toluene mixtures. As hypothesized, it was found that the threshold for soot formation does vary with fuel composition. It was also found to vary based on combustion temperatures, but there seemed to be little variability associated with changes in the mixture density.

Fuel Volatility Study The fuel volatility study provides good confirmation of the hypothesis that PM arises from fuel films. Blending isopentane and isooctane produces a fuel with a volatile fraction and a less-volatile fraction. The volatile fraction, isopentane, should evaporate readily either in-flight or upon surface contact, leaving behind only isooctane in fuel films, which evaporates more slowly. The reductions in PM emissions are comparable (though slightly greater than) the isopentane fraction in the fuel blend. This confirms the connection between the volume of liquid fuel in the cylinder and the PM emissions. The decrease in emissions may be greater than the volume fraction of isopentane because of evaporation interactions between the two fuel components. The size distributions are consistent for each operating condition regardless of isopentane content, signifying that only isooctane is participating in the soot-forming reactions.

Burned Gas Oxygen Content Investigation The main insight from the study of burned gas oxygen content was that the equivalence ratio of the bulk mixture does not significantly influence particulate emissions. If it did, one would expect to see a sharper change in PM emissions at the transition between lean and rich equivalence ratios. Instead, there is a steady increase in PM emissions with increasing

equivalence ratio. In this experiment, the rate of liquid fuelling was held constant and the equivalence ratio was increased by adding propane to the inlet air. Propane does not contribute significantly to the PM production, and the liquid evaporation properties should remain constant, so the main effect of the addition of propane is that the oxygen concentration in the burned gases is decreased. The increase in particle number concentration, while the particle size distributions maintain consistent shapes suggest that the soot formation mechanism does not change with decreased oxygen content. Instead, it implies that the regions where soot-forming reactions take place are enlarged, and that the soot-forming reactions are likely pyrolytic in nature, rather than combustion reactions. This result was instrumental in allowing the development of a conceptual model of soot formation in DISI engines.

5.1.2 Conceptual Model of Soot Formation in DISI Engines Under Cold-Idle Operating Conditions

As detailed in this conceptual model, it is thought that PM emissions from DISI engines operating under cold-idle conditions originate primarily in pyrolytic reactions in fuel vapour plumes created through the evaporation of liquid fuel from cylinder surfaces. During the injection process, liquid fuel may impinge direcly on cylinder surfaces including the piston crown, the liner surface and the intake valves. Fuel may also impinge indirectly on cylinder surfaces, including those mentioned above as well as other parts of the combustion chamber. This indirect impingement occurs after liquid fuel droplets splash off of the primary location of impingement. It is expected that much of the injected fuel will evaporate in-flight (that is, before striking any surfaces) and be thoroughly mixed with the incoming air, forming a uniform mixture. The volatile fraction of the fuel deposited on cylinder surfaces should also evaporate quickly. With sufficient charge motion, these vapours should be incorporated into the main charge before ignition. Some of the fuel deposited on the liner will not evaporate, instead mixing with the lubricating oil film, with which it is transported to the crankcase. While this portion of the fuel does not contribute to PM emissions,

it is, nevertheless a serious concern, as it dilutes the lubricating oil.

The remainder of the fuel that is deposited in liquid films on cylinder surfaces is likely composed of relatively low-volatility components that will evaporate comparatively slowly. The evaporation from these fuel films, driven mainly by heat transfer from cylinder surfaces will give rise to plumes of fuel vapour, or very rich mixtures of fuel vapour and air surrounding the fuel films. The mixture in the periphery of these plumes will approach the equivalence ratio of the bulk mixture, but the mixture will become progressively more fuel-rich as the centreline of the plume and the fuel film are approached.

After ignition, the main combustion event will proceed as usual. The combustion of the main charge should produce little PM. As the flame front reaches a fuel vapour plume, the periphery of the plume should be consumed in a rich pre-mixed combustion process. Depending on the ignition limits and critical sooting equivalence ratios of the fuel components, there may be some PM produced from this rich pre-mixed combustion.

Finally, the core of fuel vapour plumes are too rich to support combustion. Instead of combustion, it is expected that heat transfer from the bulk burned gases may be sufficient to initiate pyrolysis of the fuel vapours in the core of the plume. It is expected that soot precursors will be formed through these reactions, resulting in the nucleation and surface growth of soot particles. The high temperatures of the burned gases accelerate the evaporation of the fuel film, providing more fuel vapour to participate in these reactions. In addition, the high temperatures cause the soot particles to emit visible radiation (this is the luminosity often described as a diffusion flame). It is expected that these pyrolytic, soot-producing reactions are the primary source of PM in a DISI engine under cold-idle operating conditions.

5.2 Conclusions

The idea that liquid fuel films contribute to particulate matter emissions from DISI engines during start-up and cold-idle operation is not new. For over a decade, fuel

films have been known to be one of the major sources of PM. Typically, the soot-forming reactions involving fuel from these liquid films were described as pool fires or diffusion flames. It appears, however, that these descriptions were inaccurate. While soot incandescence, like that usually attributed to diffusion flames, is observed in DISI engines, the lack of oxygen in the bulk burned gases suggests that combustion reactions are unlikely in these regions.

This study has demonstrated that in a cold engine, instead of a conventional soot-producing diffusion flame (or pool fire), the soot-forming reactions occurring in fuel vapour plumes may be better described as the pyrolysis of fuel vapours in the near absence of oxygen, enabled by heat conduction from hot burned gases. Soot precursors, such as acetylenes and PAH are formed during these pyrolysis reactions, enabling soot particle nucleation and surface growth. The low oxygen concentrations result in little, if any, surface oxidation to compete with the particle growth.

These findings are significant as they offer a complete explanation of the genesis of particulate matter in-cylinder and provide the background information needed to devise methods of minimizing PM emissions. The importance of avoiding film formation is already appreciated within the engine design and calibration communities, but this study allows renewed attention to be paid to fuel blends as a means of achieving PM emissions reductions.

Additionally, one of the implications of the previously accepted explanation of the soot-forming reactions was that the key to reducing emissions was to eliminate fuel films. This is certainly still a viable strategy for PM reductions, but, given the new understanding of the soot-forming reactions as pyrolytic in nature, it may be possible to further contribute to the emissions reductions by attempting to increase the oxygen content in the regions surrounding fuel vapour plumes, or by using creative charge motion strategies to mix vapour plumes with the bulk charge.

5.3 Recommendations for Future Work

The conceptual model outlined in this work provides a good understanding of the soot formation mechanism in cold DISI engines operating at idle speeds. This is a very important operating regime to understand, since it contributes a large fraction of the total emissions permitted over the course of the regulatory certification test cycle. It is not, however, the only operating condition of interest. In particular, start-up and transient operation are also of interest. Given the transient nature of these processes, it is likely that fuel films are less persistent, so it is not clear what implications, if any, from this work may be applied to these operating regimes.

Thus, it is recommended that a similar effort to that completed in this study be conducted with a focus on engine transients. If a fast particle sizer is available, this can be completed in a similar method to that employed here. By relating emissions to physical processes known to be occurring in-cylinder, it may be possible to identify the probable locations of soot formation without requiring the use of an optical engine.

To confirm the hypothesis that pyrolytic reactions are involved in soot formation, optical experiments to visualize the growth of vapour plumes would be helpful. Laser-induced fluorescence may be used to measure equivalence ratios, providing an understanding of what reactions are possible given the known fuel and air concentrations, but this is difficult once soot has begun to form, since the soot luminosity obscures the inner portions of the fuel vapour plume. It may be necessary to complete such a project using simulations.

This page intentionally left blank

Bibliography

[1] Health effects of transport-related air pollution. http://www.euro.who.int/en/what-we-publish/abstracts/health-effects-of-transport-related-air-pollution. Last accessed: 2013-07-03.

[2] F Zhao, M.-C Lai, and D.L Harrington. Automotive spark-ignited direct-injection gasoline engines. *Progress in Energy and Combustion Science*, 25(5):437–562, October 1999.

[3] Walter Piock, Guy Hoffmann, Axel Berndorfer, Patrick Salemi, and Bernd Fusshoeller. Strategies towards meeting future particulate matter emission requirements in homogeneous gasoline direct injection engines. Technical Report 2011-01-1212, SAE International, Warrendale, PA, April 2011.

[4] Paul Whitaker, Paul Kapus, Martin Ogris, and Peter Hollerer. Measures to reduce particulate emissions from gasoline DI engines. Technical Report 2011-01-1219, SAE International, Warrendale, PA, April 2011.

[5] Federal register | national ambient air quality standards for particulate matter. https://www.federalregister.gov/articles/2013/01/15/2012-30946/national-ambient-air-quality-standards-for-particulate-matter. Last accessed: 2013-07-03.

[6] John B. Heywood. *Internal combustion engine fundamentals.* McGraw-Hill, 1988.

[7] Henning Kleeberg, Dean Tomazic, Oliver Lang, and Knut Habermann. Future potential and development methods for high output turbocharged direct injected gasoline engines. Technical Report 2006-01-0046, SAE International, Warrendale, PA, April 2006.

[8] Jon Andersson, Matthew Keenan, and Karin Akerman. Gdi particles - legislation, current levels and control. http://www.cambridgeparticlemeeting.org/sites/default/files/Presentations/2009/JAndersson%28Ricardo%29_2009_GDI_PM.pdf, March 2009. Last accessed: 2013-07-03.

[9] Eric Stevens and Richard Steeper. Piston wetting in an optical DISI engine: Fuel films, pool fires, and soot generation. Technical Report 2001-01-1203, SAE International, Warrendale, PA, March 2001.

[10] Ian Whelan, William Smith, David Timoney, and Stephen Samuel. The effect of engine operating conditions on engine-out particulate matter from a gasoline direct-injection engine during cold-start. Technical Report 2012-01-1711, SAE International, Warrendale, PA, September 2012.

[11] James A. Eng. The effect of spark retard on engine-out hydrocarbon emissions. Technical Report 2005-01-3867, SAE International, Warrendale, PA, October 2005.

[12] Tilo Landenfeld, Andreas Kufferath, and Juergen Gerhardt. Gasoline direct injection - SULEV emission concept. Technical Report 2004-01-0041, SAE International, Warrendale, PA, March 2004.

[13] Harry W. Herr. Percivall pott, the environment and cancer. *BJU International*, 108(4):479481, 2011.

[14] Claudio Pelucchi, Eva Negri, Silvano Gallus, Paolo Boffetta, Irene Tramacere, and Carlo La Vecchia. Long-term particulate matter exposure and mortality: a review of european epidemiological studies. *BMC Public Health*, 9(1):453, December 2009. PMID: 19995424.

[15] David B. Kittelson. Engines and nanoparticles: a review. *Journal of Aerosol Science*, 29(56):575–588, June 1998.

[16] Elena Boldo, Sylvia Medina, Alain Le Tertre, Fintan Hurley, Hans-Guido Mcke, Ferrn Ballester, and Inmaculada Aguilera. Apheis: Health impact assessment of long-term exposure to PM2.5 in 23 european cities. *European Journal of Epidemiology*, 21(6):449–458, June 2006.

[17] Jocelyn Kaiser. Mounting evidence indicts fine-particle pollution. *Science*, 307(5717):1858–1861, March 2005. PMID: 15790822.

[18] Annette Peters, Stephanie von Klot, Margit Heier, Ines Trentinaglia, Allmut Hrmann, H. Erich Wichmann, and Hannelore Lwel. Exposure to traffic and the onset of myocardial infarction. *New England Journal of Medicine*, 351(17):1721–1730, 2004. PMID: 15496621.

[19] Thomas A. J. Kuhlbusch and Christof Asbach. Particle characterization. In Flemming R. Cassee, Nicholas L. Mills, and David Newby, editors, *Cardiovascular Effects of Inhaled Ultrafine and Nanosized Particles*, page 5987. John Wiley & Sons, Inc., 2011.

[20] Health Effects Institute. Review Panel on Ultrafine Particles and Health Effects Institute. *Understanding the Health Effects of Ambient Ultrafine Particles.* HEI Perspectives. Health Effects Institute, 2013.

[21] James McCreanor, Paul Cullinan, Mark J. Nieuwenhuijsen, James Stewart-Evans, Eleni Malliarou, Lars Jarup, Robert Harrington, Magnus Svartengren,

In-Kyu Han, Pamela Ohman-Strickland, Kian Fan Chung, and Junfeng Zhang. Respiratory effects of exposure to diesel traffic in persons with asthma. *New England Journal of Medicine*, 357(23):2348–2358, 2007. PMID: 18057337.

[22] Tak W. Chan, Eric Meloche, Joseph Kubsh, Deborah Rosenblatt, Rasto Brezny, and Greg Rideout. Evaluation of a gasoline particulate filter to reduce particle emissions from a gasoline direct injection vehicle. Technical Report 2012-01-1727, SAE International, Warrendale, PA, September 2012.

[23] Emission standards: Europe: Cars and light trucks. `http://www.dieselnet.com/standards/eu/ld.php`. Last accessed: 2013-07-04.

[24] Office of Air US EPA and Radiation. History | clean air act | US EPA. `http://epa.gov/oar/caa/caa_history.html`. Last accessed: 2013-08-02.

[25] Emission standards: USA: cars and light-duty TrucksTier 1. `http://www.dieselnet.com/standards/us/ld.php`. Last accessed: 2013-08-02.

[26] Emission standards: USA: cars and light-duty TrucksTier 2. `http://www.dieselnet.com/standards/us/ld_t2.php`. Last accessed: 2013-08-02.

[27] 42 USC 7548 - study of particulate emissions from motor vehicles | title 42 - the public health and welfare | U.S. code | LII / legal information institute. `http://www.law.cornell.edu/uscode/text/42/7548`. Last accessed: 2013-08-02.

[28] Emission standards: USA: cars and light-duty TrucksTier 3. `http://www.dieselnet.com/standards/us/ld_t3.php`. Last accessed: 2013-08-02.

[29] M. Matti Maricq, Joseph Szente, Michael Loos, and Rainer Vogt. Motor vehicle PM emissions measurement at LEV III levels. Technical Report 2011-01-0623, SAE International, Warrendale, PA, April 2011.

[30] Heinz Burtscher and W. Addy Majewski. Particulate matter measurements. `http://www.dieselnet.com/tech/measure_dpm.php`, 2012. Last accessed: 2013-08-02.

[31] Jon D Andersson, David P Clarke, and James A Watson. UK particulate measurement programme (PMP): a near US 2007 approach to heavy duty diesel particulate measurements - comparison with the standard european method. Technical Report 2004-01-1990, SAE International, Warrendale, PA, June 2004.

[32] news: PMP publishes light-duty inter-laboratory correlation report. `http://www.dieselnet.com/news/2007/06pmp.php`. Last accessed: 2013-07-03.

[33] Per Ericsson and Andreas Samson. Characterization of particulate emissions propagating in the exhaust line for spark ignited engines. Technical Report 2009-01-2654, SAE International, Warrendale, PA, November 2009.

[34] B.S. Haynes and H.Gg. Wagner. Soot formation. *Progress in Energy and Combustion Science*, 7(4):229–273, 1981.

[35] Z. A. Mansurov. Soot formation in combustion processes (review). *Combustion, Explosion and Shock Waves*, 41(6):727–744, November 2005.

[36] Kenneth Brezinsky, Harjit S. Hura, and Irvin Glassman. Oxidation/pyrolysis chemistry as related to fuel sooting tendencies. *Energy & Fuels*, 2(4):487–493, July 1988.

[37] Chung K. Law. *Combustion Physics.* Cambridge University Press, 2006.

[38] A.V. Krestinin. Detailed modeling of soot formation in hydrocarbon pyrolysis. *Combustion and Flame*, 121(3):513–524, March 2000.

[39] D.B. Scully and R.A. Davies. Carbon formation from aromatic hydrocarbons. *Combustion and Flame*, 9(2):185–191, June 1965.

[40] J.B. Moss, C.D. Stewart, and K.J. Young. Modeling soot formation and burnout in a high temperature laminar diffusion flame burning under oxygen-enriched conditions. *Combustion and Flame*, 101(4):491–500, June 1995.

[41] R. J. Santoro, T. T. Yeh, J. J. Horvath, and H. G. Semerjian. The transport and growth of soot particles in laminar diffusion flames. *Combustion Science and Technology*, 53(2-3):89–115, 1987.

[42] M.D. Smooke, M.B. Long, B.C. Connelly, M.B. Colket, and R.J. Hall. Soot formation in laminar diffusion flames. *Combustion and Flame*, 143(4):613–628, December 2005.

[43] Irvin Glassman and Richard Yetter. *Combustion.* Academic Press, October 2008.

[44] Nicos Ladommatos, Paul Rubenstein, and Paul Bennett. Some effects of molecular structure of single hydrocarbons on sooting tendency. *Fuel*, 75(2):114–124, January 1996.

[45] Fu-Quan Zhao, Ming-Chia Lai, and David L. Harrington. A review of mixture preparation and combustion control strategies for spark-ignited direct-injection gasoline engines. Technical Report 970627, SAE International, Warrendale, PA, February 1997.

[46] M. Matti Maricq, Diane H. Podsiadlik, Diana D. Brehob, and Mohammad Haghgooie. Particulate emissions from a direct-injection spark-ignition (DISI) engine. Technical Report 1999-01-1530, SAE International, Warrendale, PA, May 1999.

[47] Richard R. Steeper and Eric J. Stevens. Characterization of combustion, piston temperatures, fuel sprays, and fuel-air mixing in a DISI optical engine. Technical Report 2000-01-2900, SAE International, Warrendale, PA, October 2000.

[48] Terrence Alger, Yiqun Huang, Matthew Hall, and Ronald D. Matthews. Liquid film evaporation off the piston of a direct injection gasoline engine. Technical Report 2001-01-1204, SAE International, Warrendale, PA, March 2001.

[49] Simone Hochgreb. Fuel distribution and combustion characteristics in a direct-injection, spark-ignited (DISI) engine under stratified operation. Technical Report 2001-01-3645, SAE International, Warrendale, PA, September 2001.

[50] M. C. Drake, T. D. Fansler, A. S. Solomon, and G. A. Szekely. Piston fuel films as a source of smoke and hydrocarbon emissions from a wall-controlled spark-ignited direct-injection engine. Technical Report 2003-01-0547, SAE International, Warrendale, PA, March 2003.

[51] Amin Velji, Kitae Yeom, Uwe Wagner, Ulrich Spicher, Martin Rossbach, Rainer Suntz, and Henning Bockhorn. Investigations of the formation and oxidation of soot inside a direct injection spark ignition engine using advanced laser-techniques. Technical Report 2010-01-0352, SAE International, Warrendale, PA, April 2010.

[52] Vincent S. Costanzo and John B. Heywood. Effect of in-cylinder liquid fuel films on engine-out unburned hydrocarbon emissions for an SI engine. Technical Report 2012-01-1712, SAE International, Warrendale, PA, September 2012.

[53] Axel Berndorfer, Stephan Breuer, Walter Piock, and Paul Von Bacho. Diffusion combustion phenomena in GDi engines caused by injection process. Technical Report 2013-01-0261, SAE International, Warrendale, PA, April 2013.

[54] Mohammad Fatouraie, Margaret Wooldridge, and Steven Wooldridge. In-cylinder particulate matter and spray imaging of Ethanol/Gasoline blends in a direct injection spark ignition engine. Technical Report 2013-01-0259, SAE International, Warrendale, PA, April 2013.

[55] J. Serras-Pereira, P. G. Aleiferis, D. Richardson, and S. Wallace. Characteristics of ethanol, butanol, iso-octane and gasoline sprays and combustion from a multi-hole injector in a DISI engine. Technical Report 2008-01-1591, SAE International, Warrendale, PA, June 2008.

[56] Daniel Sabathil, Achim Koenigstein, Peter Schaffner, Jan Fritzsche, and Arndt Doehler. The influence of DISI engine operating parameters on particle number emissions. Technical Report 2011-01-0143, SAE International, Warrendale, PA, April 2011.

[57] Stephen Sakai, Mitchell Hageman, and David Rothamer. Effect of equivalence ratio on the particulate emissions from a spark-ignited, direct-injected gasoline engine. Technical Report 2013-01-1560, SAE International, Warrendale, PA, April 2013.

[58] Michael Hedge, Phillip Weber, Jess Gingrich, Terrence Alger, and Imad Khalek. Effect of EGR on particle emissions from a GDI engine. Technical Report 2011-01-0636, SAE International, Warrendale, PA, April 2011.

[59] R. Gonzalez-Oropeza, B. J. Hill, A. E. Hassaneen, S. Samuel, and D. Morrey. Gasoline engine particulate emission and exhaust gas speciation. Technical Report 2009-01-2670, SAE International, Warrendale, PA, November 2009.

[60] Philip Price, Richard Stone, Dave OudeNijeweme, and Xiangdong Chen. Cold start particulate emissions from a second generation DI gasoline engine. Technical Report 2007-01-1931, SAE International, Warrendale, PA, July 2007.

[61] I. Whelan, S. Samuel, and A.E. Hassaneen. The effect of fuel temperature on particulate matter formation in gasoline direct-injection engines. Technical Report 2010-01-1469, SAE International, Warrendale, PA, May 2010.

[62] Emmanuel Kasseris and John Heywood. Charge cooling effects on knock limits in SI DI engines using Gasoline/Ethanol blends: Part 1-quantifying charge cooling. Technical Report 2012-01-1275, SAE International, Warrendale, PA, April 2012.

[63] Emmanuel Kasseris and John Heywood. Charge cooling effects on knock limits in SI DI engines using Gasoline/Ethanol blends: Part 2-effective octane numbers. Technical Report 2012-01-1284, SAE International, Warrendale, PA, April 2012.

[64] Philip Price, Ben Twiney, Richard Stone, Kenneth Kar, and Harold Walmsley. Particulate and hydrocarbon emissions from a spray guided direct injection spark ignition engine with oxygenate fuel blends. Technical Report 2007-01-0472, SAE International, Warrendale, PA, April 2007.

[65] John M. Storey, Teresa Barone, Kevin Norman, and Samuel Lewis. Ethanol blend effects on direct injection spark-ignition gasoline vehicle particulate matter emissions. Technical Report 2010-01-2129, SAE International, Warrendale, PA, October 2010.

[66] Longfei Chen, Mike Braisher, Alison Crossley, Richard Stone, and Dave Richardson. The influence of ethanol blends on particulate matter emissions from gasoline direct injection engines. Technical Report 2010-01-0793, SAE International, Warrendale, PA, April 2010.

[67] Carl Vuk and Steven J. Vander Griend. Fuel property effects on particulates in spark ignition engines. Technical Report 2013-01-1124, SAE International, Warrendale, PA, April 2013.

[68] Koichiro Aikawa, Takayuki Sakurai, and Jeff J. Jetter. Development of a predictive model for gasoline vehicle particulate matter emissions. Technical Report 2010-01-2115, SAE International, Warrendale, PA, October 2010.

[69] Felix Leach, Richard Stone, and Dave Richardson. The influence of fuel properties on particulate number emissions from a direct injection spark ignition engine. Technical Report 2013-01-1558, SAE International, Warrendale, PA, April 2013.

[70] Makoto Koike, Akinori Saito, Terutoshi Tomoda, and Yasuhiro Yamamoto. Research and development of a new direct injection gasoline engine. Technical Report 2000-01-0530, SAE International, Warrendale, PA, March 2000.

[71] Nobuhiko Koga, Shigeki Miyashita, Keiso Takeda, and Nobuo Imatake. An experimental study on fuel behavior during the cold start period of a direct injection spark ignition engine. Technical Report 2001-01-0969, SAE International, Warrendale, PA, March 2001.

[72] Richard S. Davis, Gary D. Mandrusiak, and Tilo Landenfeld. Development of the combustion system for general motors' 3.6L DOHC 4V v6 engine with direct injection. Technical Report 2008-01-0132, SAE International, Warrendale, PA, April 2008.

[73] Lars Schmidt, Justin Seabrook, John Stokes, Mohd Faizan Ahmad Zuhdi, Steven Begg, Morgan Heikal, and Jason King. Multiple injection strategies for improved combustion stability under stratified part load conditions in a spray guided gasoline direct injection (SGDI) engine. Technical Report 2011-01-1228, SAE International, Warrendale, PA, April 2011.

[74] Chris De Boer, Gary Bonar, Shizuo Sasaki, and Shreeram Shetty. Application of supercritical gasoline injection to a direct injection spark ignition engine for particulate reduction. Technical Report 2013-01-0257, SAE International, Warrendale, PA, April 2013.

[75] Ian Whelan, Stephen Samuel, and Ahmed Hassaneen. Investigation into the role of catalytic converters on tailpipe-out nano-scale particulate matter from gasoline direct injection engine. Technical Report 2010-01-1572, SAE International, Warrendale, PA, May 2010.

[76] Ian Whelan, David Timoney, William Smith, and Stephen Samuel. The effect of a three-way catalytic converter on particulate matter from a gasoline direct-injection engine during cold-start. Technical Report 2013-01-1305, SAE International, Warrendale, PA, April 2013.

[77] Tak W. Chan, Eric Meloche, Joseph Kubsh, Rasto Brezny, Deborah Rosenblatt, and Greg Rideout. Impact of ambient temperature on gaseous and particle emissions from a direct injection gasoline vehicle and its implications on particle filtration. Technical Report 2013-01-0527, SAE International, Warrendale, PA, April 2013.

[78] Iason Dimou, Kenneth Kar, and Wai Cheng. Particulate matter emissions from a direct injection spark ignition engine under cold fast idle conditions for

ethanol-gasoline blends. Technical Report 2011-01-1305, SAE International, Warrendale, PA, April 2011.

[79] Kevin Cedrone. *Kevin Cedrone Thesis.* Thesis, Massachusetts Institute of Technology, 2013. Thesis (Ph. D.)–Massachusetts Institute of Technology, Dept. of Mechanical Engineering, 2013.

[80] J. A. Caton. Comparisons of thermocouple, time-averaged and mass-averaged exhaust gas temperatures for a spark-ignited engine. Technical Report 820050, SAE International, Warrendale, PA, February 1982.

[81] TSI Incorporated. *Model 3934 SMPS (Scanning Mobility Particle Sizer) Instruction Manual, Revision D*, 1996.

[82] TSI Incorporated. *Model 3010 Condensation Particle Counter Instruction Manual, Revision D*, 1996.

[83] David Kayes and Simone Hochgreb. Investigation of the dilution process for measurement of particulate matter from spark-ignition engines. Technical Report 982601, SAE International, Warrendale, PA, October 1998.

[84] Maik Bergmann, Volker Scheer, Rainer Vogt, and Thorsten Benter. Comparison of the performance of real-time PM mass and number instrumentation for vehicle exhaust measurements. Technical Report 2007-24-0116, SAE International, Warrendale, PA, September 2007.

[85] Jon D. Andersson, Barbara G. A. Wedekind, Diane Hall, Richard Stradling, Chris Barnes, and Geoff Wilson. DETR/SMMT/CONCAWE particle research programme: Sampling and measurement experiences. Technical Report 2000-01-2850, SAE International, Warrendale, PA, October 2000.

[86] Brian E. Hallgren and John B. Heywood. Effects of oxygenated fuels on DI diesel combustion and emissions. Technical Report 2001-01-0648, SAE International, Warrendale, PA, March 2001.

[87] Imad Abdul-Khalek, David Kittelson, and Fred Brear. The influence of dilution conditions on diesel exhaust particle size distribution measurements. Technical Report 1999-01-1142, SAE International, Warrendale, PA, March 1999.

[88] Jorn Dinh Herner, William H. Robertson, and Alberto Ayala. Investigation of ultrafine particle number measurements from a clean diesel truck using the european PMP protocol. Technical Report 2007-01-1114, SAE International, Warrendale, PA, April 2007.

[89] Ioannis Kitsopanidis. *Experimental and computational study of soot formation under diesel engine conditions.* Thesis, Massachusetts Institute of Technology, 2004. Thesis (Ph. D.)–Massachusetts Institute of Technology, Dept. of Mechanical Engineering, 2004.

[90] Hua Zhao and Nicos Ladommatos. *Engine Combustion Instrumentation and Diagnostics.* Society of Automotive Engineers, January 2001.

[91] S. Russ, M. Thiel, and G. Lavoie. SI engine operation with retarded ignition: Part 2 -HC emissions and oxidation. Technical Report 1999-01-3507, SAE International, Warrendale, PA, October 1999.

[92] S. Park and J.B. Ghandhi. Fuel film temperature and thickness measurements on the piston crown of a direct-injection spark-ignition engine. Technical Report 2005-01-0649, SAE International, Warrendale, PA, April 2005.

[93] Imad A. Khalek, Thomas Bougher, and Jeff J. Jetter. Particle emissions from a 2009 gasoline direct injection engine using different commercially available fuels. Technical Report 2010-01-2117, SAE International, Warrendale, PA, October 2010.

[94] Pentane, 2,2,4-trimethyl-. `http://webbook.nist.gov/cgi/cbook.cgi?Name=isooctane&Units=SI&cTG=on&cTC=on&cTP=on&cTR=on&cIE=on&cIC=on&cDI=on&cSO=on`. Last accessed: 2013-07-25.

[95] Butane, 2-methyl-. `http://webbook.nist.gov/cgi/cbook.cgi?Name=isopentane&Units=SI&cTG=on&cTC=on&cTP=on&cTR=on&cIE=on&cIC=on&cDI=on&cSO=on`. Last accessed: 2013-07-25.

[96] Amir Gamal Maria. *On fuel selection in controlled auto-ignition engines : the link between intake conditions, chemical kinetics, and stratification.* Thesis, Massachusetts Institute of Technology, 2012. Thesis (Ph. D.)–Massachusetts Institute of Technology, Dept. of Mechanical Engineering, 2012.

[97] John E. Dec. A conceptual model of DI diesel combustion based on laser-sheet imaging*. Technical Report 970873, SAE International, Warrendale, PA, February 1997.

[98] R. W. Temple-Pediani. Fuel drop vaporization under pressure on a hot surface. *Proceedings of the Institution of Mechanical Engineers*, 184(1):677–696, June 1969.

[99] Sakae Yagi and Hiroshi Iino. Radiation from soot particles in luminous flames. *Symposium (International) on Combustion*, 8(1):288–293, 1961.

[100] Barry A. A. L. van Setten, Michiel Makkee, and Jacob A. Moulijn. Science and technology of catalytic diesel particulate filters. *Catalysis Reviews*, 43(4):489–564, 2001.

Appendices

Appendix A

Injector Pulse-Width Calibration

The injection pulse-width was correlated to the mass of fuel delivered per injection using a simple calibration procedure. The fuel rail was mounted in a test fixture that held the injectors in place during the calibration. The injector tip was inserted into top of a glass container and the injector was fired. The fuel was collected in the glass container and was then weighed on a microbalance to determine the mass of fuel delivered. A single injection delivers far too little fuel to obtain repeatable mass measurements, so hundreds or even thousands of pulses (depending on the length of the pulse) were completed and the final mass of fuel was averaged over the total number of pulses. The glass container was mounted in an ice bath to ensure the fuel did not vapourize after the injections. Any condensation on the container was carefully removed before the fuel was weighed. Figure A-1 is a plot of the calibration data. It is seen that, for pulse-widths longer than 500μs, the fuel mass delivered is related nearly linearly to the fuel injection pulse-width. At pulse-widths shorter than 500μs, the injector operates in its "ballistic" regime, and the relation between mass delivered and pulse-width is non-linear. There is a pressure dependence. As shown in figure A-2, the mass flow rate appears to be related to the square root of pressure.

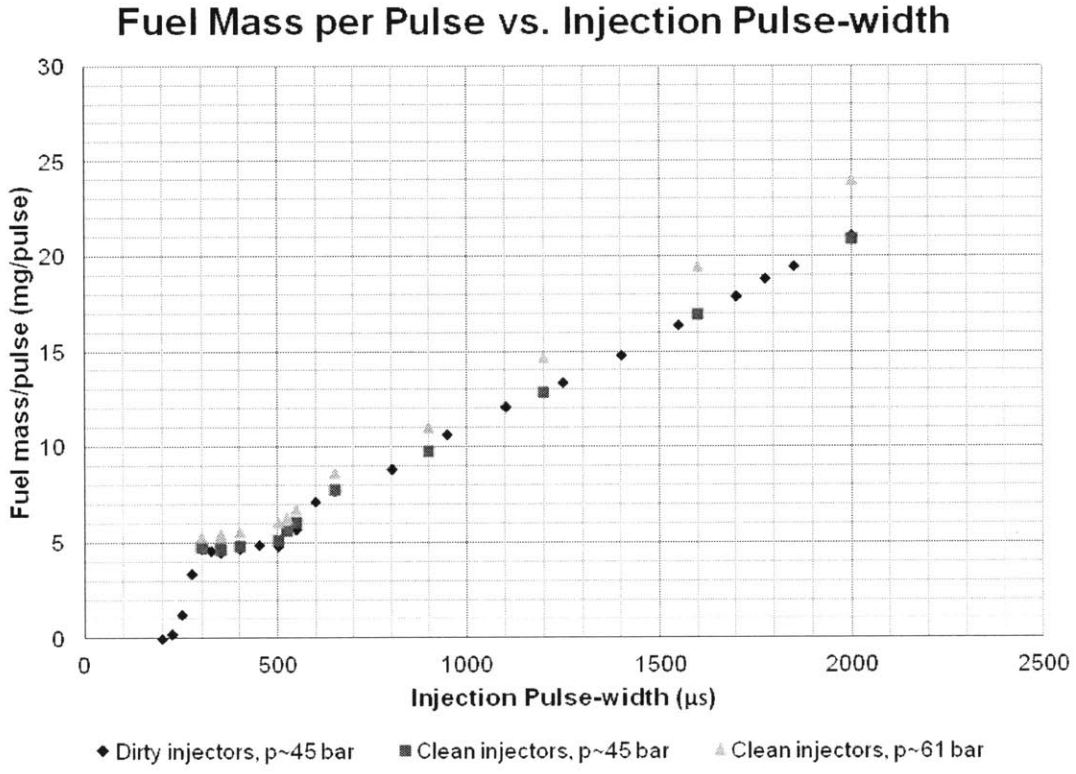

Figure A-1: Fuel Injector Mass Calibration

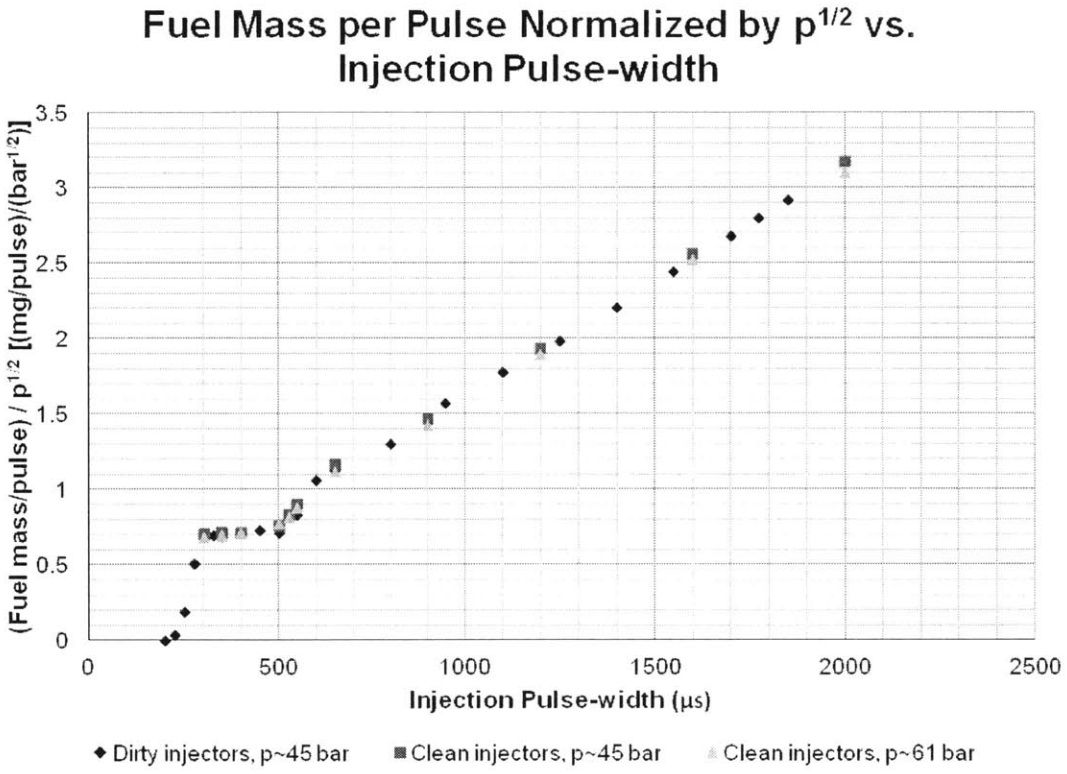

Figure A-2: Normalized Fuel Injector Mass Calibration

This page intentionally left blank

Appendix B

Haltermann HF0 437 Fuel Specifications

haltermannsolutions
fueling the world, one solution at a time.
Telephone: (800) 969-2542

Product Information

FAX: (281) 457-1469
Johann Haltermann Ltd.

PRODUCT: EPA TIER II EEE FEDERAL REGISTER

PRODUCT CODE: HF0437

Batch No.: AJ0221LT10

Tank No.: 105

Date: 10/3/2012

TEST	METHOD	UNITS	HALTERMANN Specs			RESULTS
			MIN	TARGET	MAX	
Distillation - IBP	ASTM D86	°F	75		95	87
5%		°F				110
10%		°F	120		135	126
20%		°F				149
30%		°F				175
40%		°F				204
50%		°F	200		230	223
60%		°F				234
70%		°F				244
80%		°F				263
90%		°F	305		325	319
95%		°F				342
Distillation - EP		°F			415	411
Recovery		vol %		Report		96.9
Residue		vol %		Report		1.1
Loss		vol %		Report		2.0
Gravity	ASTM D4052	°API	58.7		61.2	59.2
Density	ASTM D4052	kg/l	0.734		0.744	0.742
Reid Vapor Pressure	ASTM D5191	psi	8.7		9.2	9.2
Carbon	ASTM D3343	wt fraction		Report		0.8646
Carbon	ASTM E191	wt fraction		Report		0.8631
Hydrogen	ASTM E191	wt fraction		Report		0.1339
Hydrogen/Carbon ratio	ASTM E191	mole/mole		Report		1.847
Stoichiometric Air/Fuel Ratio				Report		14.580
Oxygen	ASTM D4815	wt %			0.05	None Detected
Sulfur	ASTM D5453	wt %	0.0025		0.0035	0.0031
Lead	ASTM D3237	g/gal			0.01	None Detected
Phosphorous	ASTM D3231	g/gal			0.005	None Detected
Silicon	ASTM 5184	mg/kg			4	<1
Composition, aromatics	ASTM D1319	vol %			35	28
Composition, olefins	ASTM D1319	vol %			10	1
Composition, saturates	ASTM D1319	vol %		Report		71
Particulate matter	ASTM D5452	mg/l			1	0.6
Oxidation Stability	ASTM D525	minutes	240			1000+
Copper Corrosion	ASTM D130				1	1a
Gum content, washed	ASTM D381	mg/100mls			5	<0.5
Fuel Economy Numerator/C Density	ASTM E191		2401		2441	2426
C Factor	ASTM E191			Report		0.9991
Research Octane Number	ASTM D2699		96.0			96.5
Motor Octane Number	ASTM D2700			Report		88.6
Sensitivity			7.5			7.9
Net Heating Value, btu/lb	ASTM D3338	btu/lb		Report		18492
Net Heating Value, btu/lb	ASTM D240	btu/lb		Report		18475
Color	VISUAL			Report		Undyed

APPROVED BY: /Ken Y. Dan